Quantifying air-void distribution and associated uncertainty in fresh and hardened concrete

by

Ragini Krishna Nikumbh

B.E., Mumbai University, 2014
M.Tech., National Institute of Technology Karnataka, Surathkal, 2017

AN ABSTRACT OF A DISSERTATION

submitted in partial fulfillment of the requirements for the degree

DOCTOR OF PHILOSOPHY

Department of Civil Engineering
Carl R. Ice College of Engineering

KANSAS STATE UNIVERSITY
Manhattan, Kansas

2023

Abstract

Freeze-thaw damage in Portland cement concrete pavements (PCCP) has been a significant concern for regions experiencing (numerous) rapid freeze-thaw cycles along with frequent precipitation. In the early 1950s Powers recommended entraining a well-distributed air-void system (comprised of equally spaced, small air voids) through the cementitious paste to minimize frost damage in PCCP. There are several methods to measure total air content in fresh concrete, such as ASTM C231 (volumetric air content using a pressure meter) and ASTM C173 (volumetric air content using a roll-o-meter). Still, air content alone is insufficient to assess an air void distribution. Hardened air-void analysis (ASTM C457) is used to accurately measure distribution in terms of total air content, paste-to-air ratio, spacing factor, and specific surface area. But this test can only be performed in hardened concrete about 28 days after it has been placed on-site, thus limiting its use for making a real-time assessment. According to ACI 201.2R, a minimum 4% total (volumetric) air content, a paste-to-air ratio between 4 to 10, along with a specific surface area in the range of 25 to 45 mm^{-1} (600 to 1100 $in.^{-1}$), and a spacing factor in the range

0.1 to 0.2 mm (0.004 to 0.008 in.), is required to ensure adequate freeze-thaw resistance of PCCP. Accordingly, limitations have been placed by various transportation agencies to ensure the required air- void distribution in PCCP. Recently, the KT-86/AASHTO T 395 (Sequential Pressure Method, referred to as the Super Air Meter - SAM) and the pressure meter were proposed as field-ready devices to improve quality control/assurance (QC/QA) practices. However, several potential shortcomings are associated with using these devices to evaluate air-void distribution in fresh concrete in real-time on the field.

To enrich the predictive capability of these traditional methods, complementary models have been proposed in this study to predict spacing factors using mixture design and fresh concrete test measurements as predictors. A set of 271 observations were used to develop the statistical

models for predicting spacing factor (PSF) measured by a commercial air-void scanning system (RapidAir, based on the ASTM C457-16 method). Significant variable(s) for model development were selected using the LASSO, Binary logistic, and Bayesian probit regression analysis models. The predictive models were evaluated on their ability to distinguish between a well-entrained air-void system (spacing factor < 0.008 in. or 0.2 mm) from a coarsely-entrained air-void system (spacing factor > 0.008 in. or 0.2 mm). It was observed that the predictive models were better and more efficient in assessing the air-void distribution than total air content or SAM number alone. Given that the models were calibrated and validated for a data set dominated by a spacing factor less than 0.008 in. (0.2 mm), its validation was limited for coarsely entrained air-void systems.

The given study focuses on examining current & alternate methods and the error associated with them to evaluate air-void distribution in fresh & hardened concrete. Distribution parameters measured by a RapidAir system are assumed to be an actual/accurate representation of the entrained air-void system. But these parameters are regulated by the RapidAir system settings (namely threshold and gain), selected by the operator during evaluation. Thus, to accurately identify and quantify this influence, a set of known air-void distributions were compared to their similar properties measured by the RapidAir system at different system settings. The known air-void distributions were generated as unique synthetic air-void structures using a Python script and printed as luster photographs using a 3200-dpi printer. A RapidAir system at different system settings scanned these photographs. The 'true' distribution parameters for these photographs were calculated from the exact size & location of air voids, recorded by the Python script. As expected, a significant error was observed between the two measurements. Later, these errors were used to minimize the influence of system settings on the distribution parameters measured for a set of concrete samples. As a result, a 'fair ground' to compare air-void structures of the same/different samples evaluated by the same/different systems and settings was provided.

Previously, researchers have recommended using alternate parameters and spacing factor definitions to evaluate air-void distribution in hardened concrete. One such parameter is the 'dispersion parameter' (DP), formerly used to quantify the dispersion of fibers in composites. The current study considers this parameter to quantify the dispersion of air voids through its cementitious paste. DP is a scalar quantity calculated as the ratio of maximum work required to disperse air voids from their current locations to their location in 'best' and 'worst' dispersion scenarios. DP helps quantify the distribution of air voids across the sample and identify the location and presence of clusters, thereby offering a better characteristic distance parameter than the 'spacing factor' to quantify the quality of air-void distribution. Overall, the given study serves as a guide to enrich QC/QA practices by assessing the accuracy & uncertainty of current & proposed methods to evaluate air-void distribution in fresh & hardened concrete.

Keywords: Concrete, air content, air void system, sequential pressure method, Super Air Meter, Volumetric paste to volumetric air ratio, statistical analysis, spacing factor, ASTM C457.

Quantifying air-void distribution and associated uncertainty in fresh and hardened concrete

by

Ragini Krishna Nikumbh

B.E., Mumbai University, 2014
M.Tech., National Institute of Technology Karnataka, Surathkal, 2017

A DISSERTATION

submitted in partial fulfillment of the requirements for the degree

DOCTOR OF PHILOSOPHY

Department of Civil Engineering
Carl R. Ice College of Engineering

KANSAS STATE UNIVERSITY
Manhattan, Kansas

2023

Approved by:

Major Professor
Dr. Christopher A. Jones

Copyright

Abstract

Freeze-thaw damage in Portland cement concrete pavements (PCCP) has been a significant concern for regions experiencing (numerous) rapid freeze-thaw cycles along with frequent precipitation. In the early 1950s Powers recommended entraining a well-distributed air-void system (comprised of equally spaced, small air voids) through the cementitious paste to minimize frost damage in PCCP. There are several methods to measure total air content in fresh concrete, such as ASTM C231 (volumetric air content using a pressure meter) and ASTM C173 (volumetric air content using a roll-o-meter). Still, air content alone is insufficient to assess an air void distribution. Hardened air-void analysis (ASTM C457) is used to accurately measure distribution in terms of total air content, paste-to-air ratio, spacing factor, and specific surface area. But this test can only be performed in hardened concrete about 28 days after it has been placed on-site, thus limiting its use for making a real-time assessment. According to ACI 201.2R, a minimum 4% total (volumetric) air content, a paste-to-air ratio between 4 to 10, along with a specific surface area in the range of 25 to 45 mm^{-1} (600 to 1100 $in.^{-1}$), and a spacing factor in the range

0.1 to 0.2 mm (0.004 to 0.008 in.), is required to ensure adequate freeze-thaw resistance of PCCP. Accordingly, limitations have been placed by various transportation agencies to ensure the required air- void distribution in PCCP. Recently, the KT-86/AASHTO T 395 (Sequential Pressure Method, referred to as the Super Air Meter - SAM) and the pressure meter were proposed as field-ready devices to improve quality control/assurance (QC/QA) practices. However, several potential shortcomings are associated with using these devices to evaluate air-void distribution in fresh concrete in real-time on the field.

To enrich the predictive capability of these traditional methods, complementary models have been proposed in this study to predict spacing factors using mixture design and fresh concrete test measurements as predictors. A set of 271 observations were used to develop the statistical

models for predicting spacing factor (PSF) measured by a commercial air-void scanning system (RapidAir, based on the ASTM C457-16 method). Significant variable(s) for model development were selected using the LASSO, Binary logistic, and Bayesian probit regression analysis models. The predictive models were evaluated on their ability to distinguish between a well-entrained air-void system (spacing factor < 0.008 in. or 0.2 mm) from a coarsely-entrained air-void system (spacing factor > 0.008 in. or 0.2 mm). It was observed that the predictive models were better and more efficient in assessing the air-void distribution than total air content or SAM number alone. Given that the models were calibrated and validated for a data set dominated by a spacing factor less than 0.008 in. (0.2 mm), its validation was limited for coarsely entrained air-void systems.

The given study focuses on examining current & alternate methods and the error associated with them to evaluate air-void distribution in fresh & hardened concrete. Distribution parameters measured by a RapidAir system are assumed to be an actual/accurate representation of the entrained air-void system. But these parameters are regulated by the RapidAir system settings (namely threshold and gain), selected by the operator during evaluation. Thus, to accurately identify and quantify this influence, a set of known air-void distributions were compared to their similar properties measured by the RapidAir system at different system settings. The known air-void distributions were generated as unique synthetic air-void structures using a Python script and printed as luster photographs using a 3200-dpi printer. A RapidAir system at different system settings scanned these photographs. The 'true' distribution parameters for these photographs were calculated from the exact size & location of air voids, recorded by the Python script. As expected, a significant error was observed between the two measurements. Later, these errors were used to minimize the influence of system settings on the distribution parameters measured for a set of concrete samples. As a result, a 'fair ground' to compare air-void structures of the same/different samples evaluated by the same/different systems and settings was provided.

Previously, researchers have recommended using alternate parameters and spacing factor definitions to evaluate air-void distribution in hardened concrete. One such parameter is the 'dispersion parameter' (DP), formerly used to quantify the dispersion of fibers in composites. The current study considers this parameter to quantify the dispersion of air voids through its cementitious paste. DP is a scalar quantity calculated as the ratio of maximum work required to disperse air voids from their current locations to their location in 'best' and 'worst' dispersion scenarios. DP helps quantify the distribution of air voids across the sample and identify the location and presence of clusters, thereby offering a better characteristic distance parameter than the 'spacing factor' to quantify the quality of air-void distribution. Overall, the given study serves as a guide to enrich QC/QA practices by assessing the accuracy & uncertainty of current & proposed methods to evaluate air-void distribution in fresh & hardened concrete.

Keywords: Concrete, air content, air void system, sequential pressure method, Super Air Meter, Volumetric paste to volumetric air ratio, statistical analysis, spacing factor, ASTM C457

Table of Contents

List of Figures

List of Tables

Acknowledgments

I want to acknowledge and express my sincere gratitude to my advisor Dr. Christopher Jones for giving me the opportunity and financial support to pursue my Doctoral studies. Thank you for the guidance, mentorship, encouragement, trust, and, most importantly, patience you have shown me during this journey, which has helped shape me into a better researcher and person. Thank you for always supporting me, creating a fun working environment, and nurturing my writing skills (which have come a long way since we started). I will also be grateful for your guidance in starting my post-academia professional career.

I would also like to thank my committee members Dr. Mustaque Hossain, Dr. Robert Peterman, and Dr. Goh - for their help and willingness to serve on the committee. I enjoyed our discussions & learning how to apply the statistical concepts better, and I appreciate your contribution to enriching our research. I sincerely appreciate Dr. Goh's technical expertise, unconditional guidance, and patience while conducting the statistical analysis. I would also like to thank Dr. Anthony Warnick for helping me understand the technical aspect of printing high-resolution images and allowing me to use the 3200-dpi printer for our research. Also, thank you, Dr. Parth Panchmatia, for your valuable comments and suggestions to improve my technical writing skills.

I would also like to acknowledge the financial support provided by the Kansas Department of Transportation (KDOT) for my research and materials donated by several companies from the industry. Thank you - Dan Wadley, Jennifer Distlehorst, Kate Andrzejewski, Hallie Bruce, and Ryan Hutchins from KDOT, for your assistance with this project. Thanks to their geology team (Kate, Hallie, and Ryan) for running many hardened air-void analysis samples/images. Your expertise helped us better understand the problem and try different ideas/solutions. Also, I sincerely appreciate the help I received from my amazing colleagues at K-State, who are always ready to help us out; some of these were Cody Delaney, Andrew Schoenecke, Clifford Temple, Trisha, Rebecca, Melissa, Jamie, Cathelyn, Cassie, Neeti, Poornima, Subodh, Faisal, Hunter Meier, Hunter Turrel, Cody, Noah, and so many more.

Finally, I would like to thank God and my amazing support group - my family and friends- for standing by me through all the difficulties and making this journey enjoyable. My parents (Ashwini and Krishan Nikumbh); my fantastic band of brothers/sisters - Subodh, Jayesh, Mangesh, Sagar, Akash, Chinmay, Harsha; my incredible friends - Nandita, Prachi, Snehal, Garima, Suraj, Aniket, Rejuna, Rohan; my whole 'Deore' family - Hirabai (Aai), Sheila mami, Mantu mama, Shalini mami, Pooja mami, Monu mama, Bunty mama, Manisha atya & mama; and sooooooo many others. Thank you, my beloved Mumma, for the wisdom, endless support, guidance, and emotional support you have given me almost daily. Your excellent advice, prayers, and belief have helped me sustain and thrive in stressful situations.

Chapter 1 - Introduction

1.1 Background

Freeze-thaw damage in concrete pavements (CP) has been a significant concern for regions experiencing cold climatic conditions. This complicated phenomenon has been explained by various theories (Marchand et al., 1995, Neville, 1996, Pigeon, 2014, Porras et al., 2020). The hydraulic pressure theory states that water, upon freezing, expands by approximately 9%, thereby creating an extra pore pressure in critically saturated (> 85%) CP (Yang et al., 2011, Li et al., 2012). When experienced over multiple freeze-thaw cycles, this excess pore pressure is known to cause micro-cracks and/or other distress in CP (Qin et al., 2016). Deicing salts used to minimize snow accumulation & ice formation for maintaining safe driving conditions on roads and bridges during snowy weather; are also known to increase the ion concentration of capillary pores in CP. The osmotic pressure theory states that water flows from gel pores (which contain less concentrated pore solution) to capillary pores to equalize the concentration of pore solution. This movement of water generates pressure in capillary pores, thereby increasing stresses in regions around the capillary pores. Furthermore, the higher concentration of pore solution caused by deicer salts lowers the freezing point of pore solution and keeps them at or near- maximum saturation (Litvan, 1976, Harnik et al., 1980, Mehta & Gerwick, 1982, Setzer, 1997, Wang et al., 2006). Overall, a combination of higher hydraulic pressure due to ice formation, an increase in osmotic pressure gradient driving water to the freezing center, an increase in capillary ice by diffusion of gel water, and vapor pressure potentials causes severe frost damage in CP (Litvan, 1976, Harnik et al., 1980, Mehta & Gerwick, 1982, Setzer, 1997, Wang et al., 2006, Li et al., 2012).

Distresses in CP are mainly observed in the form of cracking, scaling, and spalling, which are aggravated when the pavement is at maximum/critical saturation (Powers & Willis, 1950, Powers & Helmuth, 1953, Litvan, 1976, Stark, 1976, Litvan, 1988, Afrani & Rogers, 1994, Senadheera, 1995, Senadheera & Zollinger, 1996, Koubaa et al., 1997, Rollings, 1998, Scherer, 1999, Wang & Zollinger, 2000, Scherer & Valenza, 2005, Panchmatia et al., 2014, AC! 201, 2016, Weiss et al., 2018). By ensuring the use of durable aggregates (and thereby eliminating/minimizing damage due to D-cracking), researchers have tried to understand the problem associated with frost damage of paste matrix and design preventive measures (Powers & Willis, 1950, Powers & Helmuth, 1953, Pigeon et al., 1986, Weiss et al., 2018, Wu et al., 2020). In the early 1950s, entrained air voids through the cementitious paste effectively minimized the freeze-thaw effect in CP (Powers & Willis, 1950, Powers & Helmuth, 1953, Powers, 1954, Mielenz et al., 1958). This improved resistance to freeze-thaw action was attributed to a shorter distance traveled by the freezing water to reach its nearest void to release excess pore pressure generated by ice formation.

Powers described that the severity of damage generated by hydraulic pressure depends on the proportion of cementitious paste protected by air voids and the spacing factor controlled by the surrounding air voids (Powers & Helmuth, 1953). As a result, an air-void distribution is quantified in terms of total air content (A), spacing factor (L), specific surface area (a), and paste-to-air ratio (p/A). In addition, researchers have proposed alternate parameters to measure distribution, such as the Philleo factor (S) (Philleo, 1983, AC! 201, 2016). The Philleo factor (S) uses distance as an index to define the extent of hardened cement paste protected from freezing by ensuring that only a small portion of the paste (usually 10%) lies farther from the perimeter of its nearest air-void. S is calculated as per Equation 1.1(Philleo, 1983):

$$S = \frac{0.62}{N^{1/3}}\left[\left(ln\frac{1}{1-A} + 2.303\right)^{\frac{1}{3}} - \left(\ln\frac{1}{1-A}\right)^{\frac{1}{3}}\right] \quad \textbf{Equation 1.1}$$

Where, S = Philleo factor,

N = Number of air voids per unit of volume of cement paste, and

A = Air content of paste i.e., the fraction of air-entrained paste.

S is used to measure either the percentage of paste within a given distance of an air void or the distance between air voids in a specified paste percentage. It is seen to better identify the accurate air-void distribution compared to air content, as it is based on the paste content and Number of voids influencing the spacing factor (ACI 201, 2016). Consequently, it has been included as one of the recommended parameters in ACI 201.2R.

Most current recommendations for ensuring the satisfactory freeze-thaw performance of an air- entrained CP given by ACI 201.2R are based on the study by Powers (AC! 201, 2016, Powers, 1954). According to this, CP should have at least 4% A, p/A between 4 to 10 along with an a in the range of 25 to 45 mm-1 (600 to 1100 in.-1), an L in the range 0.1 to 0.2 mm (0.004 to 0.008 in.), and a maximum distance between an air void and 90% of paste (S) of approximately 0.04 mm (0.002 in.) (ACI 201, 2016). The Canadian Standards Association (CSA A23.1.19/A23.2.19, 2019) has a slightly higher limit on the average spacing factor of 0.23 mm (0.009 in.), with no single value more than 0.25 mm (0.0098 in.). Similar specifications have been made by the Kansas Department of Transportation (KDOT) Section 403 (KDOT, 2015) for on-grade concrete to ensure the quality and durability of an air-void system. These specifications must be met in addition to prequalifying coarse aggregates for construction by the KTMR-22/ASTM C666 laboratory freeze-thaw test (ASTM, 2015), where the latter also measures expansion in concrete. Some additional tests such as KTMR-21 Soundness by Freeze/Thaw (KDOT, 2019a), AASHTO T 96 Wear (AASHTO, 2022a), and KTMR-23 Wetting & Drying (KDOT, 2019b), are also used to evaluate and prequalify aggregate sources for use in on-grade construction.

The quality control/assurance (QC/QA) tests used on the field include a minimum of 5% A (by volume) in fresh concrete, as measured by KT-19/AASHTO T 196 Volumetric Method

(AASHTO, 2011, ASTM, 2016a), ASTM C231/AASHTO T 152 Pressure Method (AASHTO, 2019, ASTM, 2022b), or KT-86/AASHTO T 395

Sequential Pressure Method using a Super Air Meters, SAM (AASHTO, 2022b). Subsequently, for on- grade QC/QA, KT-71/AASHTO T 348 Air Void Analyzer) (KDOT, 2022) - AVA (AASHTO, 2018) is used to test samples behind the paver to evaluate its spacing factor, specific surface, and total air content after placement and consolidation (vibration of the mix) have occurred. AVA's maximum allowable spacing factor limit is 0.3175 mm (0.0125 in.) - above which cores must be analyzed by ASTM C457 hardened air-void analysis to evaluate the final air-void distribution for acceptance (ASTM, 2016b). Additional recommendations have been made for situations when these specifications are not satisfied on the field, as follows (KDOT, 2015):

"Obtain 2 cores from any area with an AVA spacing factor > 0.0125 inches and send to Materials Research Center for hardened air evaluation.

If the AVA spacing factor > 0.0125 inches and the average hardened air spacing factor > 0.0080 inches, then suspend paving and submit new mix design.

If the AVA spacing factor > 0.0125 inches and the average hardened air spacing factor < 0.0080 inches, then accept CP.

Take immediate steps to increase the air content whenever the air content behind the paver falls below 5.0%. Suspend paving operations when 2 consecutive air contents behind the paver fall below 4.0% and remove and replace the represented concrete.

The maximum air content is 10%. Take immediate steps to reduce the air content whenever the air content exceeds 8%."

Lindquist and Montney's KDOT - FHWA report stated that the remove-and-replace clause was reinstated in April 2008 for pavements with a spacing factor of more than 0.375 mm (0.0150 in.). However, an indistinct conclusion was made regarding the enforcement of this penalty (Lindquist & Montney, 2015, 2019). Since this penalty could incur a heavy loss in terms of time and money to the contractor and KDOT, it is vital to ascertain the reliability of the tests used for measuring the distribution parameters as soon as possible on the field. Including hardened air-void analysis by ASTM C457 method as a real-time QC/QA tool is not feasible, as it requires complete curing (14 - 28 days) of samples and significant labor/transport expense of all samples back to the central lab. Thus, the total burden of evaluating the quality of the air-void system lies on the fresh concrete properties measured as total air content by Volumetric or Pressure Method and the spacing factor by AVA or SAM. Although measuring total air content on the field is more manageable, studies have shown that the total air volume is not the sole indicator of freeze-thaw durability (Ley et al., 2012) performance. Instead, the spacing factor is a controlling factor as long as it has the minimum total air content (Ley et al., 2012). Hence, a recently developed test apparatus and method, SAM, has been investigated by several transportation agencies across the country for use as a QC/QA tool to evaluate new concrete air-void distribution properties in real-time accurately. A significant advantage is its ability to provide results in 10 to 15 minutes. Results from SAM are obtained as total air content and a system air metric number (SAM number), where the latter correlates with the ASTM C457 spacing factor and specific surface (Ley & Tabb, 2014; AASHTO, 2022b).

The air-void distribution parameters measured by the ASTM C457 method are assumed to yield its 'true' or 'actual' values. The distribution parameters can be measured using one of the three procedures outlined in ASTM C457. 'Procedure C: Contrast-Enhanced Method,' an automated version of 'Procedure A: Linear Traverse Method,' is commonly used for analysis. 'Procedure C' involves using a high-resolution camera/scanner to capture multiple high-contrast black-and-white images of the concrete surface in incremental steps. The set of images is evaluated by a computer program capable of distinguishing the fraction of air voids (brighter pixels) from the paste and aggregate (darker pixels) at a specific value of the specified percent paste (p, calculated using the mixture design), threshold and gain given by the operator (Jakobsen et al., 2005, 2006; Fonseca & Scherer, 2015). The complete process of hardened air- void analysis after sample preparation is automated in commercial systems such as the RapidAir. As a result, the measured distribution parameters are regulated by the selected system settings.

1.2 Problem Statement

Measuring the air-void properties in fresh concrete is essential to ascertain the durability of on-grade CP. The current practices efficiently measure total air content but need to be more proficient at evaluating its distribution in fresh concrete since the ASTM C457 can only assess the distribution parameters. The hardened air-void analysis is best used for vetting a mix during pre-qualification and again to verify a mix 28 days (about four weeks) after it has been placed on the field. However, because of its time and sample preparation requirements, it cannot be used as a QC/QA tool to inspect the quality of an entrained air-void system on-field. The distribution parameters measured by the ASTM C457 are assumed to represent the air-void structure in hardened concrete accurately. Still, various things could be improved with this method. This includes the dependency of measured parameters on system settings selected by the operator for commercial air-void analyzing systems. Thus, a robust tool is needed to validate the quality of entrained air-void distribution in fresh concrete & make quick decisions on the field and quantify the error or uncertainty lodged by system settings during hardened air-void analysis using a RapidAir system. This was achieved using carefully designed mixes or samples to resemble those encountered during the paving job.

1.3 Objective

Freeze-thaw damage in CP is related to unsatisfactory air entrainment in the cementitious paste. Air-void entrainment is a complicated phenomenon affected by various factors such as mixture design, chemical interaction, amount of consolidation energy introduced to a mix, how it was placed (pumped, trucked, or placed by chute), its workability, and so on. Total air content is insufficient to predict the freeze-thaw resistance of CP but is governed by the distribution of air voids. Commonly used fresh concrete tests on- field can accurately measure the total air content but is inept in evaluating its distribution. Even though hardened air void analysis is a forensically reliable QC/QA tool, it cannot accurately predict air-void distribution at the job site in real-time.

This study focuses on understanding the errors or uncertainties associated with measuring air-void distribution parameters in fresh and hardened concrete. And quantifying the variability associated with these techniques will help provide recommendations and improve the current QC/QA practices used in the field. As a result, they are improving the acceptance or rejection criteria for as-placed concrete and saving future efforts & money to replace a damaged CP because of a flawed air-void system.

In regards to this, the given study is split into three parts:

Part 1:

The first part of this study focuses on understanding the limitations associated with the current QC/QA practices, followed by using statistical techniques to develop practical solutions to identify modifications made to a pre-qualified mix on the field in real-time.

- Statistically analyze the data collected on the field (I-70 with KDOT), in Kansas State University (K-State) laboratory, and additional data procured from KDOT.

- Examine the correlation between SAM number and ASTM C457 spacing factor, followed by quantifying the error and relative uncertainty associated with the sequential pressure method for the given data set.
- Use sophisticated statistical techniques to develop predictive models to estimate the quality of air-void distribution in fresh concrete, using mixture design and fresh concrete test measurements as predictors.

The predictive models recommended during this study are an inexpensive solution recommended to enrich the current QC/QA practices.

Part 2:

The second part of this study focuses on understanding the uncertainty or error incurred by the system settings of a RapidAir system (based on the ASTM C457) on the measured air-void distribution parameters. This was achieved using a set of a known set of air-void distribution parameters. It will help understand the accuracy and repeatability of this machine when examining samples with carrying distribution parameters.

- Conduct a preliminary study using a set of concrete samples to validate the influence of system settings.
- Examine diverse types of air-void structures at different system settings for which the 'known or true' solution is known. Accordingly, a set of synthetic air-void structures were generated using a Python script and printed as high-resolution images using a 3200-dpi printer. Their 'true' distribution parameters are calculated using the size and location of air voids documented by the Python script.
- Compare the 'true' and RapidAir distribution parameters to estimate the error associated with different system settings for a set of synthetic air-void structures.

1.4 Research Methodology

Data gathered during this study included mixture designs and fresh concrete properties for concrete mixtures tested by KDOT and K-State in their laboratories and on the field. The new concrete tests conducted during this study included ASTM C138 unit weight (ASTM, 2017), ASTM C143 slump (ASTM, 2020), total air content, and SAM number. Additionally, distribution parameters in terms of the total air content, spacing factor, specific surface area, and paste-to-air ratio were measured in hardened concrete by the ASTM C457. Based on preliminary data analysis, a general trend was evident in the measured air-void properties when repetitive tests were performed. These trends formed a basis for developing equations to predict spacing factors in fresh concrete and quantifying the error associated with hardened air-void analysis conducted by the RapidAir system.

1.5 Thesis Outline

The thesis has six chapters. Chapter 1 includes an introduction to the research. Chapter 2 consists of a literature review, including general requirements and methods to assess the air-void structure in fresh and hardened concrete. The methods and predictive models to estimate the spacing factor in fresh concrete are covered in Chapter 3. Chapter 4 proposes an alternate parameter - Dispersion Parameter (DP), and a method to assess uncertainty in the distribution parameters measured by hardened air-void analysis. Chapter 5 includes overall conclusions & recommendations, and the references cited in the manuscript are listed in Chapter 6.

Chapter 2 - Literature Review

2.1 Overview

A well-entrained air-void structure comprised of a large number of small-sized, equally spaced air voids is known to improve the freeze-thaw durability of CP. The entrained air voids act as expansion chambers to relieve the excess pore pressure generated by ice formation. The improved durability properties of CP have been attributed to the short distance traveled by the freezing water to reach its nearest air- void, to release the excess pore pressure (Powers, 1945, Powers & Willis, 1950; Powers & Helmuth, 1953, Powers, 1954, Pleau & Pigeon, 1996; Pigeon, 2014). Thus, most state departments of transportation (DOTs) and other transportation agencies across the United States specify the inclusion of 4 - 6% air content with a maximum spacing factor of 0.2 mm (0.008 in.) to ensure the durability of CP. For example, KDOT Section 403 specifies the inclusion of 5 ± 0.5 % total (volumetric) air content with a spacing factor less than 0.2 mm (0.008 in.) for on-grade concrete.

Typically, the ASTM C231 pressure meter or ASTM C173 volumetric method is used to measure the total air content in fresh concrete. It provides quick results but needs to be more comprehensive to assess air-void distribution. Thus it is imperative to measure its spacing factor, which is the most significant indicator of freeze-thaw resistance (Powers & Willis, 1950, Powers, 1954, Zhang et al., 2005). Several researchers have focused on predicting this quantity of interest in fresh concrete using methods such as the sequential pressure method using SAM, AVA, and acoustic bubble spectrometer (ABS) (Chahine et al., 1998, Chahine et al., 2001, Wu et al., 2011). Additionally, alternate methods such as the point count method (Radlinski et al., 2010), ultrasonic techniques (Punurai et al., 2006, 2007, Guo et al., 2016), X-ray computed tomography (Kim et al., 2012, Lu et al., 2017), automated computation by image analysis (Chatterji & Gudmundsson, 1977, Zhang et al., 2005) or a flatbed scanner (Zalocha & Kasperkiewicz, 2005, Peterson et al., 2010, Radlinski et al., 2010), definition/equations for spacing factor (Attiogbe, 1993, Snyder, 1998), have been proposed to evaluate the air-void distribution in hardened concrete.

2.2 Air-void Distribution in Fresh Concrete

Air voids in fresh concrete are introduced in the cementitious paste by numerous actions - the motion of mixer blades and aggregates falling onto themselves forms entrapped air bubbles. At the same time, the air-entraining admixture (AEA) creates and stabilizes entrained air voids (Du & Folliard, 2005). Since AEA is used in combination with other admixtures (such as superplasticizers, retarders, and so on), it is essential to evaluate their compatibility and effect on the size, distribution, and stability of an entrained air-void structure (Du & Folliard, 2005). Additionally, mixture design parameters such as the ratio of water to cementitious material (w/cm), paste content, paste to aggregate ratio, and slump of concrete are significant in entrapping and entraining air voids (Fagerlund, 1993, Myers, 1999). Previous studies have reported an increase in air content, with an increase in a slump from 75 to 150 mm (2.95 - 5.9 in.) and a decrease in air content for a slump above 150 mm (5.9 in.). This decrease in air content has been associated with reduced stability of air bubbles for a slump above 150 mm (5.9 in.) (Powers, 1969, Du & Folliard, 2005, Dodson, 2013).

A variation in the air-void distribution of concrete mixtures evaluated during this study will be achieved by varying proportions of variables given below:

- Water to cementitious material (w/cm)
- Paste content (%)
- Slump
- Cement content and proportion of fly ash replacement

- Mixing time/procedure

2.3 Current Practices for Measuring Air-Void Distribution in Fresh Concrete

The following section will be focused on understanding the commonly used methods for assessing the air void distribution in fresh and hardened concrete.

2.3.1 AASHTO T 152 or ASTM C231: Type B Pressure Meter

The total volumetric air content in fresh concrete is typically measured by a Type B pressure meter described in ASTM C231 (ASTM, 2022b). It is based on Boyle's law and measures the pressure difference when a pressure of 14.5 psi is applied to fresh concrete. This pressure difference estimates the associated volume change caused by crushing air voids, thereby, fresh concrete's total volumetric air content. Although total air content is measured within a few minutes, a significant shortcoming of this method is its inability to quantify its distribution in fresh concrete. Air-void distribution parameters can only be entirely/accurately assessed in hardened concrete 28 days after it has been cast on-site, thus making it impossible to change the entrained air-void system. According to the precision and bias statement given by ASTM C231, the air content measured for the same sample by the same operator should not vary more than 0.5%, and that by different laboratories should be within 0.75% (ASTM, 2022b).

2.3.2 AASHTO T 348: Air Void Analyzer (AVA)

AVA is based on Stoke's law and measures the size & distribution of air voids as they rise through a column of glycerol and water (AASHTO, 2018). However, its use is limited due to its sensitivity to vibration in the testing environment, expensive equipment, difficulty in field testing, and inability to detect air bubbles larger than 0.3 mm (0.012 in.) (Tanesi et al., 2016). A precision statement presented a standard deviation of 0.018 - 0.052 mm (0.0007 - 0.002 in.) and 0.026 - 0.072 mm (0.001 - 0.003 in.) between the spacing factor (less than 0.15 mm [0.006 in.])

measurements by single and multiple operators, respectively when two tests of the same sample were conducted using 19 different AVAs (Distlehorst & Kurgan, 2007). Additionally, the specific surface measurements were presented to vary by 43% and 53% when tested on the same and different machines, respectively (Distlehorst & Kurgan, 2007, Tanesi et al., 2016). A different study recognized a weak direct relationship between the spacing factor measured by AVA and ASTM C457. It reported that the AVA measures a higher spacing factor by an average of 1.67 to 1.88 times compared to the ASTM C457 (Lindquist & Montney, 2015, 2019).

2.3.3 AASHTO T 395: Super Air Meter (SAM)

Traditionally ASTM C173/KT-19/AASHTO T 196 (air content of freshly mixed concrete by the volumetric method) or ASTM C231/KT-18/AASHTO T 152 (air content of freshly mixed concrete by the pressure method) is used to measure total air content in fresh concrete. But these methods are inept to provide a complete representation of its distribution.

Air-void distribution can be accurately quantified by hardened air-void analysis, which typically requires curing the sample for 28 days in a wet room (or lime bath), followed by about two weeks to cut, prepare and test each slide. Traditionally the volumetric or pressure method measures total air content in fresh concrete. However, these methods must be more proficient in providing a complete representation of its distribution. As a result, it cannot provide a real-time quality assessment of the entrained air-void system in the field. To tackle this inadequacy, Dr. Tyler Ley of Oklahoma State University developed the AASHTO T 395 (sequential pressure method or super air meter - SAM) equipment and test method (AASHTO, 2022b). The sequential pressure method using SAM was developed to quantify the air-void distribution in fresh concrete in real-time. Since then, it has been adopted by various state departments of transportation and transportation agencies across the United States as a potential QC/QA tool to assess the air-void distribution and total air content (Ley & Tabb, 2014, AASHTO, 2022b). A significant advantage of this inexpensive method is its ability to assess the quality of the air-void distribution in fresh concrete on the field within 10-15 minutes (Ley & Tabb, 2014, Tanesi et al., 2016, Ley et al., 2017; Dąbrowski et al., 2019).

SAM is a modified version of the traditional pressure meter. The traditional dial gauge used by a pressure meter is replaced with a digital gauge in SAM. This digital gauge is connected to a microcomputer to record and assess the measured pressure. The pressure chamber attached to the top chamber is secured to its bottom chamber (bowl) by six clamps. Sequential pressurization is used for crushing more giant air bubbles and only measuring the entrained air voids, which are more critical for freeze-thaw durability. Initially, the sequential pressure method was developed to pressurize fresh concrete using SAM in two sets of sequential pressure –- 14.5 psi (100 kPa), 30 psi (207 kPa), 45 psi (310 kPa), 60 psi (414 kPa), and 75 psi (517 kPa); and measure the associated equilibrium pressures. A SAM number of 0.5 psi relating to the pressure difference between the equilibrium pressure for 75 psi steps, was observed to correlate with a spacing factor (ASTM C457) of 0.2 mm (0.008 in.). This correlation was established for a dataset dominated by high-slump mixtures and using a single coarse aggregate source. Upon further inspection using a set of low slump paving mixtures, an offset was seen in the initial correlation between the SAM number (0.5 psi) and ASTM C457 parameters (Ley & Tabb, 2013, 2014, Tanesi et al., 2016). Subsequently, the equipment was modified due to manufacturer safety concerns, and the maximum pressure was restricted to 45 psi (310 kPa).

Currently, the Sequential Pressure Method using SAM involves three separate pressurization rounds of

14.5 psi (100 kPa), 30 psi (207 kPa), and 45 psi (310 kPa). It quantifies the total air content and spacing factor between air bubbles through the System Air Metric (SAM number) parameter (Ley & Tabb, 2014, Ley et al., 2017). The SAM number is measured as the pressure difference between the equilibrium pressure for the first (Pc1) and second (Pc2) round of 45 psi (310 kPa) steps. The total air content is measured based on the pressure difference between the applied pressure of 14.5 psi (100 kPa) and its equilibrium pressure.

2.3.3.1 Testing with Fresh Concrete

Initially, the inner side of the top lid and SAM bowl are dampened, followed by measuring the empty weight of the bowl. After that, fresh concrete is placed in the bowl in three lifts. Each layer is rodded 25 times and consolidated by at least 12 sharp mallet strikes - 3 strikes for each cardinal direction around the periphery of the bowl. The strike-off plate is slid back and forth in a sawing motion until the bowl is full. For concrete with a slump less than 2.5 in., a table vibrator consolidates at a frequency of 115 Hz for 30 seconds. The top rim of the bowl is cleaned with a damp sponge and checked for sand grains by the tip of a finger. Subsequently, the testing procedure explained below (and in Figure 2.1) is followed to determine the SAM number and total air content.

1. The lid and bowl are tightly secured using clamps while its petcocks are open.
2. Water is injected into one of the petcocks using a funnel, squeeze bottle, or similar device until air- free water emerges from the open petcock.
3. The apparatus is inclined and rocked back and forth to remove air bubbles entrapped when fresh concrete is placed in the bowl.
4. One of the petcocks is closed, and the other is left open.

5. Air pressure in the top pressure chamber is bled out by fully opening the air bleeder valve, and the corresponding gauge reading is recorded as 'start pressure.'
6. The air bleeder valve is closed, and the pressure chamber is pressurized to 14.5 psi.
7. The gauge reading stabilizes at 14.5 ± 0.05 psi. At this point, the appearance of air bubbles through the open petcock represents a pressure leak in the valve present between the top lid and bowl.
8. Excess pressure (air) is bled through the air bleeder valve.
9. In the absence of a pressure leak, the open petcock is closed, and the gauge reading is recorded for 'Step# 1: Start'. The needle valve lever is lifted open for 10 seconds while the periphery of the bowl is tapped firmly with a mallet.
10. Upon closing the needle valve lever, the gauge reading is recorded for 'Step# 1: Read'.
11. At the end of Step# 1, the gauge displays air content(%).
12. The same procedure (Steps # 6 to 10) is repeated for a pressure of 30 psi and 45 psi, and their corresponding readings are recorded as 'Step# 2: Start' & 'Step# 2: Read' and 'Step# 3: Start' & 'Step# 3: Read'.
13. At the end of Step # 12, both petcocks are slowly opened to release pressure in a bowl.
14. Steps 2 through 12 are repeated, and the corresponding readings are recorded.
15. Finally, the gauge displays the total air content (%) and SAM number

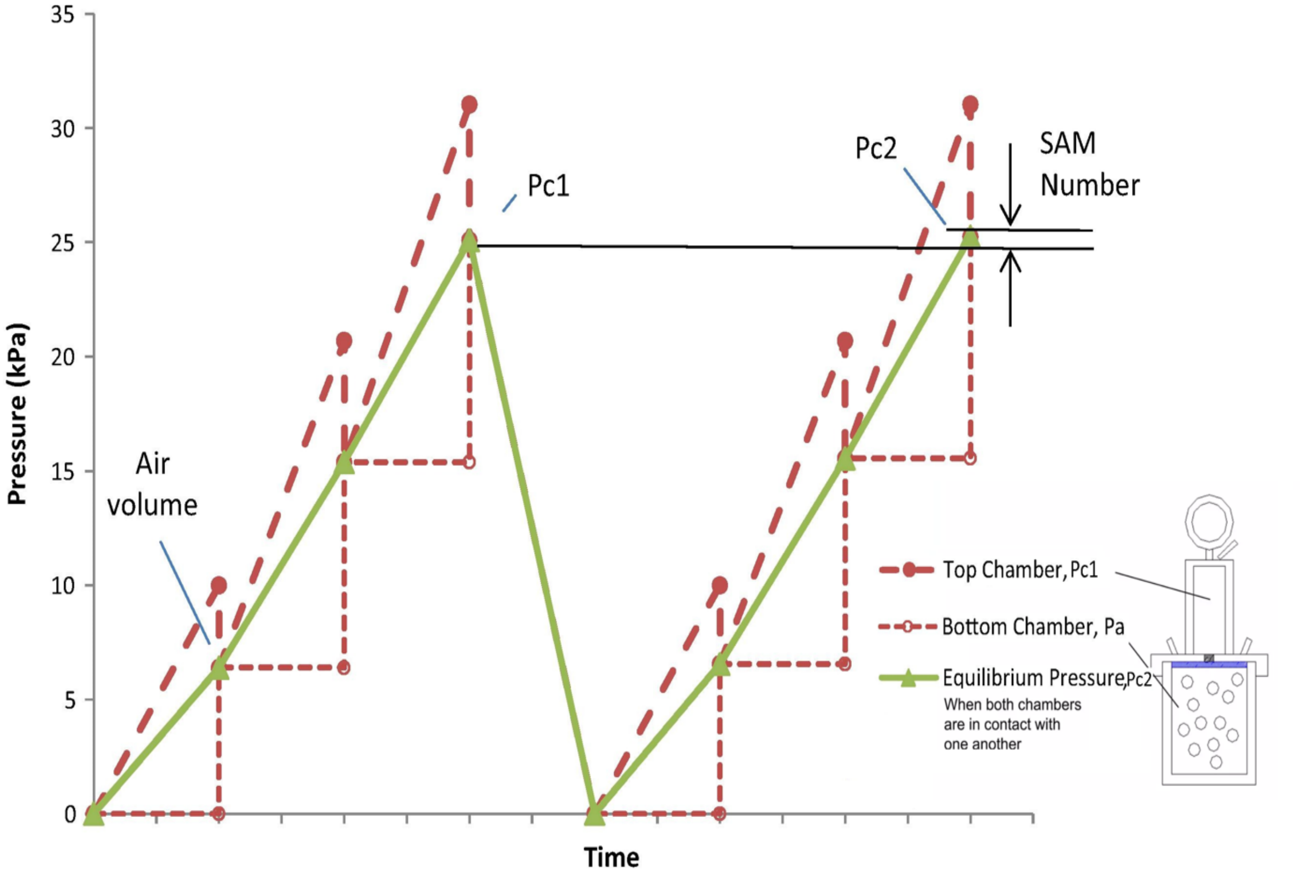

Figure 2.1: Graphical representation of the pressure steps in the top and bottom chamber in the sequential pressure method (Ley et al., 2017)

2.3.3.2 Testing with Water only

Before testing SAM with fresh concrete, it is tested with water to detect leaks and ensure it is functioning accurately. SAM is seen to function accurately if the measured air content is less than or equal to 0.30% and the SAM number is less than or equal to 0.03.

2.3.3.3 Calibration of Sequential Pressure Meter

SAM should be re-calibrated every time its pressure chamber is repaired or any part of the meter is replaced. It is calibrated using a calibration vessel - Pro Cali-Can, which has a built-in air content (by volume) of 5%. To perform calibration, the 'CALIB' option is selected from the menu, and all the steps are followed until Step# 12 with water. After the petcocks are opened (end of Step# 13), the Pro Cali-Can is placed at the center of the bowl, and readings for 'Step # 4' is recorded. Following this, the calibration results are saved.

2.3.3.4 SAM Number and Spacing Factor

SAM number has been shown to correlate with the spacing factor - measured by the ASTM C457 method (Ley & Tabb, 2014, Riding & Albahttiti, 2016, Tanesi et al., 2016, Ley et al., 2017, Dąbrowski et al., 2019, AASHTO, 2022b). A SAM number of 0.2 has been shown to correlate with a spacing factor of 0.2 mm (0.008 in.). Previously researchers have examined the correlation between SAM number and total air content (Riding & Albahttiti, 2016, Tanesi et al., 2016, Dąbrowski et al., 2019) and concluded that a decrease in SAM number is associated with an increase in total air content (Tanesi et al., 2016, Moradllo et al., 2020).

2.3.3.5 Aggregate Correction Factor, G

The aggregate correction factor (G, psi) is used to calculate the 'true' air content by correcting the effect of aggregate porosity. This is measured by placing the proportion of fine and coarse aggregates (as present in the fresh concrete mix) in the bowl. Before placement, they are soaked in water for a duration equal to when water is added to the mixer and the start of the sequential pressure method - about 15 to 30 minutes. The masses of fine and coarse aggregates in the concrete sample are calculated as per Equations 2.1 and 2.2.

Mass of fine aggregates in the sample under test (lb), Fs = S * Fb / B **Equation 2.1**

Mass of coarse aggregates in the sample under test (lb), Cs = S * Cb / B **Equation 2.2**

Where:

S = Volume of concrete sample = Volume of measuring bowl = 0.25 ft3

B = Volume of concrete produced per batch = 0.27 ft3

Fb = Total mass of fine aggregate used in mixing (lb)

Cb = Total mass of coarse aggregate used in mixing (lb)

Initially, the Pro Cali-Can is placed at the center, and water is added to the bowl until it is filled to 1/3rd of height. Slowly, the blended coarse and fine aggregates are added to the bowl by entrapping as little air as possible. Once complete, water is added to fill the bowl. The total 'apparent' air content (Ac, %) is measured at 14.5 psi pressure. Moreover, the aggregate correction factor (G, %) is calculated as the difference in the Ac (%) and the air present in the Pro Cali-Can- which is about 5%. Thus, the 'true' total air content of a concrete sample, also known as the Sample Air (As, %), is calculated as the Apparent Air (Aa, %) minus the Aggregate Correction Factor (G, %).

2.3.3.6 Accuracy of the Digital Gauge

The digital gauge used by SAM has a comprehensive range of 0.0 - 100.0 psi, with an accuracy of 0.1 psi throughout its range (Ley & Tabb, 2013). Based on its accuracy, the absolute uncertainty of the results can be calculated at the 95% confidence level, as follows (Menin, 2018):

- SAM number has absolute uncertainty of 0.14 psi $\left(= \sqrt{0.1^2 + 0.1^2}\right)$,
- Total air content has absolute uncertainty of 0.1 psi $\left(= \sqrt{0.1^2}\right)$, which is about 0.72 %.

Like the Type B pressure meter, the sequential pressure method is also based on Boyle's law. Boyle's law assumes a perfect equilibrium between the observed volume change and measured pressure difference upon consolidation. The relative uncertainty for these parameters can be calculated as their absolute uncertainty divided by the statistic of interest, i.e., observed or measured pressure difference. The SAM number refers to the pressure difference between Pc1 and Pc2 (as shown in Figure 2.1); for the total air content, it is considered between the applied pressure of 14.5 psi and its equilibrium pressure.

2.3.3.7 **Effects of Consolidation Energy**

The required amount of consolidation decreases with an increase in a slump. Thus, the required and applied amount of consolidation energy influences the accuracy of the recorded SAM number, especially for low slump mixtures (slump < 63.5 mm or 2.5 in). Higher consolidation energy is required to mobilize the buoyant air bubbles within a concrete sample. These entrapped bubbles are hard to release with just 12 mallet strikes. Thus, a higher vibration frequency is needed to release them (ACI 201, 2016). As a result, recording a significant pressure difference for low-slump mixtures may be challenging compared to high-slump mixtures (ACI 201, 2016). Thereby causing a higher degree of relative uncertainty in the measured SAM number (et al., 2019). This uncertainty adds-on to the baseline gauge accuracy, giving a wide spread of good readings recorded for a given concrete mixture. Another primary source of error is the 'N-Err' or negative error displayed as the SAM number. 'N-Err' is associated with a negative or insignificant pressure difference (when Pc1 is higher than Pc2) measured by the sequential pressure method. Hence, it is recommended to use a small tabletop vibrator such as the 'Minn-T' for consolidation and testing using SAM to evaluate low-slump mixtures.

2.4 Hardened Air-Void Analysis

Apart from ensuring stability and assessing fresh concrete entrained air void distribution, it is equally important to ascertain that the distribution parameters are accurately measured in hardened concrete. ASTM C457 method is widely used to conduct the hardened air-void by one of its three outlined procedures (ASTM, 2016b):

- Procedure A: Linear-traverse method
- Procedure B: Modified point-count method
- Procedure C: Contrast-enhanced method.

2.4.1 Introduction to the ASTM C457 Procedures

Traditionally the linear traverse method (Procedure A) involved drawing equally spaced parallel lines (Traverse) on the hardened concrete surface. This was followed by an optical microscope to manually count the traverse length intercepted by air voids, paste, and aggregates, by an index point. The frequency and traverse length measurements of the chords intercepted through the air voids and paste are recorded to calculate the hardened air void parameters as per Equations 2.3 - 2.7 (ASTM, 2016b):

- Total air content (A): the volume of air as a percentage of total volume.

$$\mathbf{A = \frac{Total\ length\ through\ air}{Total\ length\ of\ Traverse} \times 100} \qquad \textbf{Equation 2.3}$$

- Paste to air (p/A) ratio: ratio of the volumes of paste to the volume of air.

$$\mathbf{p/A = \frac{Traverse\ length\ through\ paste}{Traverse\ length\ through\ air}} \qquad \textbf{Equation 2.4}$$

- Spacing factor (L): a parameter related to the flow distance from a given air-void to its nearest neighbor in the cementitious paste.

$$\mathbf{For\ p/A \geq 4.33,\ \ L = \frac{3}{\alpha}\left[1.4\left(\frac{p}{A}+1\right)^{1/3} - 1\right]} \qquad \textbf{Equation 2.5}$$

$$\mathbf{For\ p/A < 4.33,\ \ L = \frac{p}{\alpha A}} \qquad \textbf{Equation 2.6}$$

- Specific surface (α): surface area of the air-voids per unit volume of air.

$$\mathbf{\alpha = \frac{4\ (Number\ of\ air-voids\ intercepted)}{Total\ length\ of\ Traverse}} \qquad \textbf{Equation 2.7}$$

Procedure B, called the modified point-count method, uses a 'point-count' machine that moves uniformly on the hardened concrete surface along equal distances. The machine has at least four digital counters to measure stops made in paste, air voids, and coarse & fine aggregates (ASTM, 2016b). On the other hand, Procedure C, called the contrast-enhanced method, is an automated process of Procedure A: linear-traverse method. The automated method (Procedure C) was introduced by Chatterji & Gudmundsson (Chatterji & Gudmundsson, 1977). This procedure requires painting the hardened (polished) concrete surface black and filling a white powder in its air voids. Then, a high-resolution camera captures several greyscale images of the sample surface in incremental steps. A computer program is used to distinguish between the fraction of paste, air voids, and aggregates (Chatterji & Gudmundsson, 1977, ASTM, 2016b).

For a greyscale image, the pixel value is used to measure its average brightness intensity on a scale of 0 - 255, corresponding to black, white, and shades of gray (Zhang et al., 2005). The pixel values embedded within the greyscale image are evaluated using a computer program to distinguish between the fraction of air voids (brighter pixels) and paste & aggregate particles (darker pixels) at a system setting specified (threshold and gain) by the operator (Jakobsen et al., 2005, 2006, Fonseca & Scherer, 2015). This automated process has been commercialized in systems such as the RapidAir, H-2964A, HF- MAC01 (Hachiyo Consultant Co., Ltd., and Fast Corporation), and ACES (Automated Concrete Evaluation System). Out of these, RapidAir is most widely used to perform hardened air-void analysis. Previously, round-robin studies were conducted to compare the distribution parameters for numerous samples; tested multiple times by different RapidAir systems at different systems (Zhang et al., 2005, Jakobsen et al., 2005, 2006, Jana, 2007, Peterson et al., 2009).

2.4.2 Round-Robin Studies

The study by Jakobsen et al. (2005, 2006) compared distribution parameters for three samples evaluated across seven laboratories in the USA and Europe by the RapidAir system and manual analysis. Operators could choose their preferred system settings while setting up the experiment. This included using 1 to 3 traverses per frame, rotating the samples four times (90° between each reading), threshold, pitch, and gain. The total air content readings had a standard deviation of 0.20 - 0.62 and 0.45 - 0.97 when computed by automated and manual analysis, respectively. Similarly, the standard deviation for specific surface measurements ranged between 1.58 - 2.90 mm-1 and 4.44 - 13.58 mm-1 when measured by automated and manual analysis, and the spacing factor by the automated and manual analysis fluctuated between 0.006 - 0.049 mm and 0.033 - 0.109 mm, respectively (Jakobsen et al., 2005, 2006).

The study by Zhang et al. compared nine samples' distribution parameters measured by automated and manual procedures. Assuming that the manual analysis yielded the actual/accurate distribution parameters, an error was calculated for the distribution measured by the automated procedure. Accordingly, an error of 1.38 - 5.98% was measured for the total air content, 1.76 - 8.25% for the specific surface area, and 0.52 - 8.09% for the spacing factor (Zhang et al., 2005). Conversely, Schlorholtz documented a relatively large error of 20% for the air content and 30% for the specific surface by comparing the two analysis methods (Schlorholtz, 1998). Pleau et al. (2001) reported an error of 30% for the air content, 20% for the specific surface, and 8% for the spacing factor. Other round-robin studies have drawn similar conclusions, where the distribution parameters varied using different evaluation systems or methods (Jana, 2007, Fonseca & Scherer, 2015). Of all the round-robin studies considered during this study, only one documented the threshold value used for analysis, which was 149 (Peterson et al., 2009). Since other round-robin studies did not document the threshold value, it is difficult to compare their results/errors or make an overall conclusion. Thereby further emphasizing the need to quantify the error caused by changing system settings.

2.4.1 Potential Source of Error in the Hardened Air-Void Analysis

Numerous sources of error may cause variation in the results recorded by hardened air-void analysis. This includes but is not limited to the smallest size of air-void detected, selected threshold, statistical algorithm or system or methodology used for analysis. The preceding discussion assumed the manual measurements (Procedure A) to give a more accurate presentation of the air-void distribution, but this might only sometimes be true. This is because the manual analysis is subject to human error, i.e., the operator's expertise or the microscope's resolution. On the other hand, the accuracy of automated analysis is based on the system accurately detecting both small and large air voids. A relatively low threshold is necessary to detect smaller air voids, but this causes the inclusion of more neighboring non- air pixels around the larger air voids. However, a higher threshold will include a more significant fraction of air voids as non-air, which will cause fewer air voids to be detected. Thus, the automated analysis conducted at a higher threshold exhibits a higher deviation in the total air content and a lower deviation in the spacing factor compared to the manual analysis (Peterson et al., 2009).

ASTM C457-16 provides a minimum (total) traverse length to be completed for a sample, with few recommendations/guidelines to select the system settings for analysis. The absence of 'true measurements' for evaluating a given air-void distribution causes difficulty in comparing samples analyzed by different systems or settings. This might be associated with the dependence of thresholds and gain on camera resolution or the accuracy of a system in detecting the significant distribution parameter. Accordingly, the study focuses on understanding the variation or error for air-void distribution parameters in different system settings.

Chapter 3 - Evaluation of Air-Void Distribution in Fresh Concrete

3.1 Concrete Batching and Sample Collection

The concrete mixtures prepared in the K-State laboratory were mixed and cured following a procedure like ASTM C192 Standard Practice for Making and Curing Concrete Test Specimens in the Laboratory (ASTM, 2019). Coarse and fine aggregates for the concrete mixtures batched in the K-State lab were oven-dried at 110°C for 24 hours. The weight of water required for mixing was calculated to achieve the targeted water-to-cementitious material ratio (w/cm), where a moisture correction factor was incorporated to account for the water absorbed by aggregates. Admixtures were separately mixed with the mixing water before adding to the mixer. Based on the batch size, batching was done in a 2 ft^3 pan mixer or a 4 ft^3 paddle mixer. All the fresh concrete test measurements were recorded within 10 to 15 minutes of mixing, to maintain a consistent minimum waiting periods for all the mixtures. Fresh concrete tests were conducted to measure the slump and air-void properties, which was followed by collecting two samples for hardened air-void analysis. Samples for hardened air-void analysis were collected in an oyster pail take-out container (bottom dimension of 4.5 in. x 3.5 in. x 5 $in.^3$) and prepared by a procedure similar to ASTM C31/AASHTO T 23 making and curing concrete test specimens in the field (AASHTO, 2017, ASTM, 2022a). This was followed by curing the fresh concrete samples in a moist room maintained at 23° C (73° F) and 100% relative humidity environment, for 28 days.

A total dataset of 271 observations was collected for concrete mixtures tested in the K-State laboratory and on the field. A comparison between the spacing factor measured by AASHTO T 395 Sequential Pressure Method (SAM), predictive models, and ASTM C457 hardened air void analysis are presented in the following sections. This section examines the limitations associated with SAM number and spacing factor. Also, predictive models will be statistically developed to minimize this uncertainty for the recorded dataset.

3.2 Correlation Development

When developing a model using two or three variables, linear regression analysis is commonly preferred. However, as the number of variables increases, this technique has an issue with exaggerating the coefficients of input parameters, which may indicate their false significance (Brunner & Austin, 2009). Hence, when several variables are involved in model development, statistical tools such as the least absolute shrinkage and selection operator (LASSO), Binary Logistic, or Bayesian Probit regression models are used to make unbiased conclusions. This section is based on using these three regression techniques to identify significant variables and develop predictive models.

3.2.1 LASSO Regression

The LASSO regression analysis is an extension of linear regression. It encourages simple, sparse models (i.e., models with fewer parameters) and is well-suited when working with high levels of multicollinearity. Based on an optimization technique, LASSO regression minimizes the sum of the square of errors (SSE) by multiplying a LASSO penalty factor (λ) to the sum of absolute coefficient values. Thus, by minimizing LASSO regression, the coefficient of insignificant parameters i.e., parameters not contributing to the predicted/expected value 'y', is reduced to zero (Tibshirani, 1996). Mathematically, the LASSO regression is defined by Equation 3.1:

$$\text{LASSO regression} = \sum_{i=1}^{n}\left(y_j - \sum_{j=1}^{p} x_{ij}\beta_j\right)^2 + \lambda\left(\sum_{j=0}^{p}\left|\beta_j\right|\right) \qquad \textbf{Equation 3.1}$$

Where:

y = Known value of the observations

x = Known values of the predictor or variables

β = Coefficient of the predictor or variables

λ = LASSO penalty or Tuning parameter

n = Number of observations

p = Number of predictors or variables.

3.2.2 Binary Logistic Regression (BLR)

Linear regression assumes a linear relationship given by Equation 3.2:

$$\boldsymbol{y} = \mathbf{SF_i} = \mathbf{f(X_i)} + \boldsymbol{\varepsilon_i} \text{, where } \mathrm{X_i} = \text{ predictors and } \varepsilon_\mathrm{i} = \text{Error}$$ **Equation 3.2**

However, BLR applies a logit transformation to the log odds probability of y. This statistical technique is often used for classification and predict the relationship between predictors (Xi) and the predicted or dependent variable (y), where y is in a binary form (0 or 1). The binary form of models developed in this study is given by Equation 3.3:

$$\mathbf{y_i} = \begin{cases} \mathbf{1 \text{ if } SF_i \leq 0.2 \text{ mm}} \\ \mathbf{0 \text{ if } SF_i > 0.2 \text{ mm}} \end{cases}$$ **Equation 3.3**

The log odds or natural logarithm of odds refers to the probability of success to failure, which can be calculated as per Equation 3.4. And the corresponding logistic function can be calculated as per Equation 3. 5 respectively (Tranmer & Elliot, 2008, Harrell & Harrell, 2015),

$$\boldsymbol{\widehat{\pi_i}} = \mathbf{Logit(P_i)} = \frac{\mathbf{exp(P_i)}}{\mathbf{1-exp\ (P_i)}} = \frac{\mathbf{1}}{\mathbf{1-exp\ (-P_i)}}$$ **Equation 3.4**

where $\widehat{\pi_i}$ = probability of $\mathrm{y_i}$; if $\widehat{\pi_i} \geq 0.5 \Rightarrow \widehat{y_i} = 1$ or else $\widehat{y_i} = 0$

$$\mathbf{ln}\left(\frac{\mathbf{P_i}}{\mathbf{1-P_i}}\right) = \mathbf{exp}(\widehat{\boldsymbol{\beta_0}} + \widehat{\boldsymbol{\beta_1}}\mathbf{X_{i1}} + \widehat{\boldsymbol{\beta_2}}\mathbf{X_{i2}} + \cdots + \widehat{\boldsymbol{\beta_p}}\mathbf{X_{ip}})$$ **Equation 3.5**

where $\widehat{\boldsymbol{\beta_0}}$ **= coefficient of parameters** $(\mathbf{X_i})$

$\boldsymbol{\beta}_\mathbf{i}$ was estimated via maximum likelihood estimation (MLE). The best value of $\boldsymbol{\beta}_i$'s is estimated using multiple iterations to maximize the log odds and logistic regression function. The overall predictive probability of the model was obtained by summing up the conditional probabilities for each observation.

3.2.3 Bayesian Probit Regression (BPR)

BPR is a type of conditional modeling where a binary target variable (Y) is described by a linear combination of other variables (Xi). This modeling type uses the posterior probability for each of the regression coefficient(s) to predict 'Y' based on a given dataset. Commonly, a Bernoulli distribution is used to describe the relationship between Xi and Y for a normal linear model (Lamnisos et al., 2012, Chakraborty & Khare, 2017). In this model, and under a particular choice of prior probabilities for the parameters also known as the conjugate priors, the posterior distribution can be found analytically. The prior distribution can be given by Equation 3.6 as follows (Lamnisos et al., 2012, Chakraborty & Khare, 2017):

$$\mathbf{y_i \sim Bernoulli\ (p_i)\ with\ p_i = P(y_i = 1) = \Phi(x_i^T \boldsymbol{\beta})} \qquad \textbf{Equation 3.6}$$

where i = 1, . . . , n, where Φ(.)is the CDF of a standard normal distribution, $\beta = (\beta_1, . . . , \beta_p)^T$ and $x = (x_1, . . . , x_{ip})^T$. Similar to Equation 3.3, BPR models also assumes a binary 'y' as given by Equation 3.7

$$\mathbf{y_i = \begin{cases} 1 \text{ if } z_i > 0 \\ 0 \text{ if } z_i \leq 0 \end{cases}} \qquad \textbf{Equation 3.7}$$

Where $z_i = x_i^T\beta + \epsilon_i,\ \epsilon_i \sim N(0,1)$

And its likelihood can be given by Equation 3.8 as:

$$\mathbf{p(y|\boldsymbol{\beta}) = \prod_{i=1}^{n}\{\Phi(x_i^T\boldsymbol{\beta})\}^{y_i}\{1 - \Phi(x_i^T\boldsymbol{\beta})\}^{1-y_i}} \qquad \textbf{Equation 3.8}$$

We have assumed that, p(β) α 1 i.e., the posterior distribution is proportional to the likelihood. Thus, the joint posterior distribution can be expressed by Equation 3.9 as:

$$\mathbf{p(\beta, z|y) \propto p(y|z, \beta)p(\beta)p(\beta) = p(y|z)p(z|\beta)p(\beta)} \quad \textbf{Equation 3.9}$$

where $p(y|\beta) = \prod_{i=1}^{n} N(z_i|x_i^T\beta, 1)$

Thus, the given below logic can be implemented using the Gibbs sampler in 'R' to develop the predictive models and obtain the required coefficients (βi) for Xi using Equation 3.10 and 3.11.

$$\boldsymbol{\beta|z, y \sim N_d(X^TX)^{-1}X^Tz, ((X^TX)^{-1})} \quad \textbf{Equation 3.10}$$

$$\mathbf{z_i|\beta, z_{-i}, y \overset{ind}{\sim} \begin{cases} N(x_i^T\beta, 1)\mathbb{I}(z_i > 0) \text{ if } y_i = 1 \\ N(x_i^T\beta, 1)\mathbb{I}(z_i \le 0) \text{ if } y_i = 0 \end{cases}} \quad \textbf{Equation 3.11}$$

Where $X = (x_1, . . . , x_n)^T$ and $z = (z_1, . . . , z_n)^T$.

3.3 Statistically Assessing the Predictive Models

Model development is critical and involves shortlisting potential parameters vital in predicting the spacing factor. A predictive model is expected to be well correlated, i.e., it should have a higher R^2 and correlation factor. But for a potential QC/QA tool, it is more important for the model to accurately determine whether a fresh concrete mixture has a well- or coarse-entrained air-void structure. In such cases, the statistical hypothesis or confirmatory data analysis method is more important than a well-correlated model. The predictive models developed during this study were mainly evaluated on their ability to distinguish the quality of air-void distribution. Following the recommendations given by ACI 201.2R and KDOT section 403, a spacing factor of 0.2 mm (0.008 in.) was used as a threshold to assess the predictive capacity of the developed models. Statistical terms such as sensitivity, specificity, and accuracy were used to examine their predictive capability (Altman & Bland, 1994, ACI 201, 2016).

Sensitivity and specificity (as shown in Figure 3.1) refer to a model's ability to uniquely identify the true-positive and false-negative results respectively with certainty. Its accuracy measures the overall ability to correctly identify the true-positive and true-negative results (Altman

& Bland, 1994). For this study, true-positive and true-negative results refers to a model accurately recognizing a spacing factor less than 0.2 mm (0.008 in.), and greater than 0.2 mm (0.008 in.), respectively. Thus, sensitivity and specificity refers to a model accurately recognizing a spacing factor less than 0.2 mm (0.008 in.) and greater than 0.2 mm (0.008 in.), respectively, when compared to the spacing factor measured in hardened concrete by the ASTM C457 method. For this study, the model's accuracy has been determined based on its ability to precisely separate data points with a spacing factor less than 0.2 mm (0.008 in.) and greater than 0.2 mm (0.008 in.).

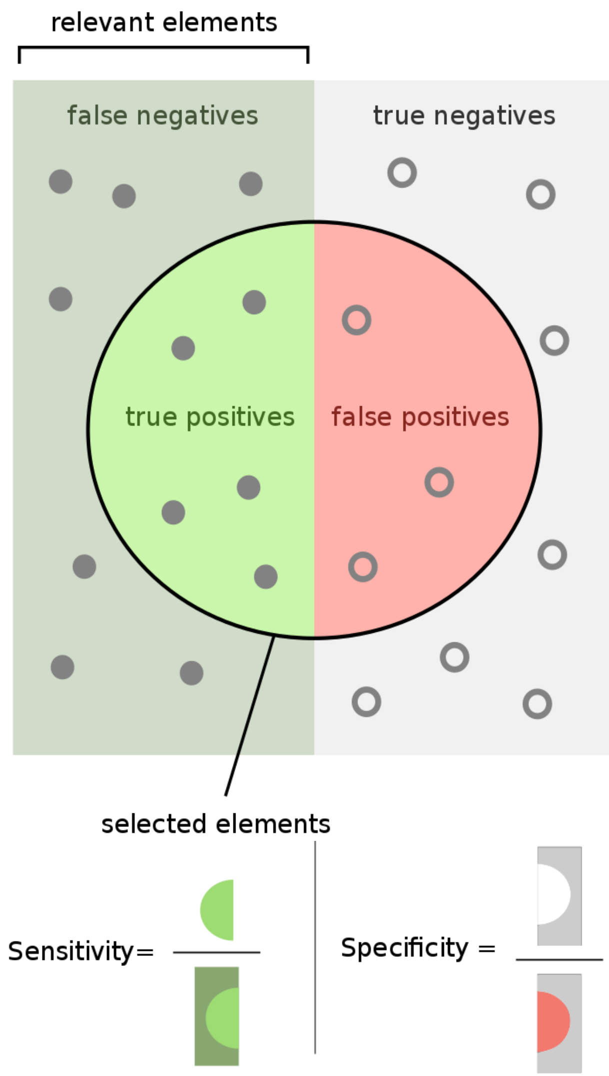

Figure 3.1: Representation of Sensitivity and Specificity (Walber, 2022).

3.4 Parameter Selection Models to Predict Spacing Factor in Fresh Concrete

Low-slump concrete mixtures are preferred for on-grade paving, but their high stiffness and low workability presents problems when testing with SAM. As a result, causing specific challenges related to the accuracy and repeatability of test, for use on the field. This study intends to improve the current recommendations for assessing the quality of air-void distribution with a focus on spacing factor, in fresh concrete on the field. Statistical methods were used to assess the uncertainty of current methods for the dataset collected during this study. The main objective of these predictive models was to reduce the error associated with current test methods.

A test matrix of various mix design and fresh test measurement parameters was established to predict an array of commonly evaluated air-void parameters. Both fresh & hardened properties were evaluated for each concrete mixture. The measured results were then statistically analyzed during model development to predict spacing factor in fresh concrete, as the output 'Y'. The set of input variables (Xi, shown in Table 3.1) was shortlisted based on their importance stated in literature, ease of measurement, and variation recorded in the dataset. The process of variable selection and elimination was automated by using LASSO, BLR, and BPR models. The models were formulated using a combination of the shortlisted individual parameters and their cross-products terms (to accommodate multicollinearity between parameters).

Table 3.1: Fresh concrete and mixture design parameters considered for model development.

Variable	Explanation based on the Introduction section
Shortlisted variables	
Total air content (Fresh concrete property)	Defines the total air content and influences air-void distribution. Assumed relation (Moradllo et al., 2020): ↑Air content = ↓ Spacing factor
SAM number (Fresh concrete property)	An empirical quantity correlated to the spacing factor measured by the ASTM C457 method (Ley & Tabb, 2013, 2014, Riding & Albahttiti, 2016, Tanesi et al., 2016, Ley et al., 2017, Moradllo et al., 2020, Becker et al., 2021). • ↑ SAM number = ↑ Spacing factor • SAM number of 0.2 is known to correlate to a spacing factor of 0.2 mm (0.008 in.)
Slump (Fresh concrete property)	Controls the flowability of concrete mixtures, and thus its compaction/consolidation, along with the pressure change detected by an air meter. Assumed relation (Powers, 1969, Du & Folliard, 2005, Dodson, 2013): • Slump: 75 – 150 mm (2.95 – 5.9 in.) ↑ Slump = ↑ Air content • Slump above 150 mm (5.9 in.) ↑ Slump = ↓ Air content (associated with reduced stability of air bubbles).
Paste percentage (Mixture design parameter)	The air bubbles are distributed through the cementitious paste. Additionally, as seen in Equations 2.5 – 2.6, the spacing factor in hardened concrete is dependent on the paste-to-air ratio and specific surface area. ↑ Spacing factor = ↑ Air content and ↓ Specific surface area.

Excluded variables	
Mixture design parameters: • **Ratio of water to cementitious material** • **Fly ash content** • **Ratio of fine to coarse aggregates** • **Dosage of admixtures** • **Type of admixture / admixture interaction**	These parameters may be significant, but due to relatively small or no variations recorded in their variable range during this study, these parameters were excluded.

Following model development, the ASTM C457 spacing factor and predicted spacing factor (PSF) were compared using the statistical parameters given in Section 3.3, $R^{2,}$ and correlation factor. Sophisticated statistical regression techniques given in Section 3.2 were used to form an unbiased conclusion of the input parameters and predictive models. The process of developing the predictive models itself will broaden our understanding regarding the influence of these parameters on the spatial distribution of air voids in fresh concrete.

3.5 Fresh Air-Void Distribution Parameters

A SAM number was targeted between 0 to 0.80, and the measured values ranged between 0.02 to 0.80. The range and division of total number of observations for fresh concrete properties measured for all the concrete mixtures and mixture design properties are given in Table 3.2.

Table 3.2: Distribution of dataset for mixture design and fresh concrete properties.

Mixture design variables			
Cementitious Paste Targeted range: 20 – 30%	**# Observations**	**Water to cementitious material ratio**	**# Observations**
20 - 25%	208 (76.75%)	not recorded	122 (45.02%)
25 - 30%	56 (20.66%)	< 0.40	6 (2.21%)
30 - 35%	5 (1.84%)	0.40 – 0.45	137 (50.55%)
35 - 55%	2 (0.74%)	> 0.45	6 (2.21%)
Fresh concrete properties			
Total Air Content Targeted range: 4 – 6%	**# Observations**	**Slump Targeted range: 0 – 63.5 mm (0 – 2.5 in.)**	**# Observations**
< 4%	7 (2.58%)	not recorded	114 (42.07%)
4 - 6%	95 (35.06%)	0 mm or in.	8 (2.95%)
6 - 8%	92 (33.95%)	0 – 63.5 mm (0 – 2.5")	70 (25.83%)
> 8%	77 (28.41%)	63.5 – 127 mm (2.5 – 5")	71 (26.20%)
		> 127 mm or 5"	8 (2.95%)

A comparison between fresh properties i.e., total air content and SAM number measured by AASHTO T 395, and hardened air-void distribution parameters assessed by the RapidAir system (based on the ASTM C457), is given in this section. The study focuses on assessing the air-void distribution in on-grade concrete pavement mixes. Additionally, as explained in section

2.3.7, the energy required to consolidate a low-slump concrete mixtures can influence the variability measured for distribution parameters in fresh concrete. This hypothesis will be further examined in this section for the recorded set of low-slump (slump ≤ 2.5 in.) mixtures. Observations for the same mixture tested multiple times using the same/different SAM device(s), by the same/different operator, in the laboratory, and on the field, have been summarized in Table 3.3 and Figure 3.2. The associated relative uncertainty of total air content and SAM number for low-slump concrete mixtures is calculated as per Equation 3.12 (Menin, 2018):

$$\textbf{Relative Uncertainity} = \frac{\textbf{Absolute Uncertainity}}{\textbf{Measured result or pressure difference}} \qquad \textbf{Equation 3.12}$$

Table 3.3: Repeatability of total air content and SAM number, when the same mixture is tested multiple times by the same/different meter and operators in the field or the lab.

		Total air content			SAM number		
		Coefficient of variation	**Variance**	**Relative uncertainty**	**Coefficient of variation**	**Variance**	**Relative uncertainty**
Field test: Different meters and operators	Range	1.1 – 4.9%	0.01 – 0.13	1.0 – 1.4%	0 – 78.9%	0 – 0.06	17.7 – 176.8%
	Average	3.2%	0.08	1.2%	20.3%	0.01	70.3%
Field test: Same meter and same/different operators	Range	0 – 4.5%	0 – 0.04	1.0 –1.5%	0 – 8%	~0	27.7 – 141.4%
	Average	0.1%	0.001	1.1%	0.2%	~0	64.7%
Laboratory test: Same meter and operator	Range	0 – 3.3%	0 – 0.12	1.0 – 1.6%	17 – 93.0%	0 – 0.12	22.4 – 157.1%
	Average	2.2%	0.03	1.4%	46.2%	0.03	82.8%

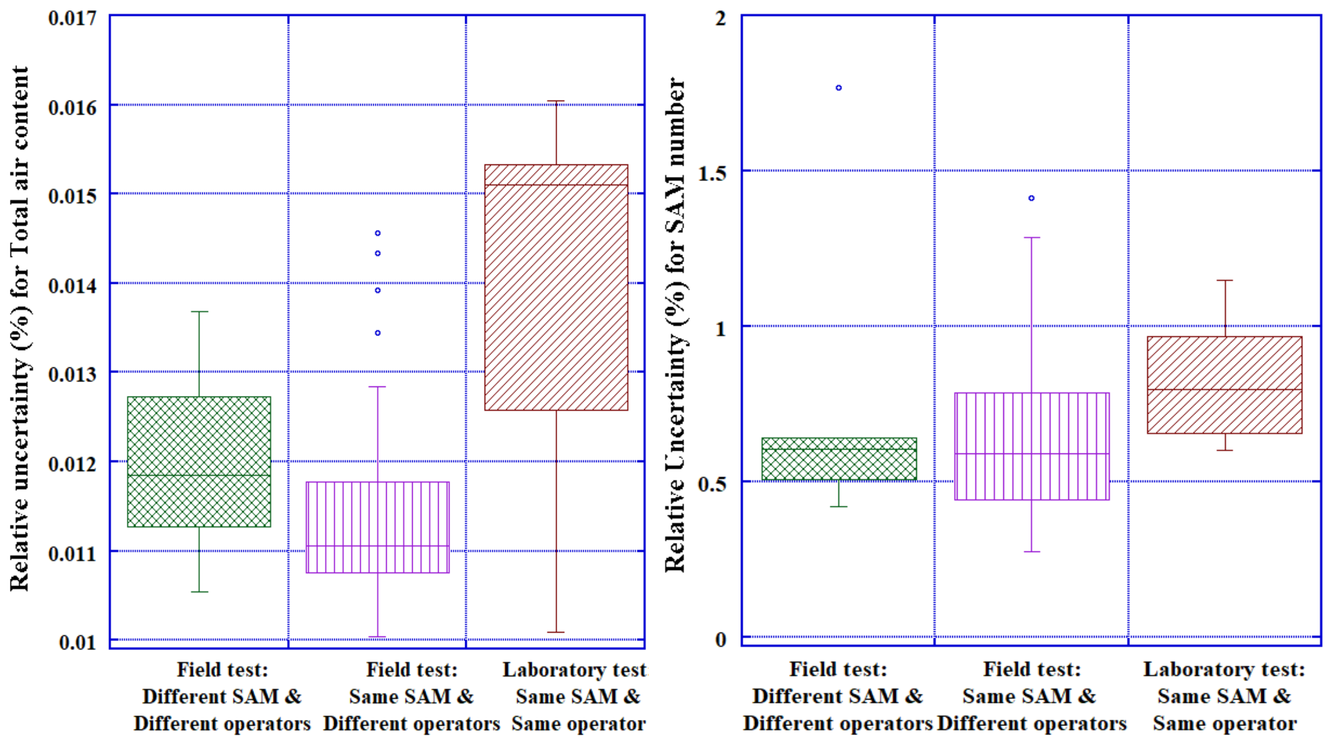

Figure 3.2: Box and whisker plot representing the average relative uncertainty measured between results recorded for the same mixture in the laboratory and field, using the same/different meter and operator.

As seen in Figure 3.2 and Table 3.3, the measured relative uncertainty for SAM number is about 59 times higher than that for total air content. The magnitude and spread of interquartile ranges (box lengths) for SAM number appear to be much larger than that for total air content. The contrast in estimated relative uncertainty is a result of the contrasting magnitude of pressure difference associated with these parameters. For example, a total air content of 5% has an equilibrium pressure of 7.50 psi when a 14.5 psi pressure is applied, so the corresponding pressure difference is 7 psi. Likewise, for a SAM number of 0.2, the pressure difference between Pc2 and Pc1 is approximately equal to 0.2 psi. Since the accuracy of the digital gauge over its complete range is 0.1 psi, it has a better probability of accurately measuring the total air content than the SAM number. Similar results were reported by a study, where the SAM number had a 154% higher coefficient of variation per site than the total air content (Riding & Albahttiti, 2016). To minimize the relative uncertainty and probability of getting erroneous results for the SAM number, a digital gauge with higher accuracy (such as 0.01 psi) is recommended.

The strength of a good QC/QA tool lies in its ability to present unbiased results with consistent repeatability. In addition to higher absolute uncertainty, the low repeatability (Figure 3.2 and Table 3.3) of these results indicates their dependence on equipment and operator. A SAM number of 0.2, correlates with a spacing factor of 0.2 mm or 0.008 in. (Ley & Tabb, 2014), and a total volumetric air content between 4 – 6% is recommended by ACI 201.2R and various transportation agencies across the United States. Thereby signifying a problem with solely using the SAM number and, to a lesser extent, total air content as a reliable QC/QA tool, for testing low-slump on-grade concrete mixtures. Minimizing these shortcomings using the statistical models proposed later in this study, could improve the current recommendations for assessing air-void distribution in fresh concrete.

3.6 Hardened Air-Void Parameters

Along with assessing the air-void distribution in fresh concrete, hardened air-void analysis was conducted as per the ASTM C457 method. For the 271 observations used in this study, the total air content, specific surface area, and spacing factor were observed between 2.25 – 13.8%, 7.74 – 940.3 mm^{-1} (0.305 – 37.02 in^{-1}), and 0.06 – 0.69 mm (0.002 – 0.027 in.), respectively. Based on the box and whisker plot shown in Figure 3.3, the probability of getting a higher spacing factor increases with a decrease in the air content and vice-versa.

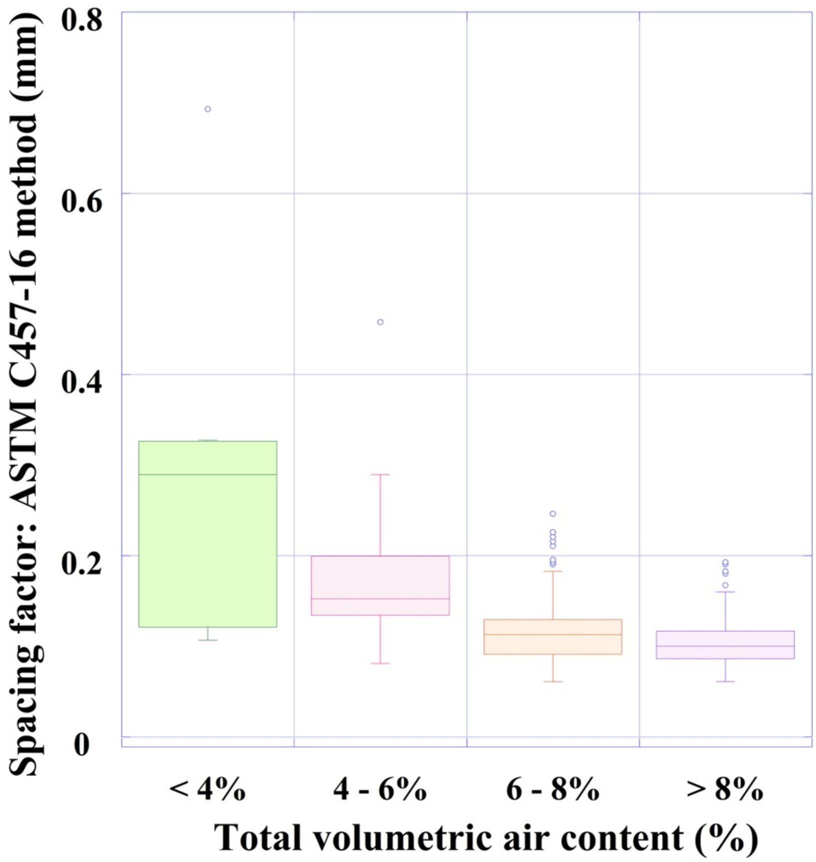

Figure 3.3: Box and whisker plot between the spacing factor (mm) measured by the ASTM C457 method and total air content measured in fresh concrete.

Additionally, a large distribution of spacing factor (0.107 – 0.693 mm) is seen for air content less than 4%, but this might be due to the limited number of observations (i.e., 7 observations) recorded in this range. The former conclusion is supported by the succeeding ranges of air content, where 95 observations have 4 – 6% air content, 92 observations for 6 – 8% air content, and 77 observations for an air content greater than 8%. Since entrained concrete mixtures with an air content ≤ 4% would be rejected in the field, those above 6% have a better probability of obtaining the required spacing factor (less than 0.2 mm or 0.008 in.). The higher variation recorded in spacing factor for a range of 4 - 6% (by volume) air content, advocates the need to build a convenient and precise QC/QA tool to detect quality of distribution in this critical range.

3.7 Predictive Model Development

A strong QC/QA tool is identified by its ability to accurately detect a truly deficient sample from a given set of samples. The statistical parameters discussed in sections 3.2 and 3.5. indicates that the total air content and SAM number in fresh concrete are weak indicators of the observed spacing factor in hardened concrete. These shortcomings could result in the rejection of a desirable concrete mixture (distribution parameters within permissible limits), or acceptance of an impermissible mixture. This can be a concern, especially for borderline cases where the SAM number is slightly greater or less than 0.2, and the observed total air content is between 4 and 6%. The AASHTO T 395 Sequential Pressure Method and SAM, are based on crushing the larger entrapped air voids by sequential pressurization, to only measure the entrained air voids. Thus, the correlation of SAM number to spacing factor helps assess a phenomenologically different aspect of measurement in fresh concrete, i.e., the entrained air voids contributing towards freeze-thaw durability, which sustains and can be observed in the hardened air-void analysis. Thus, despite its poor relative uncertainty, this method could still be useful for QC/QA in concert with other lower uncertainty predictors. Thus, an emphasis has been placed in this study to optimize its accuracy and repeatability, by developing predictive models using statistical tools.

3.7.1 Model Optimization: LASSO Regression

In this section, LASSO regression is used to develop models for predicting spacing factor using variables identified in Table 3.1. For a few observations in the complete dataset, some values such as slump and mixture design parameters. The observations with missing values were eliminated from the complete database (271 observations) to form the reduced dataset (157 observations). The reduced dataset was used to design an unbiased base model by randomly splitting it in a 60:40 fashion for calibration and validation i.e., 60% or 94 data points were used for calibrating the model, and 40% or 63 data points were used to validate the calibrated model.

Initially, a base model was formulated using the reduced dataset as per Equation 3.13. For the base model, individual parameters and their cross-terms were based on contributors such as the total air content (%), SAM number, paste content (%), and slump (in.).

$$\textbf{Base Model: } \mathbf{PSF = -0.23\ SAM\ no. + 0.24\ Paste + 0.46\frac{1}{Air\ content} - 0.21\frac{1}{Slump} + 0.87\frac{Paste}{Air\ content} + 0.70\ SAM\ no. \times Paste + 0.36\frac{SAM\ no.}{Slump} - 0.22\frac{Paste}{Slump} + 0.86\frac{1}{Air\ content \times Slump} + 0.95\frac{SAM\ no. \times Paste}{Air\ content}} \quad \textbf{Equation 3.13}$$

The predicted spacing factor (PSF) computed using the base model is compared to the spacing factor measured by the RapidAir in Figure 3.4 (a). The identity line shown in Figure 3.4 indicates a direct relationship between PSF and the measured spacing factor. For the validation dataset, PSF from the base model had an R^2 and correlation factor of 0.36 and 0.60, respectively, with a sensitivity, specificity, and accuracy of 94%, 67%, and 90.5%, respectively. Additionally, statistical parameters were calculated for the combined calibration and validation dataset, which had a sensitivity, specificity, and accuracy of 93%, 56%, and 88.5%, respectively. Similarity between the statistical parameters for both datasets, emphasizes the model's strong sensitivity and poor specificity. The presence of outliers in Figure 4.3(a) about the identity line, with its reduced specificity and R^2, reflects the model's shortcoming caused by over-fitting to a dataset dominated by a spacing factor less than 0.2 mm (0.008 in.).

Some of the other shortcomings associated with the base model included a narrow range of paste percentages, inclusion of insignificant parameters or cross-terms (between parameters), and so on. Thereafter, rigorous testing was done using LASSO to include or exclude a set of variables from the base model. For example, as seen in Equations 2.5 and 2.6, the spacing factor in hardened concrete is based on specific surface area and paste-to-air ratio (p/A). By analogy with the ASTM C457 paste-to-air ratio (p/A), the paste percentage and total air content were combined to form a term called the 'volumetric paste to volumetric air ratio (V_P/V_A)'. V_P/V_A was calculated as the ratio of volumetric paste (V_P) i.e., the paste percentage calculated from the mixture design to the volume of air (V_A) or total air content measured in fresh concrete. V_P/V_A attempts to measure the air-void distribution in cementitious paste in fresh concrete, like that measured by the Philleo factor (S).

Subsequently, SAM number and V_P/V_A were individually evaluated (Table 3.4 and Figure 3.4(b)). Similar to the base model, it exhibited a strong specificity (0.88 and 0.81, respectively), along with a weak sensitivity (0.43 and 0.67, respectively) and accuracy (48.4% and 68.5% respectively). Given the significance of the sequential pressure method (SAM)'s broad application on the field and its known correlation to the spacing factor in hardened concrete, it is vital to improve its limitation associated with poor sensitivity and accuracy for use as a potential QC/QA tool (Table 3.4).

A predictive model is expected to be well correlated, i.e., it should have a high R^2 and correlation factor. But it is more important for the model to accurately differentiates between true positive and negative results i.e., between a spacing factor less and more than 0.2 mm (0.008 in.), in real-time. Thus, the non-linear form of parameters was evaluated along with its linear form. Ultimately, the final model was developed as per Equation 3.14, to balance the strengths and weaknesses of its constituting variables (SAM number and V_P/V_A) and yield maximum accuracy.

$$\textbf{Final model: } \mathbf{PSF = 0.026\,\frac{V_P}{V_A}^{1.5} \times SAM\ no^{0.2}} \qquad \textbf{Equation 3.14}$$

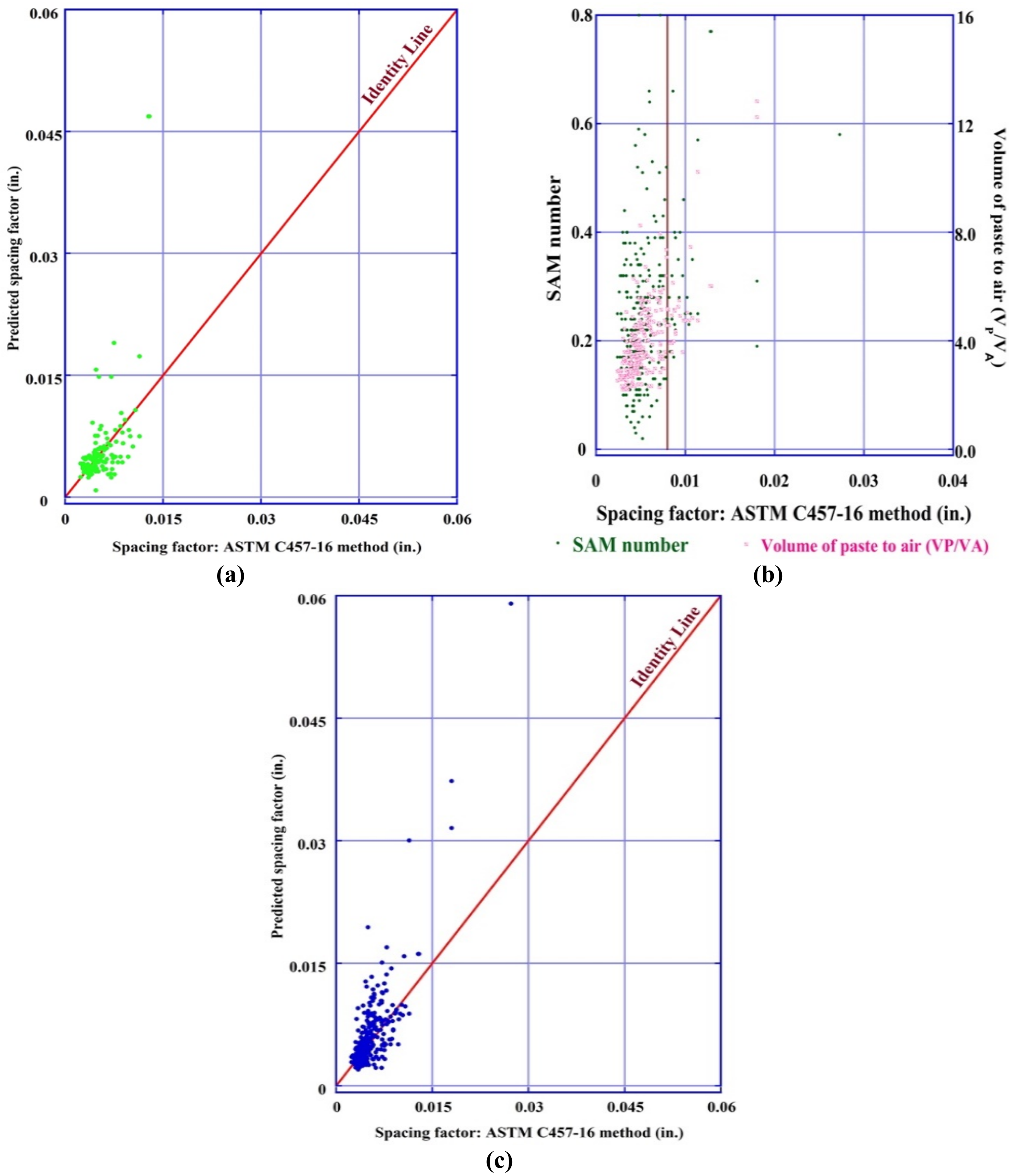

Figure 3.4: (a) PSF by the base model using reduced dataset; (b) SAM number and V_P/V_A, and (c) PSF by final model, for the complete dataset, vs ASTM C457 spacing factor.

All data points for variables used in final model was available for the complete dataset (271 observations). Thus, the robustness of final model was evaluated using the complete dataset. Similar to the reduced dataset used by base model, the complete dataset was split in a 60:40 fashion, where 162 observations were used for calibration, and the rest (135 observations) were used for validation. The validation dataset displayed a sensitivity, specificity, and accuracy of 91%, 93%, and 91.7% respectively. Even for the entire dataset, as seen in Figure 3.4 (c) and the PSF using the final model showed high accuracy (81.1%). Due to simple parameters and good statistical indicators (R^2 = 0.63 and correlation factor = 0.79), the final model shows promise for use as a strong QC/QA tool.

Table 3.4: Summary of statistical analysis with the complete dataset for SAM number, V_P/V_A, and PSF from the final model.

Threshold	**SAM number = 0.2**	**V_P/V_A = 4**	**Final model: PSF = 0.2 mm (0.008 in.)**
Sensitivity (%)	43	67	82
Specificity (%)	88	81	72
Accuracy (%)	48.4	68.5	81.1

The air-void distribution measured by SAM number and that by the PSF (final model) is compared to the spacing factor measured by ASTM C457 method. The corresponding upper and lower limit for the 95% confidence interval is shown in Figure 3.5. Based on this, an interpretation can be made that the PSF by final model measures spacing factor 90.41% (245 out of 271 observations) accurately within the boundaries of confidence interval, while 66.42% (180 out of 271 observations) of the measured SAM number lies within the boundary of 95% confidence interval. Using V_P/V_A to develop the PSF (final model) resulted in a more robust model with potential for use in QC/QA.

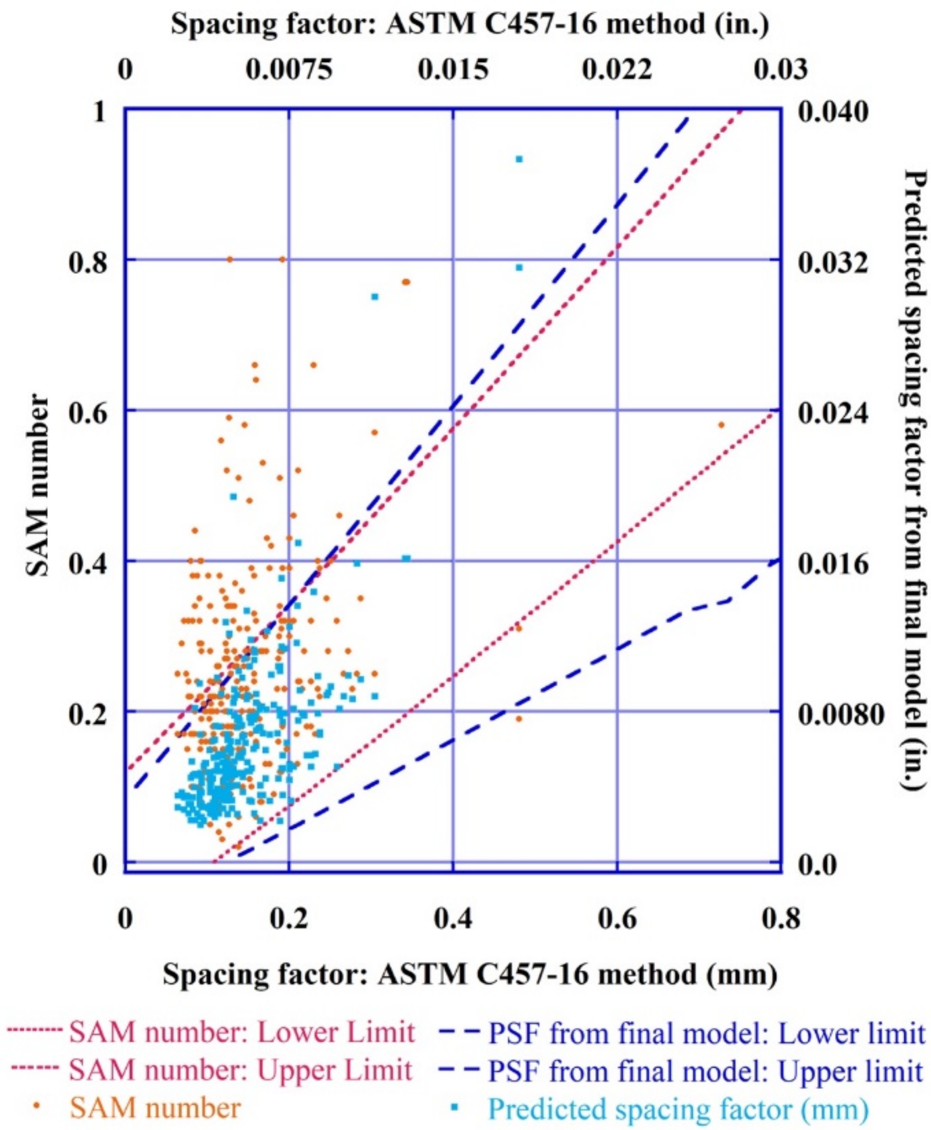

Figure 3.5: SAM number and PSF by final model versus the spacing factor measured by ASTM C457method, bound by the lower and upper limits of 95% confidence level.

In addition to the thresholds specified in Table 3.4, alternate thresholds were examined to identify the presence of an alternate optimum threshold for the SAM number, V_P/V_A, and PSF calculated by both the base and final model. The alternate thresholds were compared to a spacing factor of 0.2 mm (0.008 in.) measured by the ASTM C457 method, as shown in Figure 3.6. Increasing the threshold value for spacing factor resulted in higher accuracy and sensitivity but poor specificity.

Since a balanced model must accurately identify both positive and negative results, the sensitivity and specificity must be optimized simultaneously. Comparing the statistical parameters in Figure 3.6, the optimization points for combined sensitivity and specificity (highlighted by red circles) for V_P/V_A and PSF computed by the base and final models remain consistently high between (78% & 75%, 83% & 78%, and 82% % 72% respectively), while that for the SAM number is lower at 60% & 62%. For the given dataset, these parameters optimize at an alternate threshold for SAM number of 0.3, V_P/V_A of 4.7, and PSF of 0.2 mm (0.008 in.). The continuously rising trend of accuracy and sensitivity might be associated with the limitations of the given dataset. These thresholds might be better suited for the dataset used in this study, but an adjustment may be needed to suit different data or region-specific results. Thus, for use as a robust on-site QC/QA tool, it may be beneficial to specify a range of allowable values for the fresh concrete properties, rather than stating a single minimum or maximum limiting threshold value for the measured fresh concrete properties.

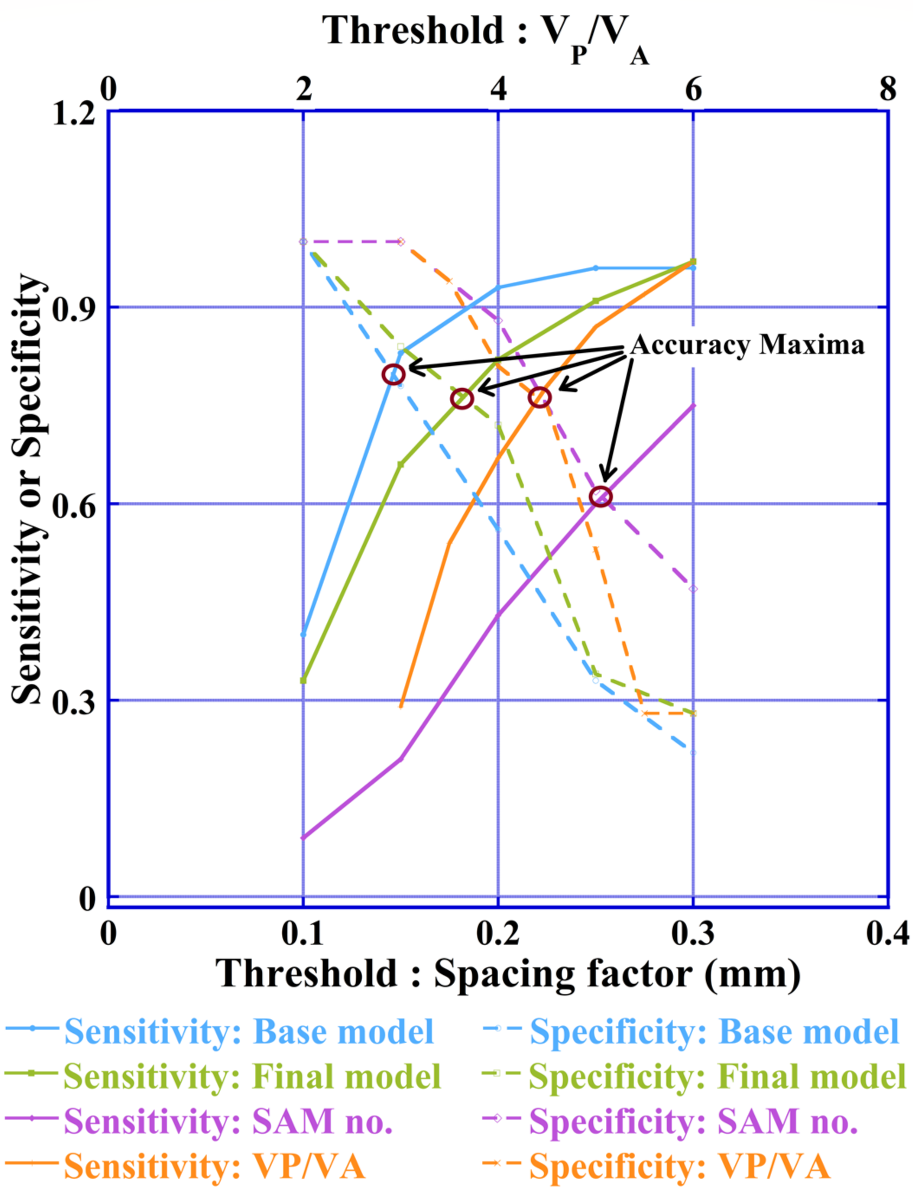

Figure 3.6: Sensitivity and Specificity, measured for the PSF by the base and final model, SAM number, and V_P/V_A at different thresholds.

3.7.2 Model Optimization: Binary Logistic Regression (BLR)

The accuracy of predictive models and significance of variables established by the LASSO regression, was further verified using the BLR and BPR models. The supplementary regression models were selected to verify the developed models were unaffected by the influence of chosen statistical technique and yielded true accuracy of models.

The significance of individual and cross-term variables (given in Table 3.1) to predict 'y' by BLR model, was measured using their p-value. Variables with a p-value ≤ 0.05 were qualified as significant and those with a p-value > 0.05 as insignificant. The predictive models formed using the significant variables, were then statistically analyzed using the measured sensitivity, specificity, and accuracy for the given dataset. The logic given by Equation 3.4 and 3.5 can be further simplified (as given by Equation 3.15) for using the predictive models recommended by BLR on the field:

$$\mathbf{ln\left(\frac{P_i}{1-P_i}\right) = exp(\widehat{\beta_0} + \widehat{\beta_1}X_{i1} + \widehat{\beta_2}X_{i2} + \cdots + \widehat{\beta_p}X_{ip})} \qquad \textbf{Equation 3.15}$$

where $\widehat{y_i} = 1$ is assigned when $\ln\left(\frac{P_i}{1-P_i}\right) \geq 0$ or else $\widehat{y_i} = 0$.

Like LASSO regression, the reduced dataset was randomly (shuffled) and split 60:40 for calibration: validation. Accordingly, the best fit model was obtained as per Equation 3.16.

$$\mathbf{ln\left(\frac{P_i}{1-P_i}\right) = 1.8\ SAM\ number + 2.8\ Paste - 1.2\frac{V_P}{V_A} - 64} \qquad \textbf{Equation 3.16}$$

The recommended model exhibited a sensitivity, specificity, and accuracy of 92.8%, 71.4% and 89.8% respectively, for the calibration dataset. Similarly, the model had an overall sensitivity, specificity, and accuracy of 93.8%, 57.9% and 85.5% respectively. Each of these variables in the best fit model (Equation 3.16) and their terms in the models will be observed in the range given below:

- SAM number: 0.02 to 0.80 ⇒ 1.8 SAM number: 0.036 to 1.44
- Paste (%): 10 to 50, commonly varying between 20 to 30% ⇒ 2.8 Paste: 56 to 84
- $\frac{V_P}{V_A}$ commonly varies between 0 to 20 ⇒ $1.2\frac{V_P}{V_A}$: 0 to 24

Although the intercept for best fit model (given by Equation 3.16) seems to be large, it should be noted that similar to LASSO regression, the predicted variable or output from BLR model (Equation 3.16) will also be controlled by the paste (%) and V_P/V_A terms.

3.7.3 Model Optimization: Bayesian Probit Regression (BPR)

The predictive models formulated using BPR, used a logic similar to that used by BLR & LASSO. A sample set with 10,000 repetitions was used for posterior distribution, out of which the first 2000 samples were eliminated. Finally, the best fit model by BLR is given by Equation 3.17, following the procedure outlined in Section 3.2.3.

$$\ln\left(\frac{P_i}{1-P_i}\right) = -16.8\ \text{Air content} - 3.5\ \text{Paste} + 0.7\text{Air content} \times \text{Paste} + 83 \qquad \textbf{Equation 3.17}$$

The best fit model formulated by BPR had a sensitivity, specificity, and accuracy of 86.7%, 62.5% and 84.3%, respectively. Additionally, the V_P/V_A and SAM number parameters were evaluated by the BPR model, and its statistical significance is given in Table 3.5. Although the model formulated by Equation 3.18 had the highest specificity and accuracy, the model formed by Equation 3.19 was simple in formation and allowed effortless application on the field.

Table 3.5: Models formulated with SAM number and V_P/V_A, using BPR.

$\ln\left(\frac{P_i}{1-P_i}\right) =$	**– 6. 2 SAM number + 2.9 (Equation 3.18)**	**– 0.6 V_P/V_A + 3.3 (Equation 3.19)**
Sensitivity	85.3%	85.5%
Specificity	50.0%	57.14%
Accuracy	81.9%	83.1%

3.8 Model Limitations

A common conclusion can be drawn from the best fit models developed using three regression modelling techniques in this study, which highlights the significance of V_P/V_A in identifying the quality of an air-void structure or distribution. However, these predictive models were developed using a finite set of pavement concrete mixtures containing raw materials (such as coarse and fine aggregates) sourced from Kansas. It is recommended that these models be calibrated for locally available materials. Therefore, caution is warranted when applying the models described herein for concrete mixtures far outside the following parameter ranges:

- Fresh air content: 1.8 – 11.6 %
- Hardened air content: 3.98 – 12.76 %
- SAM number: 0.07 – 0.77
- Slump: 0 – 5 in.
- Spacing factor: 0.081 – 0.69 mm
- w/cm: 0.40 – 0.47
- Cementitious paste: 21.12 – 28.82 %
- Volumetric paste to air ratio (VP/VA): 2.2 – 16.

The models would need to be further calibrated for applications outside the specified range. Additionally, the models are biased towards a spacing factor less than 0.2 mm (0.008 in.) due to insufficient data points with a spacing factor greater than 0.2 mm (0.008 in.). This limitation can be minimized by calibrating the models over a larger data set with almost equal or evenly distributed data points (i.e., same number of mixtures have a spacing factor greater than 0.2 mm or 0.008 in., as those that have a spacing factor less than 0.2 mm or 0.008 in.).

3.9 Recommendations

Ensuring durability of concrete pavements is of the highest priority, so recommendations are provided below to account for potential changes to the specifications for quantifying air voids in fresh concrete, in the field.

- Include V_P/V_A as one of the specifications in Section 403 for on-grade concrete to improve QC/QA tools.
- V_P/V_A can be included with an example of the recommendations given below:
  - Reject concrete if air content ≤ 4%
  - For air content: 4 – 6%:
    - Calculate V_P/V_A:
    - If $V_P/V_A \leq 3.85$: place concrete
    - If $V_P/V_A > 3.85$: remix to increase air content and lower V_P/V_A before placing concrete, re-test.
  - For air content: 6 – 8%
    - Place concrete
    - No need to calculate V_P/V_A
  - For air content: 8 – 10%:
    - Remix concrete to lower air content, and re-test.
  - For air content ≥ 10%
    - Reject concrete.

Chapter 4 - Quantifying Uncertainty/Error Associated with an Automated Air-Void Scanning (RapidAir) System

ASTM C457 method is commonly used to perform hardened air-void analysis on a 2D concrete surface, which is assumed to represent the air-void structure in 3D. The distribution parameters measured by this method are defined to evaluate different aspects of the air-void structure. The distribution parameters as defined by ASTM C457, can be interpreted as follows:

- Spacing factor (L) → Dispersion of air-voids through a given area i.e., the average distance from one air-void to its nearest one.
- Specific surface area (α) → Average of the surface area or size of air void.
- Paste-to-air ratio (p/A) → Proportion of entrained air-voids with respect to cementitious paste.
- Total air content (A) → Proportion of the combined area of all the air voids in comparison to the sample area being evaluated.

As per the hydrostatic pressure theory proposed by Powers, total air content is insufficient to predict the freeze-thaw resistance of PCCP. Whereas spacing between the entrained air voids (i.e., spacing factor) ensures the required durability (Powers & Willis, 1950; Mielenz et al., 1958; Hong-fa & Jia-Chun, 2010, Wu et al., 2020). In other words, ensuring a uniform distribution of numerous tiny air bubbles entrained throughout the cementitious paste is essential. Numerous research studies have been focused on understanding the significance of a critical spacing factor on the freeze-thaw durability of PCCP (Powers, 1954, Mielenz et al., 1958, Pleau & Pigeon, 1996, Snyder, 1998, Hong-fa & Jia-Chun, 2010, Radlinski et al., 2010, Shon et al., 2018, Igarashi et al., 2021). Although there has been a tentative conclusion over the required spacing factor value, they made a common conclusion on the importance of a spacing factor. Since the spacing factor suggested by Powers acts as a characteristic distance parameter, it has been included in the specifications/design codes by most departments of transportation or transportation agencies.

The original hardened air-void analysis process was tedious, as it involved manually counting air voids through a microscope. With the advancement of technology, this process has been optimized by using a high-resolution camera to capture numerous greyscale images of a sample, i.e., air-void structure. These images are then analyzed by software, which can distinguish between the air & non-air fraction and estimate their distribution parameters. This automated process has been commercialized in systems such as RapidAir. However, more specifications should be given to ensure the proper applicability of this methodology or the associated accuracy for the commercialized systems. Based on the estimated precision statement given by the ASTM C457, the spacing factor and air content for samples prepared and tested in the same laboratory varied by 22.6% & 1.61%, respectively, and those prepared in one laboratory and tested in other laboratories varied by 2.01 - 2.07% and 17.5 - 20.1% respectively (ASTM, 2016b).

Additionally, the round-robin studies discussed in Section 2.4.2, showed a higher variation in the measured distribution parameters. It further pointed out the problem associated with the poor reproducibility and repeatability of results measured by different RapidAir systems. The operator reached a common conclusion regarding the dependence of measured distribution parameters on the selected system and settings (threshold, gain, pitch, and total traverse length). The influence of these parameters can be explained as follows:

- Threshold – Influences the greyscale pixel values in being identified as air voids. This affects the number and size of air voids classified as air voids.
- Gain – Impacts the apparent brightness of pixels in the greyscale image.
- Pitch – Influences the total traverse length.

Since most laboratories can choose their preferred system setting during hardened air-void analysis, all the specimens may be evaluated in different settings. Hence, it is essential to quantify the degree of uncertainty or error associated with different system settings. In the long run, this will help ensure that the measured distribution parameters are unbiased (i.e., free from the influence of system settings). Thereby demonstrating how easily the evaluated parameters can be manipulated to achieve a set of target values and further signifying the need to regulate the system settings.

4.1 Preliminary Analysis

An attempt is made in this chapter to quantify the associated uncertainties or variations introduced by different system settings of RapidAir. A preliminary analysis was conducted using two sets of 21 hardened concrete samples. Suppose the measured (fresh and hardened concrete) air-void distribution parameters have a negligible influence on system settings. In that case, the average value of observations for all samples at a given setting should remain constant. This average value has been used to understand the variance associated with the distribution parameters in three commonly used system settings. The observed results have been summarized in Table 4.1.

Table 4.1: Average distribution parameters i.e., Air content (%), Spacing factor (mm), and Specific surface area (mm^{-1}) measured at different threshold and gain settings.

Threshold / Gain	Average air content (%)	Average spacing factor (mm)	Average spacing factor (mm^{-1})
165 / 63	5.93	0.31	15.61
165 / 31	5.26	0.38	14.21
185 / 31	5.10	0.38	13.99
Standard Deviation	0.44	0.04	0.88
Coefficient of Variation	0.08	0.11	0.06

As seen in Table 4.1, at the same threshold (165) but different gain settings (31 and 63), a difference of 0.67% was observed in the measured air content, 0.07 mm for the spacing factor, and 1.4 mm-1 for the specific surface area. For this set of samples, the average air content of 5.31% was measured in fresh concrete. The air content measured at 165 threshold / 63-gain setting was the closest to that measured in fresh concrete. Since the actual 'true measurements' for distribution parameters of the evaluated specimens were unavailable, it is difficult to ascertain which settings gave accurate results. Thus, another set of 21 samples was selected and analyzed using the same RapidAir system and scanned over a broader range of threshold/gain settings. Since the pixel value associated with air voids lies within 100 - 255 on the grayscale, the samples were evaluated at 63 gain and a threshold of 125, 165, 185, 200, & 250, along with 31 gain and a threshold of 165 & 185. The corresponding results are shown in Figure 4.1.

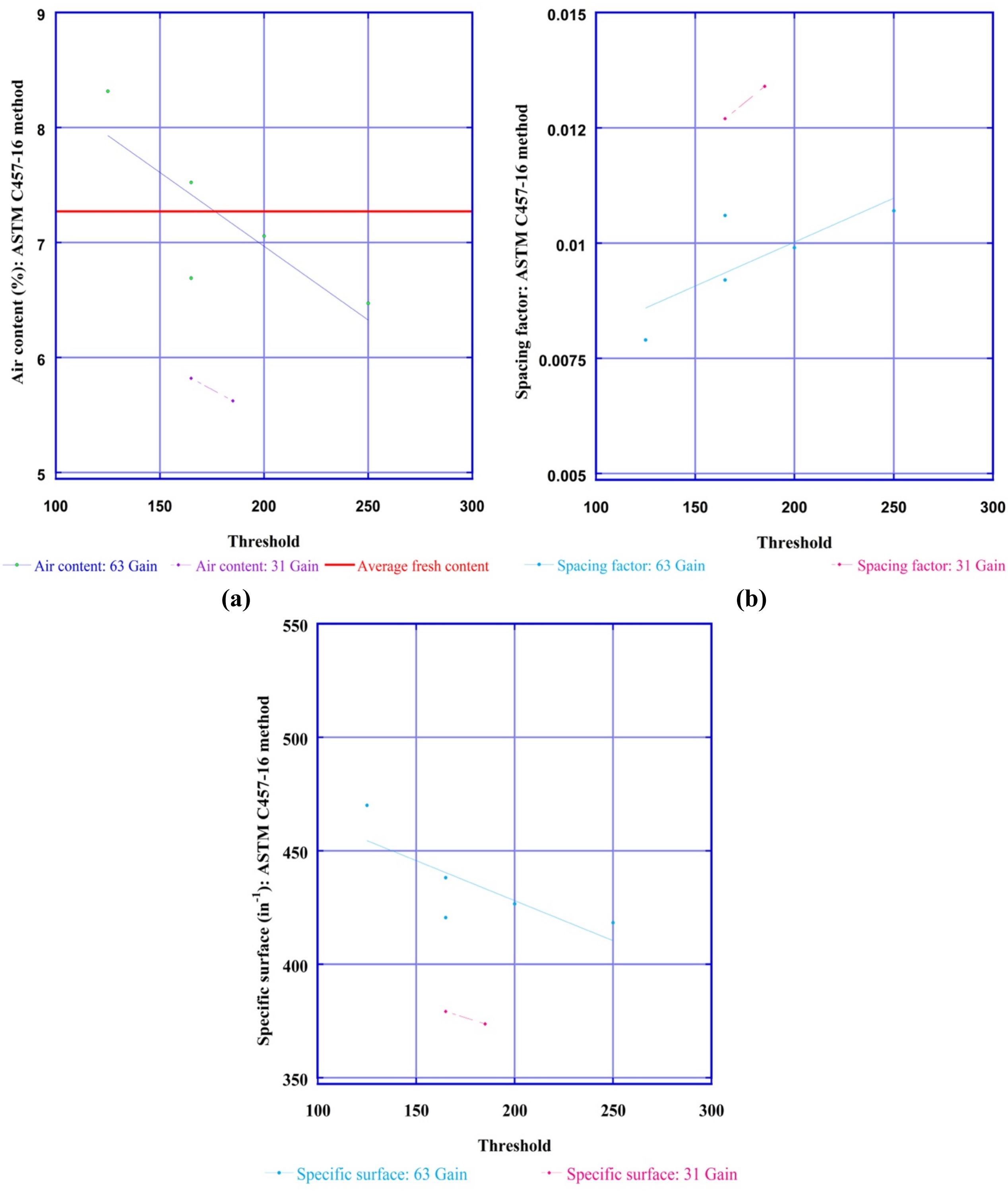

Figure 4.1: Average air-void parameters: (a) Air content (%), (b) Spacing factor (mm), and (c) Specific surface area (mm^{-1}) measured at the different threshold and gain settings

Similar to the observations in Table 4.1, Figure 4.1 shows a similar trend. The average values of air content and specific surface area decreased with an increase in threshold, and that of the spacing factor increased. On the other hand, the average fresh air content was 7.27% and was used to calculate the associated variation with hardened air content. This was done due to the unavailability of the 'true measurements' for distribution parameters. The wide variation observed in Figure 4.1 further emphasizes the need to quantify error associated with distribution parameters evaluated at different system settings. The following section aims to quantify this error using a set of known air-void structures.

4.2 True Air-Void Distribution Parameters using Synthetic Images

A significant problem associated with identifying the exact error/uncertainty in different system settings is the absence of a 'true value' for distribution parameters. This was achieved using a set of unique air- void structures randomly generated using a Python script. They were printed as 100 x 100 mm2 (4 x 4 in.2) luster photographs using a 3200-dpi printer. During further discussion, they will be referred to as 'Synthetic air-void structures.' Each synthetic air-void structure was unique, and the Python script documented its air voids' exact location and size. Accordingly, these properties were used to calculate the 'true measurements' for the distribution parameters. These were calculated using the formula given by Equation 4.1 - 4.5, which were adopted from their mathematical definitions given in Section 2.4.1.

- $\textbf{Air content} = \frac{\textbf{Sum of the area of all air-voids}}{\textbf{Area of the concrete specimen or image}} \times \mathbf{100}$ **Equation 4.1**
- $\textbf{Specific Surface area} = \frac{\textbf{Total surface area of all air-voids}}{\textbf{Total volume of air-voids}} \times \mathbf{100}$ **Equation 4.2**
- $\textbf{Spacing factor} = \textbf{average of } (\textbf{maximum distance from an air} - \textbf{void to its nearest air} - \textbf{void})$ **Equation 4.3**
- $\textbf{Paste content} = \mathbf{100} - \textbf{Air content}$ **Equation 4.4**

- $\text{Paste to air ratio} = \frac{\text{Paste content}}{\text{Air content}}$ **Equation 4.5**

4.2.1 Verifying 'Synthetic Air-Void Structures' by Keyence Microscope.

Initially, the accuracy of synthetic images printed by the high-resolution printer was verified by scanning the images under a (digital) Keyence microscope. Thereby verifying the accuracy of readings recorded by the Python script and later printed by the high-resolution printer. This was done to measure the precision of air-void structures printed as synthetic images. The evaluated quantities and their 'true' dimensions documented by the Python script are given in Figure 4.2 and Table 4.2, respectively. The air voids were printed with an average accuracy of 97%, and the distance between air voids was measured with an average accuracy of 87.30%.

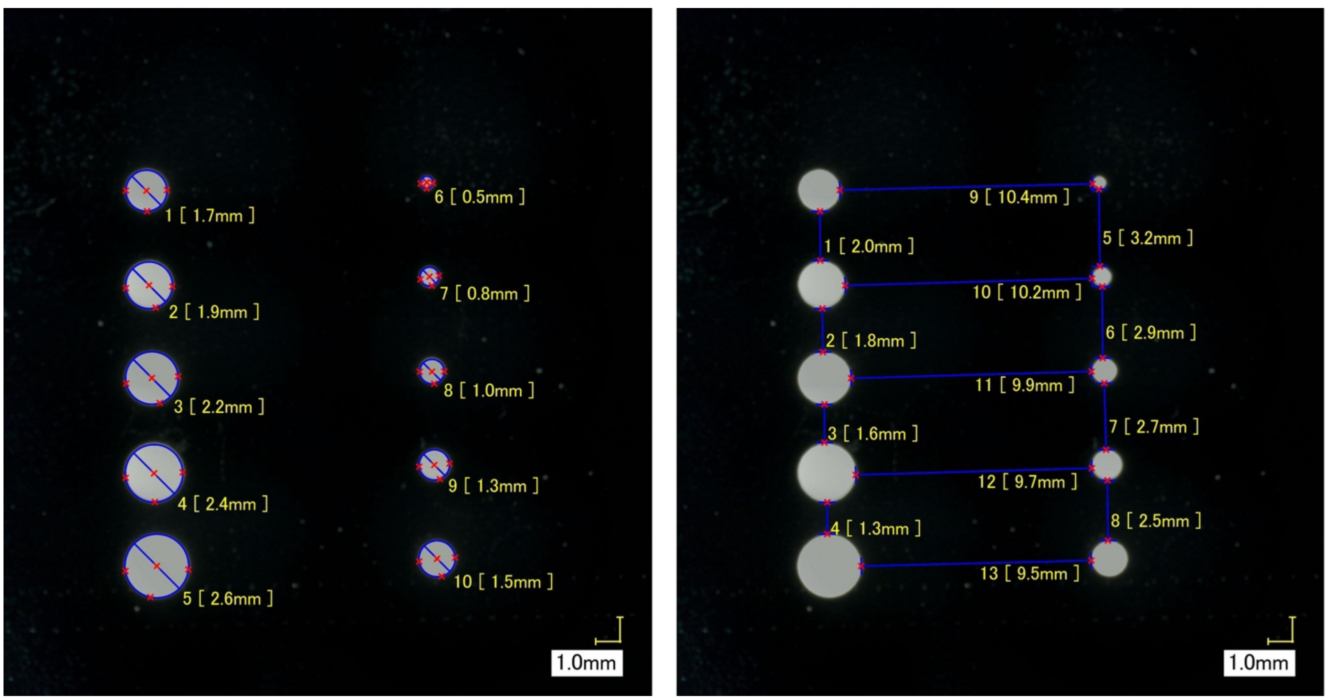

Figure 4.2: Size and distance between air voids for images measured by microscope.

Table 4.2: Properties of air-void structures in the first set of synthetic images.

Air Void #	Radius (mm)	Error (%)	Distance #	Distance (mm)	Error (%)
1	1.75	2.86	1	2.37	15.43
2	2.00	5.00	2	2.11	14.49
3	2.25	2.22	3	1.86	13.75
4	2.50	4.00	4	1.62	19.75
5	2.74	5.11	5	3.61	11.23
6	0.51	1.96	6	3.35	13.43
7	0.76	5.26	7	3.11	13.04
8	1.00	0.00	8	2.87	12.74
9	1.25	4.00	9	11.57	10.11
10	1.50	0.00	10	11.32	9.89
-	-	-	11	11.08	10.61
-	-	-	12	10.83	10.39
-	-	-	13	10.58	10.21

4.2.2 First Set of Synthetic Air-Void Structures

After assessing the accuracy of the printed air-void structures using a Keyence microscope, a set of 8 synthetic images were randomly generated and evaluated using a RapidAir system. They were evaluated at a threshold/gain of 165 / 31 by the Research Geology Section located within the KDOT Materials and Research Center in Topeka, KS. Two sets of images were prepared for an air content of 2%, 4%, 6%, and 8%. The properties of the set of images shown in Figure A.1 - A. 8 are given in Figure 4.3 and Table 4.3. Figure 4.3 shows the distribution of air-void sizes encompassed in the synthetic air-void structures. Their 'true' distribution parameters were calculated using the properties documented by the Python script and compared to the corresponding distribution parameters measured by the ASTM C457 (shown in Table 4.3). The scanned prints had a total traverse length of 2360.1 mm (92.92 in.). Images 2b, 4b, 6b, and 8b were evaluated at a paste value of 20%, and the rest were evaluated at a paste value of 15%.

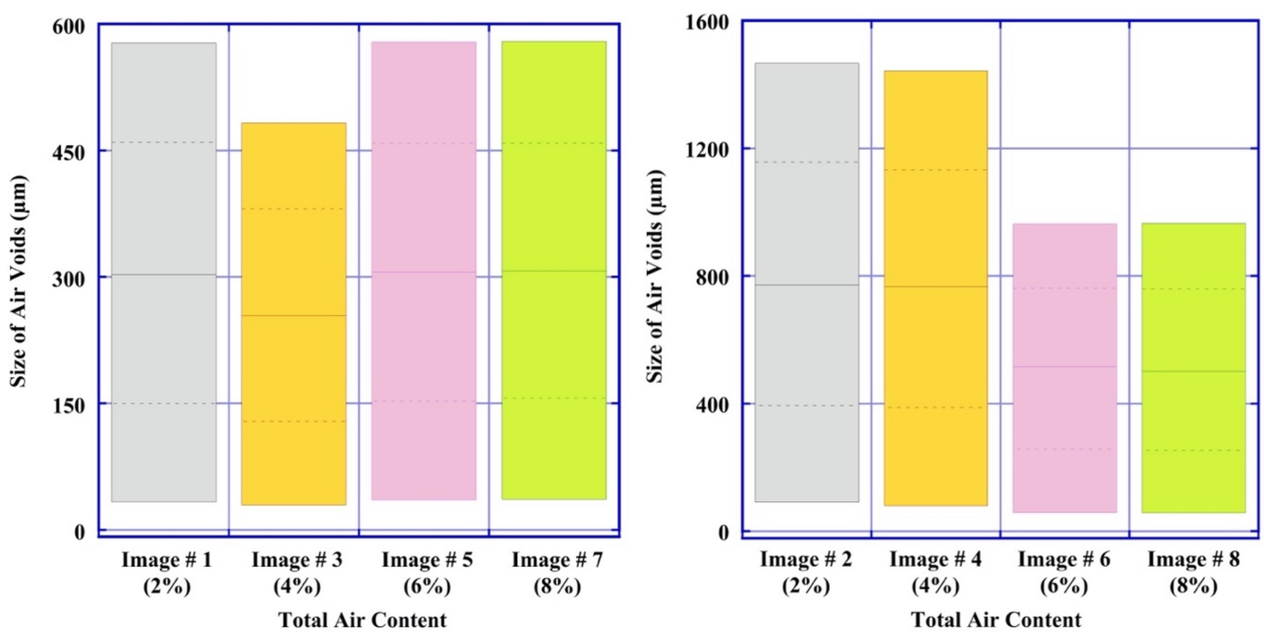

Figure 4.3: Air Void Size Distribution for synthetic air-void structures (Figure A.1 - A.8).

Table 4.3: Properties of air-void structures in the first set of synthetic images.

Image #	Measured 'true' parameters				RapidAir measurement (ASTM C457)			
	Air content (%)	# Voids	Air void size (µm)	Spacing factor (mm)	Air content (%)	# Voids	Spacing factor (mm)	Specific Surface (mm^{-1})
1	2	8,493	2.5 – 304.7	0.30	2.38	303	0.195	21.55
2a	1.5	994	5.3 – 762	0.96	1.84	99	0.636	9.10
2b					1.55	99	0.658	10.79
3	4	24,460	2.6 – 254	0.13	3.86	564	0.105	24.74
4a		2,731	5.1 – 761.9	0.41	4.61	263	0.336	9.67
4b					4.63	273	0.432	10
5	6	25,396	2.5 – 304. 8	0.11	6.46	822	0.072	21.56
6a		9,098	5.1 – 507.9	0.18	6.92	534	0.166	13.07
6b					7.31	579	0.204	13.42
7	8	33,694	2.6 – 304.8	0.08	9.12	1083	0.054	20.13
8a		12,329	5.1 – 507.8	0.14	8.63	662	0.134	13.01
8b					9.33	715	0.165	12.99

The ASTM C457 distribution parameters were compared to its 'true or known' values, and the associated error is tabulated in Table 4.4. Overall, a higher error was associated with the measured spacing factor that air content. A substantial proportion of air voids were not detected by the RapidAir system, which might be due to their small sizes. Additionally, the observed error for total air content was higher for images with larger air voids (Image# 4, 6, 8), and air content of 4%, 6%, and 8% was lower than that for smaller air voids (Image# 3, 5, 7).

Table 4.4: Error associated with the distribution parameters measured by the RapidAir.

Sample #	True air content (%)	Air content	# Voids	Spacing factor
1	2	19.00	96.43	34.78
2a	1.5	22.67	90.04	33.45
2b		3.33	90.04	31.12
3	4	3.50	97.69	20.08
4a		15.25	90.37	17.55
4b		15.75	90.00	5.91
5	6	7.67	96.76	32.26
6a		15.33	94.13	8.85
6b		21.83	93.64	11.98
7	8	14.00	96.79	32.72
8a		7.88	94.63	1.76
8b		16.63	94.20	21.32

4.2.3 Second Set of Synthetic Air-Void Structures

After that, another set of 10 synthetic air-void structures (Figure A.9 - A.18) was generated with varying air-void sizes and distribution, as shown in Table 4.5. These synthetic images were used to quantify the error associated with different system settings (threshold and gain) on the measured air-void count, size, and distribution. The images were scanned at a gain of 63 and 31 for threshold values specified in Table 4.5.

Table 4.5: Properties of air-void structures in the second set of synthetic images.

Image #	Air content (%)	# Voids	Threshold	Radius (µm)	Spacing factor (mm)
1	2	964	150, 175, 200, 250	521.0	0.76
2	4	219	200, 250	1542.0	1.37
3	8	3307	200, 250	562.3	0.22
4	6	87	200, 250	2992.9	1.90
5	8	4054	150, 175, 200, 250	508.0	0.20
6	4	414	175, 200, 225, 250	437.5 – 1745.0	0.96
7	6	748	175, 200, 225, 250	1023.2	0.59
8	6	2515	175, 200, 225, 250	560.0	0.42
9	8	2127	175, 200, 225, 250	703.11	0.44
10	4	97	175, 200, 225, 250	2339.7	2.13

The size of air voids was selected as per the acceptable or observed (size) range of entrained air voids. Air-void structure of Images# 1, 3, and 5 was created with smaller voids, and Images# 4, 5, and 7 with larger size voids. The size of (randomly distributed) circles in these images was varied across a wide range to identify the number, sizes, and distribution of air voids accurately detected at different settings. The effect of pitch, i.e., the distance between successive traverses, using equal spacing circles along the X or Y direction (Images# 8, 9, and 10). Lastly, Image# 6 was developed to combine all these variables and understand their combined effect.

The 'true value' of distribution parameters for these images was compared to their similar values recorded by the RapidAir system at system settings given in Table 4.5. For both 31- and 63-gain settings, the error associated with distribution parameters was higher and scattered across a wide range for smaller voids (Images # 1, 3, 5). Conversely, images with larger voids (Images # 2, 4, 7) and Image # 6 had a well-converged error. Furthermore, the error for the 63-gain setting was truncated at a threshold value of 150 & 250 and dispersed for the 31-gain setting. Overall, the error associated with 63-gain setting was lower than that at 31-gain. Upon comparing the error associated with individual distribution parameters, the hierarchy of error (low to high) ranged as - total air content (error< 80%), the spacing factor (Images # 1, 3, 5 at 31-gain: error< 300% and the remaining images had an error< 80%), and lastly the specific surface (error< 700%).

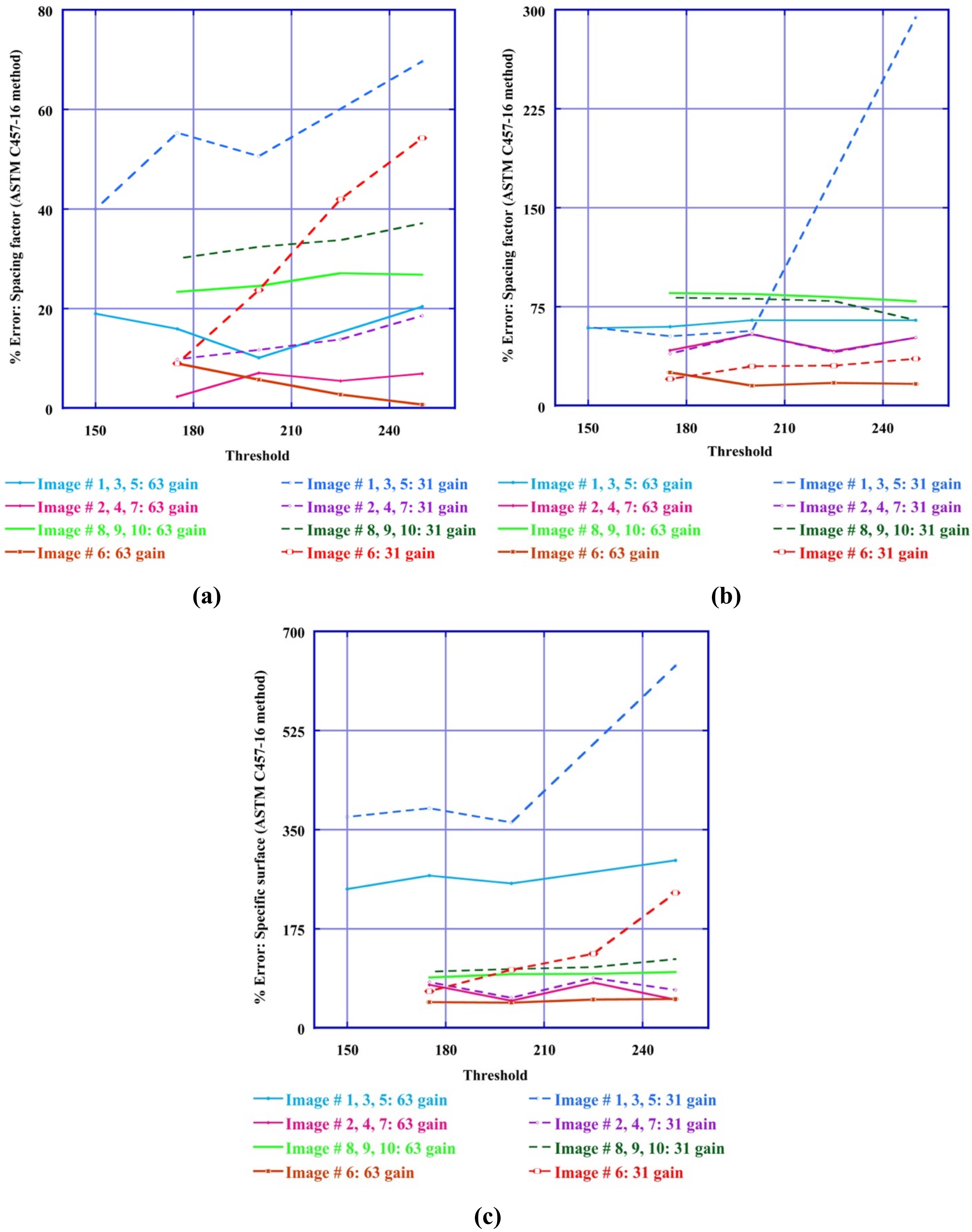

Figure 4.4: % error for the air-void parameters measured by the RapidAir system for the synthetic air-void systems at varying system settings.

4.3 Alternative Dispersion Metrics

The current standard practices/specifications to assess air-void distribution are based on research from the early 1950s (Powers & Willis, 1950, Powers, 1954, Mielenz et al., 1958). Since then, alternate recommendations have been made to visualize air-void distribution, different definitions to calculate spacing factor (assuming different spatial arrangements of the air-void structure), or parameters to assess the dispersion of air-voids through its cementitious paste (Punurai et al., 2006; Peterson et al., 2010, Radlinski et al., 2010, Zhu et al., 2011, Kim et al., 2012, Hasholt, 2014, Fonseca & Scherer, 2015, Guo et al., 2016, Ley et al., 2017, Lu et al., 2017, Shon et al., 2018; Dąbrowski et al., 2019, Becker et al., 2021, Igarashi et al., 2021). Although very few or hardly any new revisions have been made to transportation agencies' specifications or design codes. This inconsistency signifies an urgent need to evaluate these options and check if they can improve the current/modern construction practices.

ASTM C457 method helps homogenize the distribution of an air-void structure into a single scalar quantity known as the 'spacing factor.' Commonly, the spacing factor is used to qualify the quality (i.e., well or coarse) of an air-void distribution or dispersion through the cementitious paste. Moreover, the value of distribution parameters is dependent on the assumed spatial arrangement of air voids. Based on the assumed arrangement, the measured 'true/actual' values of distribution parameters vary from sample to sample. Thus, in addition to quantifying the uncertainty/error associated with hardened air-void analysis (performed by RapidAir), it is imperative to reanalyze the currently used distance (spacing factor) parameter to quantify distribution, i.e., dispersion. Accordingly, an alternative scalar quantity, known as the 'dispersion parameter (DP), has been studied in this section to quantify dispersion on a scale of worst to best. DP has been previously used to quantify the dispersion of fibers in composites (Yazdanbakhsh et al., 2011). Although the medium and material of evaluation are different, the overall quantification concept remains the same.

Yazdanbakhsh et al. assumed a DP = 0 for the worst-case scenario and a DP = 1 is assigned to the best- case scenario. Accordingly, a given dispersion was assigned a value between 0 to 1 to quantify it on a scale of worse to best. DP was calculated as the ratio of maximum "work" required to disperse an air- void system to obtain the worst dispersion and the best dispersion (Yazdanbakhsh et al., 2011), calculated as per Equation 4.6:

$$\mathbf{DP = 1 - \frac{Wa}{Ww}} \qquad \textbf{Equation 4.6}$$

where, W_a and W_w correspond to the work required to disperse air voids from their current locations to their location in the 'best and 'worst' dispersion scenarios, respectively. The work done is calculated as per Equation 4.7, given below:

$$\textbf{Work done} = \sum_{i=0}^{n} \mathbf{A_i} \times \mathbf{d_i} = \sum_{i=0}^{n} \mathbf{A_i} \times \sqrt{(\mathbf{x}-\mathbf{x_i})^2 + (\mathbf{y}-\mathbf{y_i})^2} \qquad \textbf{Equation 4.7}$$

where n = total number of air voids in the given air-void structure

A_i, (x_i, y_i) = Area and (x,y) coordinates of the i^{th} air-void.

(x,y) = (x,y) coordinates for the best or worst-case scenario.

The worst-case scenario was considered when all the fibers were clustered at either one of the corners of the sample. Moreover, the associated work was calculated to move them from their current location to the assumed location for worse dispersion.

The best-case scenario refers to a cubical spatial arrangement where a given sample area is split into numerous small squares. Moreover, the center of each of these smaller squares was taken to be the location for the 'best dispersed' case. All the fibers falling under each of the smaller squares were considered as a group, and work done was calculated to move the group from their centroid to the vertex of a 'best dispersed' air-void location.

4.4 Quantifying Air-Void Distribution using Dispersion Parameter

This section proposes an alternate method to quantify the air-void distribution using the 'DP' parameter conceptualized in Section 4.3. DP for an air-void distribution is proposed by modifying Equation 4.6., to identify the clustering of air voids and their overall distribution across a surface. Unlike Section 4.3, the proposed DP considers five reference points for the worst-case scenario shown in Figure 4.5 (a) - four corners and the center of a square specimen. However, the best-dispersed case remains the same and can be achieved by meshing the sample into (100 x 100) smaller squares (shown in Figure 4.5 (b)). Thus, DP was calculated as the ratio of work required to disperse air voids from their given location to their assumed reference points for worst to best case. Accordingly, it can be calculated by Equation 4.8:

$$\mathbf{DP} = \frac{\textbf{Work done to achieve to worst−dispersion}}{\textbf{Work done to achieve to best−dispersion}} \qquad \textbf{Equation 4.8}$$

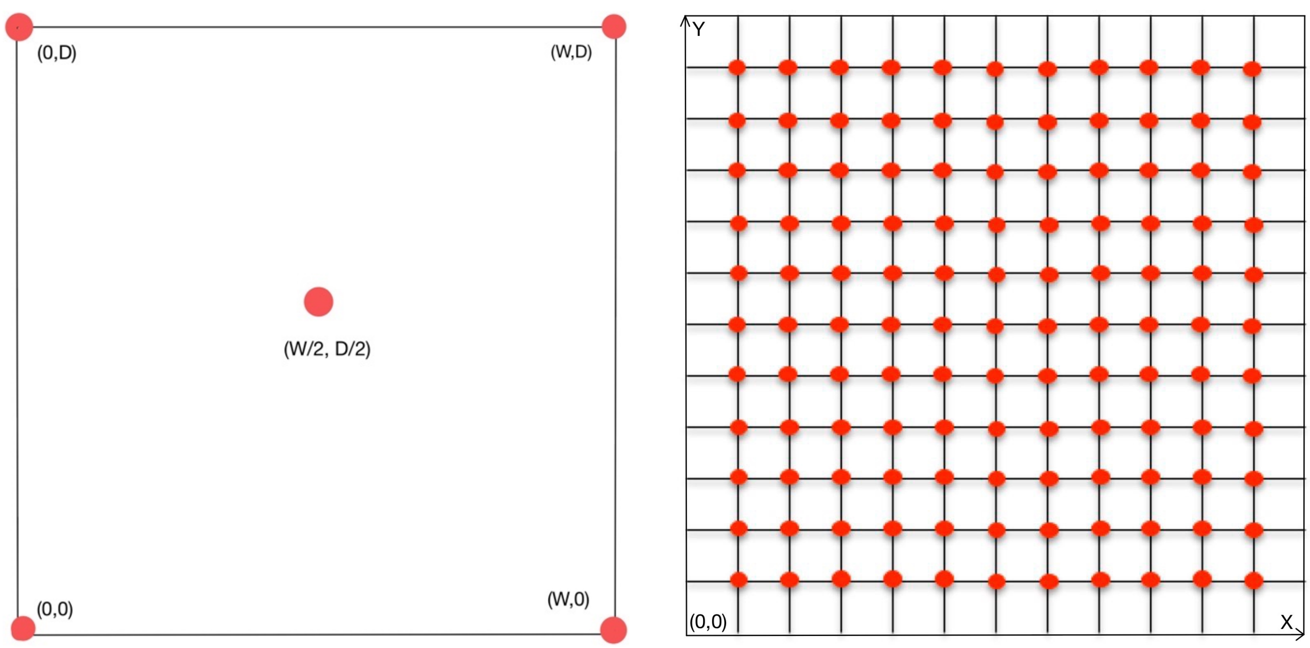

(a) **Worst-case scenario** **(b) Best-case scenario**

Figure 4.5: Example of references points used to calculate DP for the (a) Worst- and (b) Best-case scenarios.

For a well-dispersed air-void structure, the mean distance traveled by air voids (within each of the (smaller) sub-squares) to each of the five reference points considered for the worst-case scenario positions will remain constant. However, the mean DP will vary for the reference points for a coarsely dispersed air-void structure. The standard deviation (STDEV) or the coefficient of variation (COV) between DPs measured for the five reference points can be used to identify if the air voids are well distributed or clustered towards a reference point. As a result, a smaller STDEV or COV between the DP for five reference points will be required to qualify an air-void structure as well-distributed. Similarly, a higher STDEV or COV will signify coarse distribution.

The accuracy of the proposed 'DP' parameter to quantify air-void distribution is evaluated using synthetic air-void structures (images) to quantify their accuracy. The estimated mean DP values w.r.t the five reference points for the synthetic air-void structures are given in Table 4.6. Moreover, the associated STDEV or COV between the DPs is given in Table 4.7 and Figure 4.6.

Table 4.6: Average DP measured for synthetic images.

Image #	Average DP measured w.r.t Reference point					Average for reference points	STDEV between reference points
	(0, 0)	(W, 0)	(0, D)	(W, D)	Center (W/2, D/2)		
1	0.00390	0.00395	0.00396	0.00384	0.00765	0.00466	0.00167
2	0.00064	0.00065	0.00063	0.00061	0.00129	0.00076	0.00030
3	0.00616	0.00615	0.00625	0.00618	0.01252	0.00745	0.00284
4	0.00174	0.00165	0.00160	0.00161	0.00316	0.00195	0.00067
5	0.00628	0.00623	0.00626	0.00621	0.01262	0.00752	0.00285
6	0.00415	0.00417	0.00418	0.00424	0.00851	0.00505	0.00193
7	0.00651	0.00650	0.00647	0.00649	0.01298	0.00779	0.00290
8	0.00495	0.00489	0.00492	0.00490	0.01001	0.00593	0.00228
1	0.00061	0.00065	0.00058	0.00065	0.00126	0.00075	0.00029
2	0.00015	0.00016	0.00015	0.00015	0.00028	0.00018	0.00006
3	0.00196	0.00192	0.00191	0.00195	0.00399	0.00235	0.00092
4	0.00006	0.00005	0.00006	0.00006	0.00013	0.00007	0.00003
5	0.00234	0.00232	0.00235	0.00224	0.00461	0.00277	0.00103
6	0.00027	0.00028	0.00026	0.00029	0.00060	0.00034	0.00014
7	0.00050	0.00048	0.00045	0.00045	0.00092	0.00056	0.00020
8	0.00105	0.00084	0.00103	0.00080	0.00226	0.00120	0.00060
9	0.00082	0.00082	0.00083	0.00081	0.00192	0.00104	0.00049
10	0.00005	0.00004	0.00005	0.00006	0.00015	0.00007	0.00005

As seen in Table 4.7 and Figure 4.6., the average COVs for DP measured w.r.t the reference points are well-correlated ($R^2 = 0.97$ and 0.92) with the spacing factor (mm). This suggests that DP measures dispersion similarly to the spacing factor. However, it is essential to understand that the spacing factor, a scalar quantity, normalizes the nearest distance neighbors for air voids. At the same time, DP provides an understanding of the overall air-void distribution across the sample area. As a result, it enriches hardened air-void analysis by providing a 20 representation of the air-void distribution instead of the 1D representation given by the spacing factor.

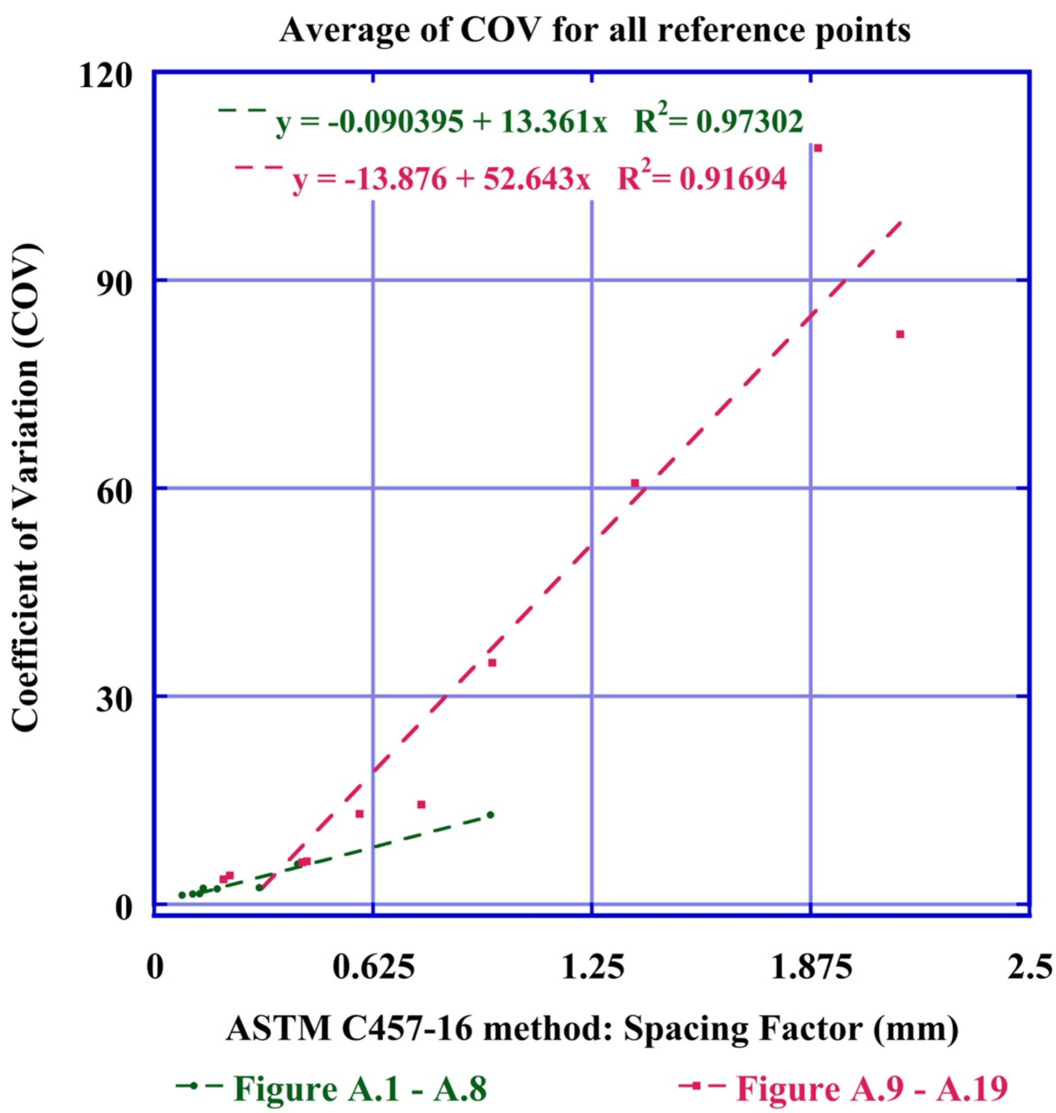

Figure 4.6: COV between DPs measured vs spacing factor (mm) for synthetic images.

Table 4.7: COV between DPs measured for synthetic images.

Image #	COV between DP measured w.r.t Reference point					Average COV for reference points	STDEV between reference points	Spacing factor (mm)
	(0, 0)	(W, 0)	(0, D)	(W, D)	Center (W/2, D/2)			
Figure A.1. – A.8.								
1	2.26	2.96	3.01	1.82	2.00	2.41	0.55	0.30
2	12.47	17.67	11.92	9.14	13.37	12.91	3.09	0.96
3	1.36	1.39	1.54	1.59	1.90	1.56	0.22	0.13
4	7.38	6.66	5.34	5.38	4.52	5.85	1.15	0.41
5	1.62	1.51	1.31	1.37	1.71	1.50	0.17	0.11
6	2.28	2.21	2.10	2.23	2.41	2.25	0.11	0.18
7	1.31	1.33	1.35	1.31	1.33	1.33	0.02	0.08
8	2.07	1.91	1.88	1.83	3.99	2.33	0.93	0.14
Figure A.9. – A.19								
1	12.65	16.76	12.80	15.68	14.00	14.38	1.80	0.76
2	61.51	84.81	57.74	39.97	59.60	60.73	15.98	1.37
3	4.21	4.00	3.85	4.48	4.32	4.17	0.25	0.22
4	127.17	91.13	91.10	134.89	101.02	109.06	20.64	1.90
5	3.47	3.83	4.54	3.18	3.06	3.62	0.60	0.20
6	32.15	32.07	20.01	48.79	41.22	34.85	10.84	0.96
7	17.50	13.20	11.57	10.46	12.45	13.04	2.70	0.59
8	5.24	9.95	4.85	3.79	6.58	6.08	2.38	0.42
9	5.01	5.03	6.83	5.85	8.33	6.21	1.40	0.44
10	64.65	55.93	66.03	103.50	120.93	82.21	28.34	2.13

4.5 Recommendations

Currently, the hardened air-void analysis conducted using the RapidAir system (based on the ASTM C457: Procedure C), is assumed to yield the actual distribution parameters for an air-void structure. However, there are several shortcomings associated with this method, of which the major ones are:

1. The selected system and settings influence measured distribution parameters.
2. 'Spacing factor' homogenizes the distance between air voids into a single scalar quantity, i.e., provides a 1D dimension for 2D distribution or sample.

With that objective, this chapter was focused on quantifying the uncertainties associated with hardened air void analysis and identifying an alternate dispersion parameter (DP) to assess air-void distribution. Accordingly, the following recommendations have been made:

1. The synthetic images create an ideal format to calibrate or quantify the error associated with different RapidAir systems and settings. Comparing the 'true' distribution parameter with those evaluated by a RapidAir system will help quantify the influence of system settings on the distribution parameters. This illustrates how easily results could be manipulated to achieve target values. Concerning this, it is important to conduct a round-robin study before developing a calibration system using synthetic images. The suggested round-robin studies can be conducted by circulating the same set of synthetic images with different laboratories (without revealing their 'true' distribution parameters). Comparing the RapidAir measurements recorded at different settings, the error can be mapped for different systems and parameters. The observed error in distribution parameters can be used to recommend the optimized system settings for different RapidAir systems.

2. Use DP as a variable to quantify air-void distribution across the sample surface, which will better identify if the air voids are well-distributed or clustered in a sample.ss

Chapter 5 - Conclusions

Air entrainment in concrete pavements is known to improve the freeze-thaw durability of the cementitious paste (Powers, 1945, Powers & Willis, 1950, Powers & Helmuth, 1953, Mielenz et al., 1958). For high freeze-thaw resistance, state departments of transportation recommend a total air content higher than 4%, along with a spacing factor less than 0.02 mm (0.008 in.). Therefore, the total air content can be reliably measured in fresh concrete and is widely used as a QC/QA tool on-site. More recently, the SAM number has been implemented to evaluate the distribution of air voids in fresh concrete. A SAM number less than 0.2 is considered an acceptable threshold for identifying concrete mixtures with a spacing factor of less than 0.2 mm (0.008 in.). However, this study demonstrated that the variability in SAM number is significant, specifically for concrete mixtures with a slump less than 3.175 cm (1.25 in.). The higher variability in the total air content and SAM number measured on-site makes it difficult to use either of these as an individual QC/QA tool.

This study used LASSO, Binary Logistic, and Bayesian Probit regression models to enhance these methods' predictive capabilities by developing models using fresh concrete properties and mixture design parameters as predictors. The following observations were made during this study:

- The spacing factor measured by the ASTM C457 method decreased with an increase in the total air content. The range of the measured spacing factors also decreased as the total air content increased.
- Concrete mixtures with an air content greater than 6% (by volume) also satisfied the spacing factor requirement (< 0.2 mm or 0.008 in.) recommended for freeze-thaw durable concrete.

- The relative uncertainty (Figure 3.2 and Table 3.3) calculated for the total air content is much lower than that for the SAM number for on-grade concrete mixtures tested using the same and different SAM meters by the same and different operators in the laboratory and field.
- Based on the statistical analysis of data collected from 157 concrete mixtures, the base model expressed by Equation 3.13 was developed and validated to predict the spacing factor using parameters obtained from mixture design and fresh concrete properties.
- The final Predictive model given by Equation 3.14, formulated using SAM number and VP/VA, was found to accurately differentiate between spacing factors less and more significant than 0.2 mm (0.008 in.), thus, creating a simple and efficient on-site QC/QA tool to evaluate the air entrainment in fresh concrete.
- The SAM number, V_P/V_A, and PSF were calculated using the base model. PSF calculated using the final model exhibited an accuracy of 48.4%, 68.5%, 88.5%, and 81.1%, respectively, in discriminating between the spacing factors with good air systems, i.e., less than 0.2 mm (0.008in.) and those greater than 0.2 mm (0.008 in.), for the complete dataset (271 observations).
- The models were developed using a data set dominated by a spacing factor less than 0.2 mm (0.008 in.), so they need to be further calibrated over a more extensive data set with equally distributed spacing factor data points to improve their predictive capacity and accuracy.
- The best-fit models developed by all three regression techniques were dominated by the new concrete parameter, VP/VA. Thus, emphasizing it is significance in quantifying air-void distribution in hardened concrete.

Furthermore, the uncertainties associated with hardened air-void analysis performed by a RapidAir system were also evaluated during this study. To quantify the error or uncertainty, a set of synthetic air-void structures were developed using a Python script and printed as high-resolution images. The exact location and sizes of the air voids in these images were documented by the Python script and were used to calculate their 'known or true' distribution parameters. Hence, the error associated with different systems and settings was estimated by comparing the 'actual or known' observations with the measured similar properties by the RapidAir. Accordingly, the following observations have been made:

- ASTM C457 method normalizes the distribution of air voids across the sample surface (2D) into a scalar (1D) quantity known as the 'spacing factor.'
- The system settings, such as threshold and gain, influence air-void distribution parameters evaluated by a RapidAir system.
- The error can be minimized for the spacing factor, air content, or specific surface at a given system setting. Thus, a system setting can be selected for analysis based on the quantity or parameter of interest.

Additionally, an alternate 'Dispersion parameter' (DP) has been recommended in this study to quantify the observed distribution of air voids across a sample surface.

- The proposed DP was well correlated (R^2 = 0.97 and 0.92) to the spacing factor for both sets of synthetic air-void images.
- Unlike the spacing factor, DP gives a 2D representation of the distributed air voids across the sample surface. This helps identify whether the air voids are well distributed across the sample surface or clustered in an area.

Chapter 6 - References

AASHTO. (2017). AASHTO T 22: Standard Method of Test for Compressive Strength of Cylindrical Concrete Specimens. In: American Association of State and Highway Transportation Officials (AASHTO).

AASHTO. (2022a). AASHTO T 96: Standard Method of Test for Resistance to Degradation of Small-Size Coarse Aggregate by Abrasion and Impact in the Los Angeles Machine. In: American Association of State and Highway Transportation Officials (AASHTO).

AASHTO. (2019). AASHTO T 152: Standard Method of Test for Air Content of Freshly Mixed Concrete by the Pressure Method. In: American Association of State and Highway Transportation Officials (AASHTO).

AASHTO. (2011). AASHTO T 196: Standard Method of Test for Air Content of Freshly Mixed Concrete by the Volumetric Method. In: American Association of State and Highway Transportation Officials (AASHTO).

AASHTO. (2018). AASHTO T 348: Standard Method of Test for Air-Void Characteristics of Freshly Mixed Concrete by Buoyancy Change. In: American Association of State and Highway Transportation Officials (AASHTO).

AASHTO. (2022b). AASHTO T 395: Standard Method of Test for Characterization of the Air-Void System of Freshly Mixed Concrete by the Sequential Pressure Method. In: American Association of State and Highway Transportation Officials (AASHTO).

ACI Committee 201. (2016). ACI 201.2R-16 Guide to Durable Concrete. Farmington Hills, MI: American Concrete Institute.

Afrani, I., & Rogers, C. (1994). The effects of different cementing materials and curing on concrete scaling. *Cement, Concrete and Aggregates*, *16*(2), 132-139.

Altman, D. G., & Bland, J. M. (1994). Statistics Notes: Diagnostic tests 2: predictive values. *Bmj*, *309*(6947), 102.

ASTM. (2022a). ASTM C31 / C31M-22, Standard Practice for Making and Curing Concrete Test Specimens in the Field. In. West Conshohocken, PA: ASTM International.

ASTM. (2017). ASTM C138 / C138M-17a, Standard Test Method for Density (Unit Weight), Yield, and Air Content (Gravimetric) of Concrete. In. West Conshohocken, PA: ASTM International.

ASTM. (2020). ASTM C143 / C143M-20, Standard Test Method for Slump of Hydraulic-Cement Concrete. In. West Conshohocken, PA: ASTM International.

ASTM. (2016a). ASTM C173 / C173M-16, Standard Test Method for Air Content of Freshly Mixed Concrete by the Volumetric Method. In. West Conshohocken, PA: ASTM International.

ASTM. (2019). ASTM C192 / C192M-19a, Standard Practice for Making and Curing Concrete Test Specimens in the Laboratory. In. West Conshohocken, PA: ASTM International.

ASTM. (2022b). ASTM C231 / C231M-17a, Standard Test Method for Air Content of Freshly Mixed Concrete by the Pressure Method. In. West Conshohocken, PA: ASTM International.

ASTM. (2016b). ASTM C457 / C457M-16, Standard Test Method for Microscopical Determination of Parameters of the Air-Void System in Hardened Concrete. In. West Conshohocken, PA: ASTM International.

ASTM. (2015). ASTM C666 / C666M-15, Standard Test Method for Resistance of Concrete to Rapid Freezing and Thawing. In. West Conshohocken, PA: ASTM International.

Attiogbe, E. K. (1993). Mean spacing of air voids in hardened concrete. *Materials Journal*, *90*(2), 174-181.

Becker, H. H., Ley, M. T., Welchel, D., Peery, J., Leflore, J., Brorsen, B. W., & Khatibmasjedi, M. (2021). Determining the air void efficiency of fresh concrete mixtures with the Sequential air method. *Construction and Building Materials*, *288*, 122865.

Brunner, J., & Austin, P. C. (2009). Inflation of Type I error rate in multiple regression when independent variables are measured with error. *Canadian Journal of Statistics,* 37(1), 33-46.

Chahine, G. L., Duraiswami, R., & Frederick, G. (1998). Detection of air bubbles in hp ink cartridges using DYNAFLOW's acoustic bubble spectrometer (ABS) technology. In. DYNAFLOW.

Chahine, G. L., Kalumuck, K. M., Cheng, J.-Y., & Frederick, G. (2001). Validation of bubble distribution measurements of the ABS acoustic bubble spectrometer with high speed video photography. *http://resolver.caltech. edu/cav2001:sessionA7.004*.

Chakraborty, S., & Khare, K. (2017). Convergence properties of Gibbs samplers for Bayesian probit regression with proper priors. *Electronic Journal of Statistics,* 11(1), 177-210.

Chatterji, S., & Gudmundsson, H. (1977). Characterization of entrained air bubble systems in concretes by means of an image analysing microscope. *Cement and Concrete Research*, *7*(4), 423-428.

Dodson, V. H. (2013). *Concrete admixtures*. Springer Science & Business Media.

Du, L., & Folliard, K. J. (2005). Mechanisms of air entrainment in concrete. *Cement and concrete research*, *35*(8), 1463-1471.

Dąbrowski, M., Glinicki, M. A., Dziedzic, K., & Antolik, A. (2019). Validation of sequential pressure method for evaluation of the content of microvoids in air entrained concrete. *Construction and Building Materials*, *227*, 116633.

Distlehorst, J. A., & Kurgan, G. J. (2007). Development of precision statement for determining air void characteristics of fresh concrete with use of air void analyzer. Transportation research record, 2020(1), 45-49.

Fagerlund, G. (1993). The long time water absorption in the air-pore structure of concrete.

Fonseca, P., & Scherer, G. (2015). An image analysis procedure to quantify the air void system of mortar and concrete. *Materials and Structures*, *48*(10), 3087-3098.

Guo, S., Dai, Q., Sun, X., & Sun, Y. (2016). Ultrasonic scattering measurement of air void size distribution in hardened concrete samples. *Construction and Building Materials*, *113*, 415422.

Harnik, A. B., Meier, U., & Rösli, A. (1980). *Combined Influence of Freezing and Deicing Salt on Concrete--Physical Aspects*. West Conshohocken, PA: ASTM International.

Harrell, J., Frank E., & Harrell, F. E. (2015). Binary logistic regression. *Regression modeling strategies: With applications to linear models, logistic and ordinal regression, and survival analysis*, 219-274.

Hasholt, M. T. (2014). Air void structure and frost resistance: A challenge to Powers' spacing factor. *Materials and structures*, *47*(5), 911-923.

Hong-fa, & Jia-Chun, W. (2010). Influence of Structural Characteristics of Air Bubbles on Salt Frost Resistance of Concrete [J]. *Journal of South China University of Technology (Natural Science Edition)*, *11*.

Igarashi, S., Taniguchi, M., & Yamashita, S. (2021). Correlation between Conventional Spacing Factors of Air Voids in Concrete and Characteristic Distances Defined by Point Process Statistics. *Journal of Advanced Concrete Technology*, *19*(8), 886-896.

Jakobsen, U., Pade, C., Thaulow, N., Brown, D., Sahu, S., Magnusson, O., & De Schutter, G. (2005). The Rapidair system for air void analysis of hardened concrete—a round-robin study. *Proceedings of the 10th Euroseminar on Microscopy Applied to Building Materials, Paisley, UK*, *21*, 25.

Jakobsen, U., Pade, C., Thaulow, N., Brown, D., Sahu, S., Magnusson, O., & De Schutter, G. (2006). Automated air void analysis of hardened concrete—a Round Robin study. *Cement and Concrete Research*, *36*(8), 1444-1452.

Jana, D. (2007). A round robin test on measurements of air void parameters in hardened concrete by various automated image analyses and ASTM C 457 methods. Proceedings of the 29th International Conference on Cement Microscopy,

Kansas Department of Transportation (2015). Standard Specification for State Road & Bridge Construction:). Section 403 – ON GRADE CONCRETE. Topeka, KS: Kansas Department of Transportation.

KTMR-21 Kansas Test Method. (2019a). Soundness and modified soundness of aggregates by freezing and thawing. Topeka, KS: Kansas Department of Transportation (KDOT).

KTMR-23 Kansas Test Method (2019b). Wetting and Drying Test of Sand-Gravel Aggregate for Concrete. Topeka, KS: Kansas Department of Transportation (KDOT).

Kim, K. Y., Yun, T. S., Choo, J., Kang, D. H., & Shin, H. S. (2012). Determination of air-void parameters of hardened cement-based materials using X-ray computed tomography. *Construction and Building Materials*, *37*, 93-101.

Koubaa, A., Snyder, M. B., & Peterson, K. R. (1997). *Mitigating Concrete Aggregate Problems in Minnesota*. Minnesota Department of Transportation, Research Services Section.

Lamnisos, D., Griffin, J. E., & Steel, M. F. (2012). Cross-validation prior choice in Bayesian probit regression with many covariates. *Statistics and Computing*, *22*, 359-373.

Ley, T., Felice, R., & Freeman, J. M. (2012). Concrete pavement mixture design and analysis (MDA): assessment of air void system requirements for durable concrete.

Ley, T., & Tabb, B. (2013). *Development of a Robust Field Technique to Quantify the Air-Void Distribution in Fresh Concrete* (No. OTCREOS9. 1-31-F). Oklahoma Transportation Center.

Ley, M. T., & Tabb, B. (2014). A test method to measure the freeze thaw durability of fresh concrete using overpressure. T&DI Congress 2014: Planes, Trains, and Automobiles, 79-87.

Ley, M. T., Welchel, D., Peery, J., Khatibmasjedi, S., & LeFlore, J. (2017). Determining the airvoid distribution in fresh concrete with the Sequential Air Method. *Construction and Building Materials*, *150*, 723-737.

Li, W., Pour-Ghaz, M., Castro, J., & Weiss, J. (2012). Water absorption and critical degree of saturation relating to freeze-thaw damage in concrete pavement joints. *Journal of Materials in Civil Engineering*, *24*(3), 299-307.

Lindquist, W., & Montney, R. (2015). *Comparison of Spacing Factors as Measured by the Air-Void Analyzer and ASTM C457.* Kansas Department of Transportation.

Lindquist, W., & Montney, R. (2019). Comparison of spacing factors as measured by the air-void analyzer and ASTM C457. *International Journal of Pavement Engineering,* 20(2), 183-190.

Litvan, G. G. (1976). Frost action in cement in the presence of de-icers. *Cement and Concrete Research,* 6 (3), 351-356.

Litvan, G. G. (1988). *The mechanism of frost action in concrete: Theory and practical implications*. National Research Council Canada, Institute for Research in Construction.

Lu, H., Alymov, E., Shah, S., & Peterson, K. (2017). Measurement of air void system in lightweight concrete by X-ray computed tomography. *Construction and Building Materials*, *152*, 467-483.

Moradllo, M. K., Qiao, C., Ghantous, R. M., Zaw, M., Hall, H., Ley, M. T., & Weiss, W. J. (2020). Quantifying the freeze-thaw performance of air-entrained concrete using the time to reach critical saturation modelling approach. Cement and Concrete Composites, 106, 103479.

Marchand, J., Pleau, R., & Gagné, R. (1995). Deterioration of concrete due to freezing and thawing. *Materials Science of Concrete*, 4(4), 283-354.

Mehta, P. K., & Gerwick, B. C. (1982). Cracking-corrosion interaction in concrete exposed to marine environment. *Concrete International,* 4(10), 45-51.

Menin, B. (2018). h, k, NA: Evaluating the Relative Uncertainty of Measurement. *American Journal of Computational and Applied Mathematics,* 8(5), 93-102.

Mielenz, R., Wolkodoff, V., Backstrom, J., Flack, H., & Orgin, E. (1958). Effects of the Air Void System in Concrete. Part 1–Entrained Air in Unhardened Concrete. Proceedings, American Concrete Institute,

Myers, D. (1999). *Surfaces, interfaces, and colloids* (Vol. 415). Wiley New York.

Neville, A. M. (1996). Properties of concrete. 4th and final ed. *England: Addison Wesley Longman Limited*, 282-283.

Panchmatia, P., Olek, J., & Whiting, N. (2014). Joint deterioration in concrete pavements.

Peterson, K., Carlson, J., Sutter, L., & Van Dam, T. (2009). Methods for threshold optimization for images collected from contrast enhanced concrete surfaces for air-void system characterization. *Materials Characterization*, *60*(7), 710-715.

Peterson, K., Sutter, L., & Radlinski, M. (2010). The practical application of a flatbed scanner for air-void characterization of hardened concrete. In *Recent Advancement in Concrete Freezing-Thawing (FT) Durability*. ASTM International.

Philleo, R. E. (1983). A Method for Analyzing Void Distribution in Air-Entrained Concrete. *Cement, concrete and aggregates,* 5 (2), 128-130.

Pigeon, M. (2014). *Durability of concrete in cold climates*. CRC Press.

Pigeon, M., Pleau, R., & Aitcin, P.-C. (1986). Freeze-thaw durability of concrete with and without silica fume in ASTM C 666 (Procedure A) test method: internal cracking versus scaling. *Cement, concrete and aggregates*, *8*(2), 76-85.

Pleau, R., & Pigeon, M. (1996). The use of the flow length concept to assess the efficiency of air entrainment with regards to frost durability: Part I—description of the test method. *Cement, concrete and aggregates*, *18*(1), 19-29.

Pleau, R., Pigeon, M., & Laurencot, J.-L. (2001). Some findings on the usefulness of image analysis for determining the characteristics of the air-void system on hardened concrete. *Cement and Concrete Composites*, *23*(2-3), 237-246.

Porras, Y., Jones, C., & Schmiedeke, N. (2020). Freezing and thawing durability of high early strength Portland cement concrete. *Journal of Materials in Civil Engineering*, *32*(5), 04020077.

Powers, T. C. (1945). A working hypothesis for further studies of frost resistance of concrete. Journal Proceedings,

Powers, T. C. (1954). Void space as a basis for producing air-entrained concrete. Journal Proceedings,

Powers, T. C. (1969). The properties of fresh concrete.

Powers, T. C., & Helmuth, R. (1953). Theory of volume changes in hardened portland-cement paste during freezing. Highway research board proceedings,

Powers, T. C., & Willis, T. (1950). The air requirement of frost resistant concrete. Highway Research Board Proceedings,

Punurai, W., Jarzynski, J., Qu, J., Kurtis, K. E., & Jacobs, L. J. (2006). Characterization of entrained air voids in cement paste with scattered ultrasound. *Ndt & E International*, *39*(6), 514-524.

Punurai, W., Jarzynski, J., Qu, J., Kim, J.-Y., Jacobs, L. J., & Kurtis, K. E. (2007). Characterization of multi-scale porosity in cement paste by advanced ultrasonic techniques. *Cement and Concrete Research*, *37*(1), 38-46.

Qin, X.-c., Meng, S.-p., Cao, D.-f., Tu, Y.-m., Sabourova, N., Grip, N., & Elfgren, L. (2016). Evaluation of freeze-thaw damage on concrete material and prestressed concrete specimens. *Construction and Building Materials*, *125*, 892-904.

Radlinski, M., Olek, J., Zhang, Q., & Peterson, K. (2010). Evaluation of the critical air-void system parameters for freeze-thaw resistant ternary concrete using the manual point-count and the flatbed scanner methods. In *Recent Advancement in Concrete Freezing-Thawing (FT) Durability*. ASTM International.

Riding, K.A. & Albahttiti, M. (2016). *Concrete Pavement Quality Control Testing Requirements Needed for the Super Air Meter* (No. FHWA-KS-16-14). Kansas Department of Transportation (KDOT). Bureau of Research.

Rollings, R. S. (1998). Joint spalling in newly constructed concrete pavements. *Journal of performance of constructed facilities,* 12(3), 137-144.

Scherer, G. W. (1999). Crystallization in pores. *Cement and Concrete research*, *29*(8), 1347-1358.

Scherer, G., & Valenza, J. (2005). Mechanisms of frost damage. *Materials science of concrete*, *7*(60), 209-246.

Schlorholtz, S. (1998). *Image Analysis for Evaluating Air Void Parameters of Concrete* (No. Iowa DOT Project HR-396).

Senadheera, S. P. (1995). *Spalling in concrete pavements: its relationship to coarse aggregate in concrete and a framework for design.* Texas A&M University.

Senadheera, S. P., & Zollinger, D. G. (1996). *Influence of coarse aggregate in portland cement concrete on spalling of concrete pavements.* Center for Transportation Research, Bureau of Engineering Research.

Setzer, M. (1997). Action of frost and deicing chemicals: basic phenomena and testing. *Freeze–thaw durability of concrete*, 3-22.

Shon, C.-S., Abdigaliyev, A., Bagitova, S., Chung, C.-W., & Kim, D. (2018). Determination of air-void system and modified frost resistance number for freeze-thaw resistance evaluation of ternary blended concrete made of ordinary Portland cement/silica fume/class F fly ash. *Cold Regions Science and Technology*, *155*, 127-136.

Snyder, K. A. (1998). A numerical test of air void spacing equations. *Advanced cement based Materials*, *8*(1), 28-44.

Stark, D. (1976). Characteristics and utilization of coarse aggregates associated with D-cracking. In *Living with Marginal Aggregates*. ASTM International.

Tanesi, J., Kim, H., Beyene, M., & Ardani, A. (2016). Super air meter for assessing air-void system of fresh concrete. *Advances in Civil Engineering Materials*, *5*(2), 22-37.

Tibshirani, R. (1996). Regression shrinkage and selection via the lasso. *Journal of the Royal Statistical Society: Series B (Methodological)*, *58*(1), 267-288.

Tranmer, M., & Elliot, M. (2008). Binary logistic regression. *Cathie Marsh for census and survey research, paper,* 20.

Walber. (2022). Sensitivity and specificity. https://en.wikipedia.org/wiki/Sensitivity_and_specificity

Wang, K., Nelsen, D. E., & Nixon, W. A. (2006). Damaging effects of deicing chemicals on concrete materials. *Cement and concrete composites*, *28*(2), 173-188.

Wang, L. & Zollinger, D. G. (2000). Mechanistic design framework for spalling distress. *Transportation research record,* 1730(1), 18-24.

Weiss, W. J., Olek, J., Whiting, N. M., Panchmatia, P., Qiao, C., & Suraneni, P. (2018). Synthesis: Accelerating Implementation of Research Findings to Reduce Potential Concrete Pavement Joint Deterioration.

Wu, X., Hsiao, C., & Chahine, G. (2011). ABS Acoustic Bubble Spectrometer®©.

Wu, Z., Libre, N. A., & Khayat, K. H. (2020). Factors affecting air-entrainment and performance of roller compacted concrete. *Construction and Building Materials*, *259*, 120413.

Yang, W. C., Ge, Y., Zhang, B. S., & Yuan, J. (2011). Effect of saturation degree on concrete deterioration due to freeze-thaw action. Key Engineering Materials,

Yazdanbakhsh, A., Grasley, Z., Tyson, B., & Al-Rub, R. K. A. (2011). Dispersion quantification of inclusions in composites. *Composites Part A: Applied Science and Manufacturing*, *42*(1), 75-83.

Zalocha, D., & Kasperkiewicz, J. (2005). Estimation of the structure of air entrained concrete using a flatbed scanner. *Cement and Concrete research*, *35*(10), 2041-2046.

Zhang, Z., Ansari, F., & Vitillo, N. (2005). Automated determination of entrained air-void parameters in hardened concrete. *ACI materials journal*, 102(1), 42.

Zhu, J., Kee, S.-H., Han, D., & Tsai, Y.-T. (2011). Effects of air voids on ultrasonic wave propagation in early age cement pastes. *Cement and Concrete Research*, 41(8), 872-881.

Appendix A.1 – First Set of Synthetic Air-Void Systems

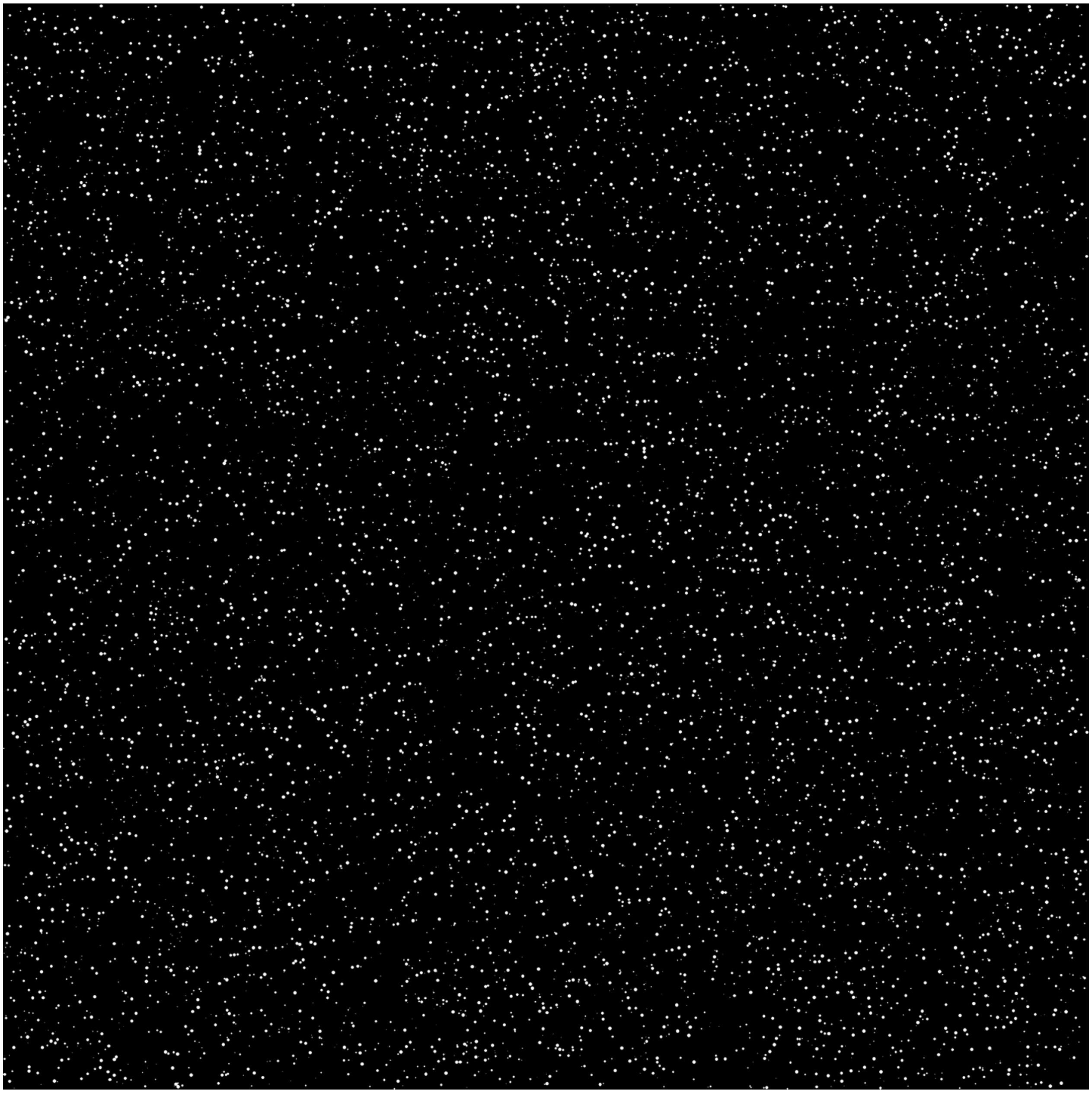

Figure A.1. Synthetic image # 1: Air content = 2%.

Figure A.2. Synthetic image # 2: Air content = 2%.

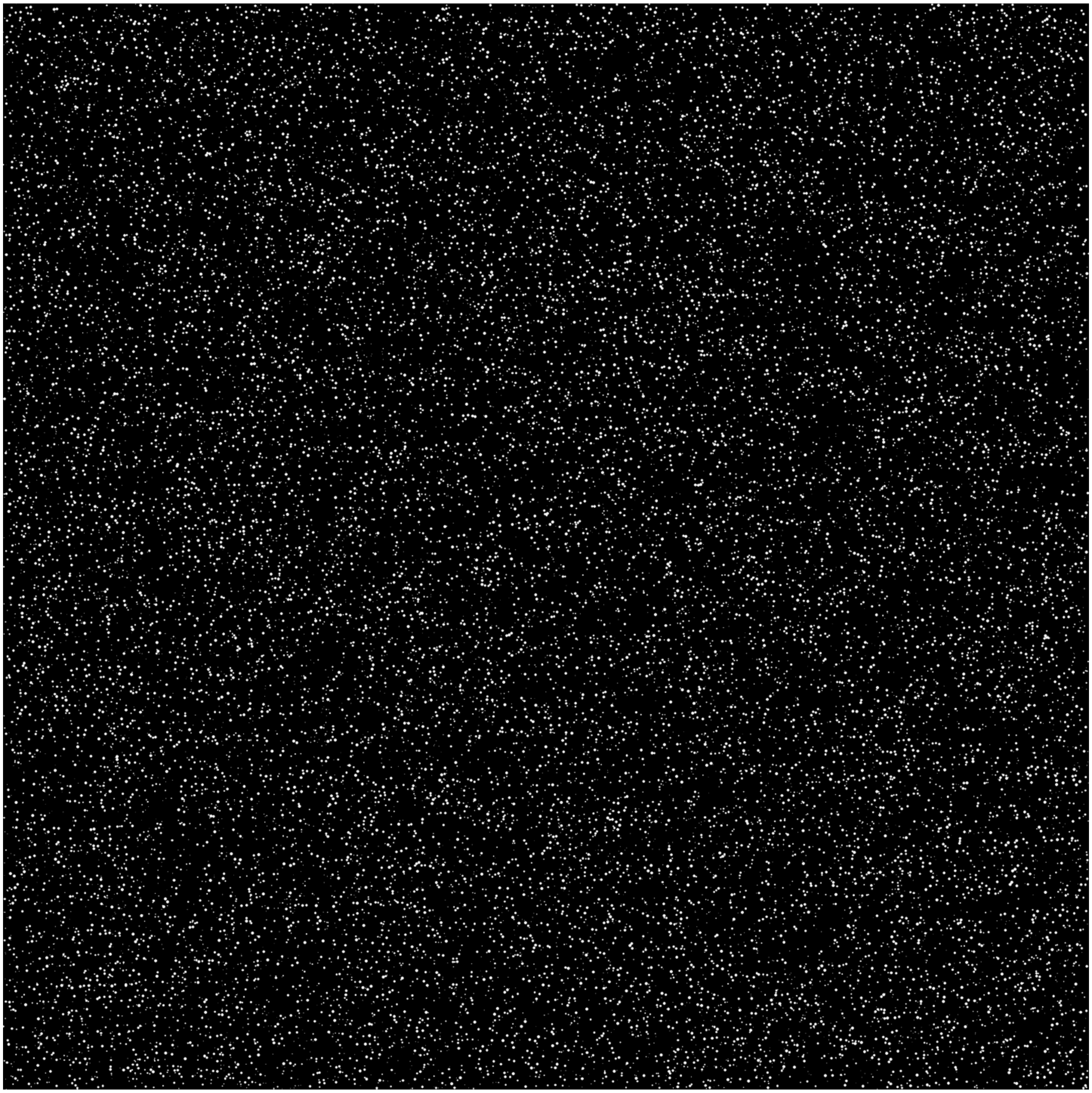

Figure A.3. Synthetic image # 3: Air content = 4%.

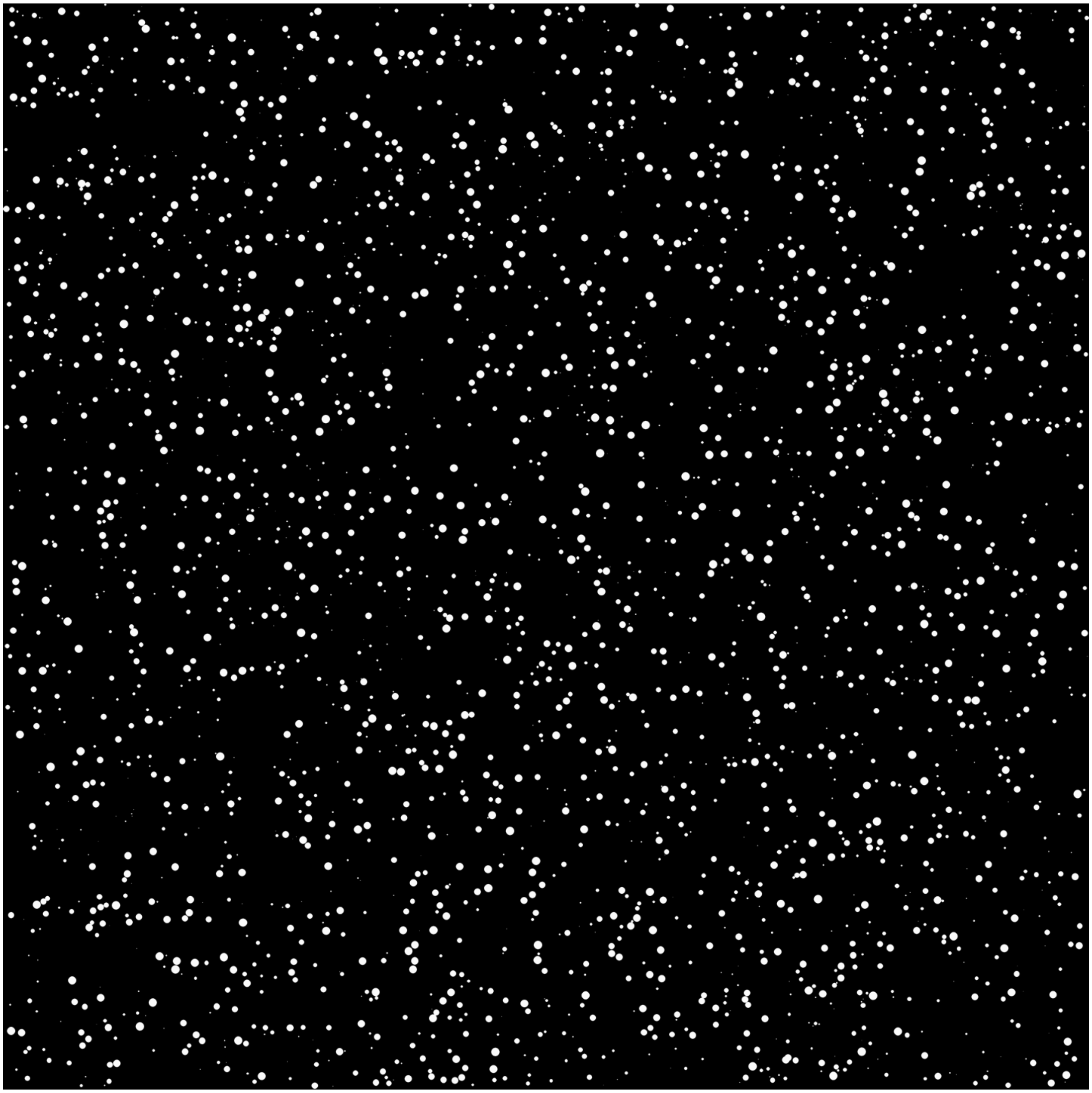

Figure A.4. Synthetic image # 4: Air content = 4%.

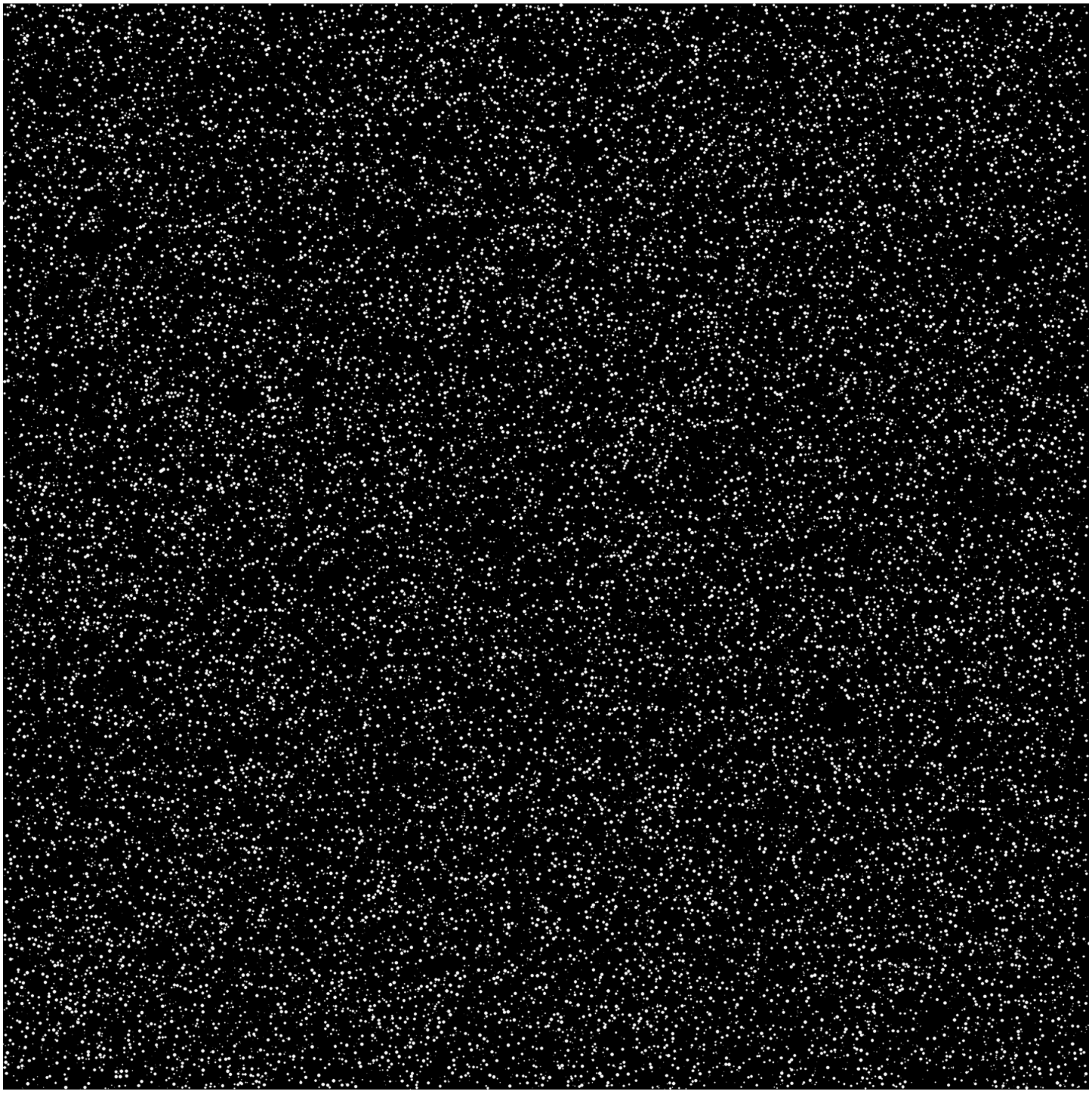

Figure A.5. Synthetic image # 5: Air content = 6%.

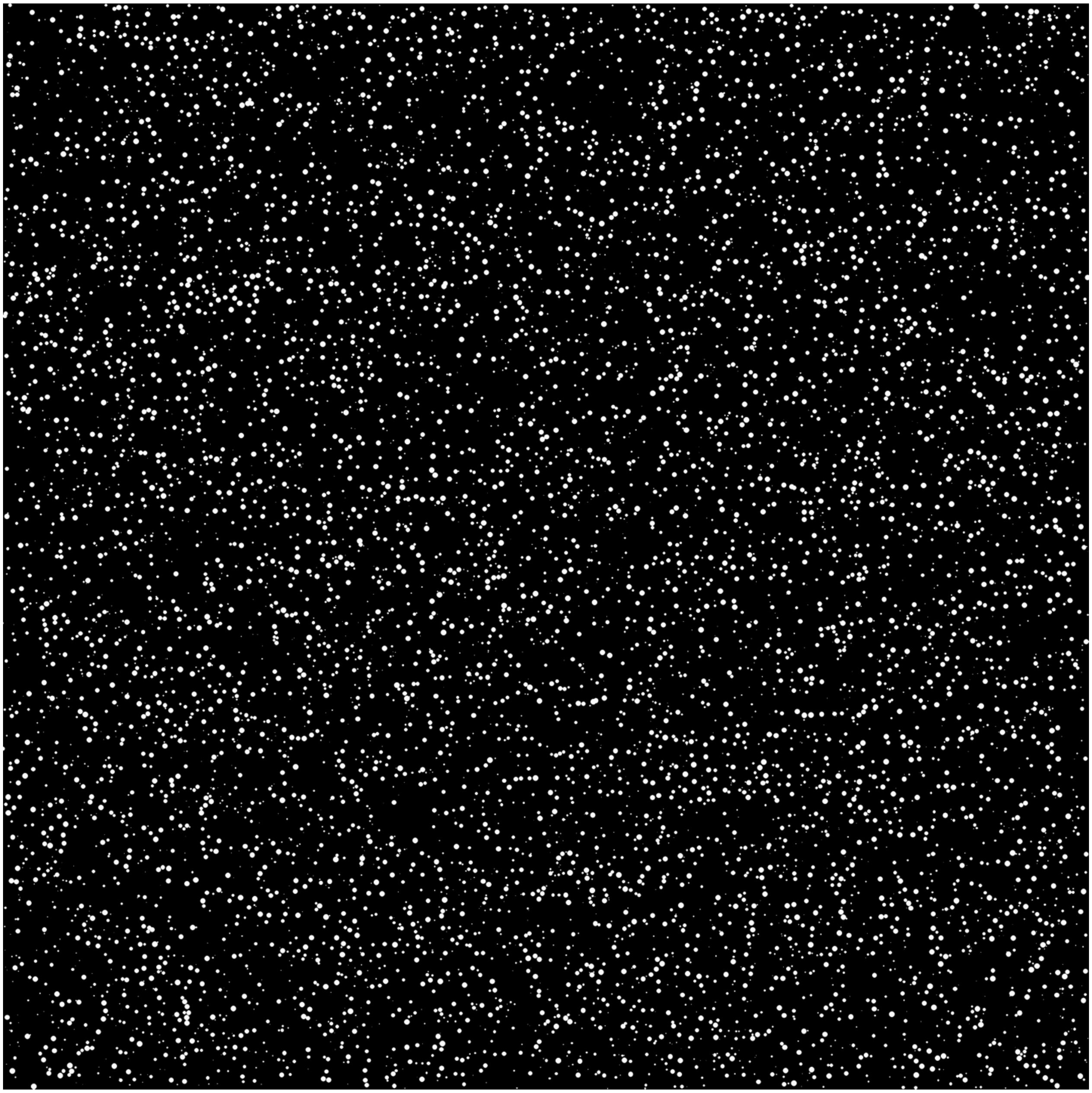

Figure A.6. Synthetic image # 6: Air content = 6%.

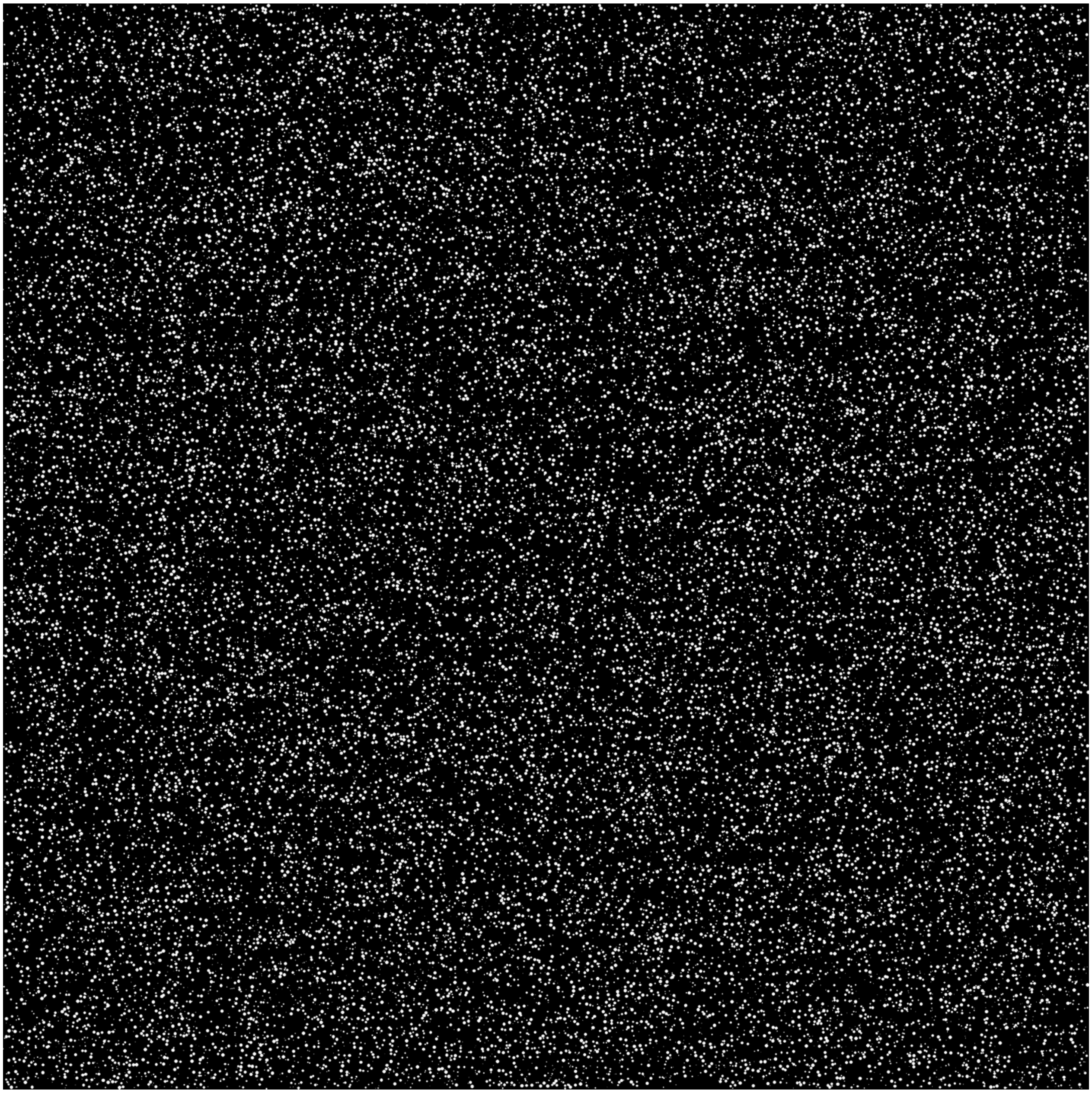

Figure A.7. Synthetic image # 7: Air content = 8%.

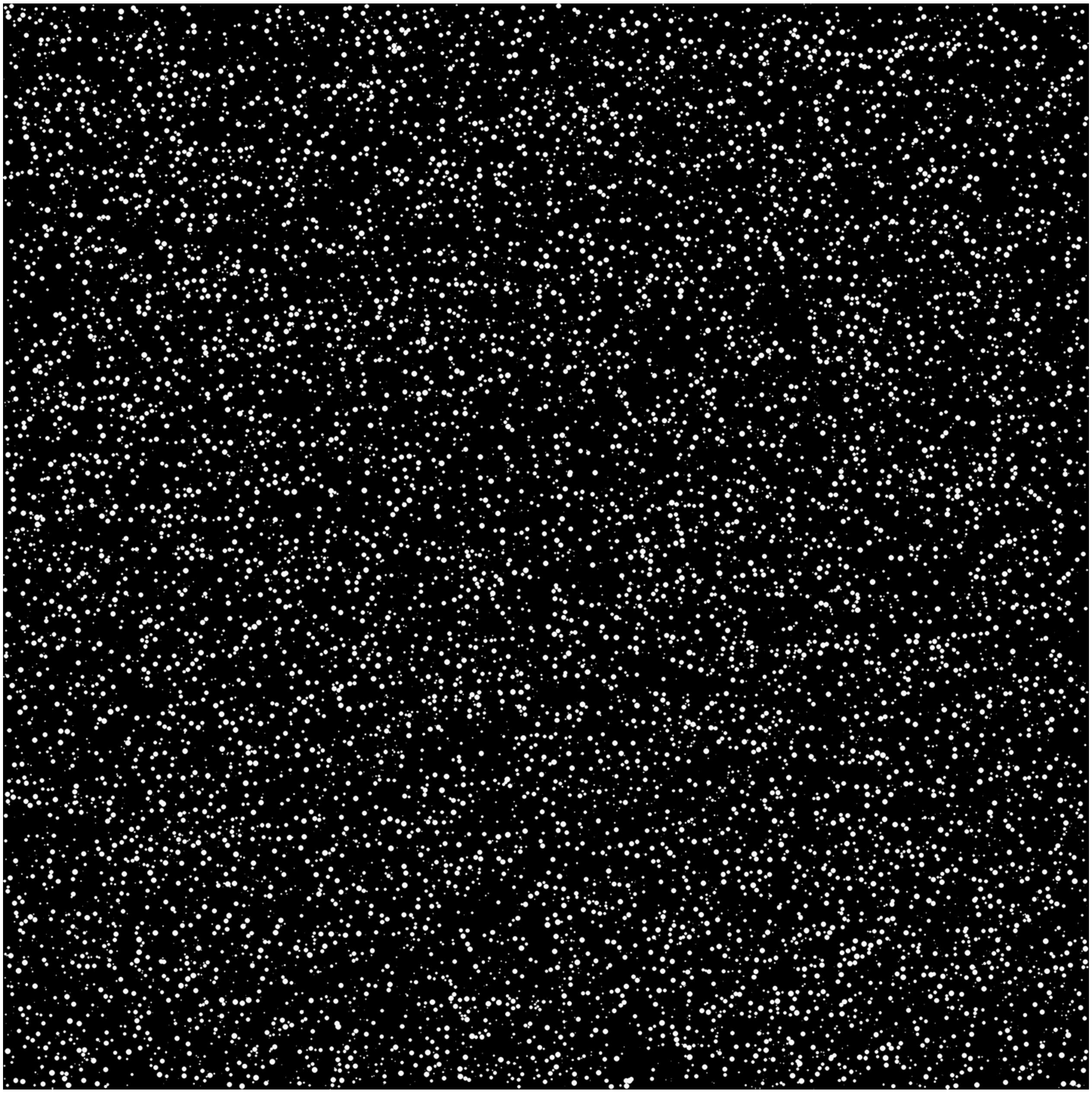

Figure A.8. Synthetic image # 8: Air content = 8%.

Appendix A.2 – Second Set of Synthetic Air-Void Systems

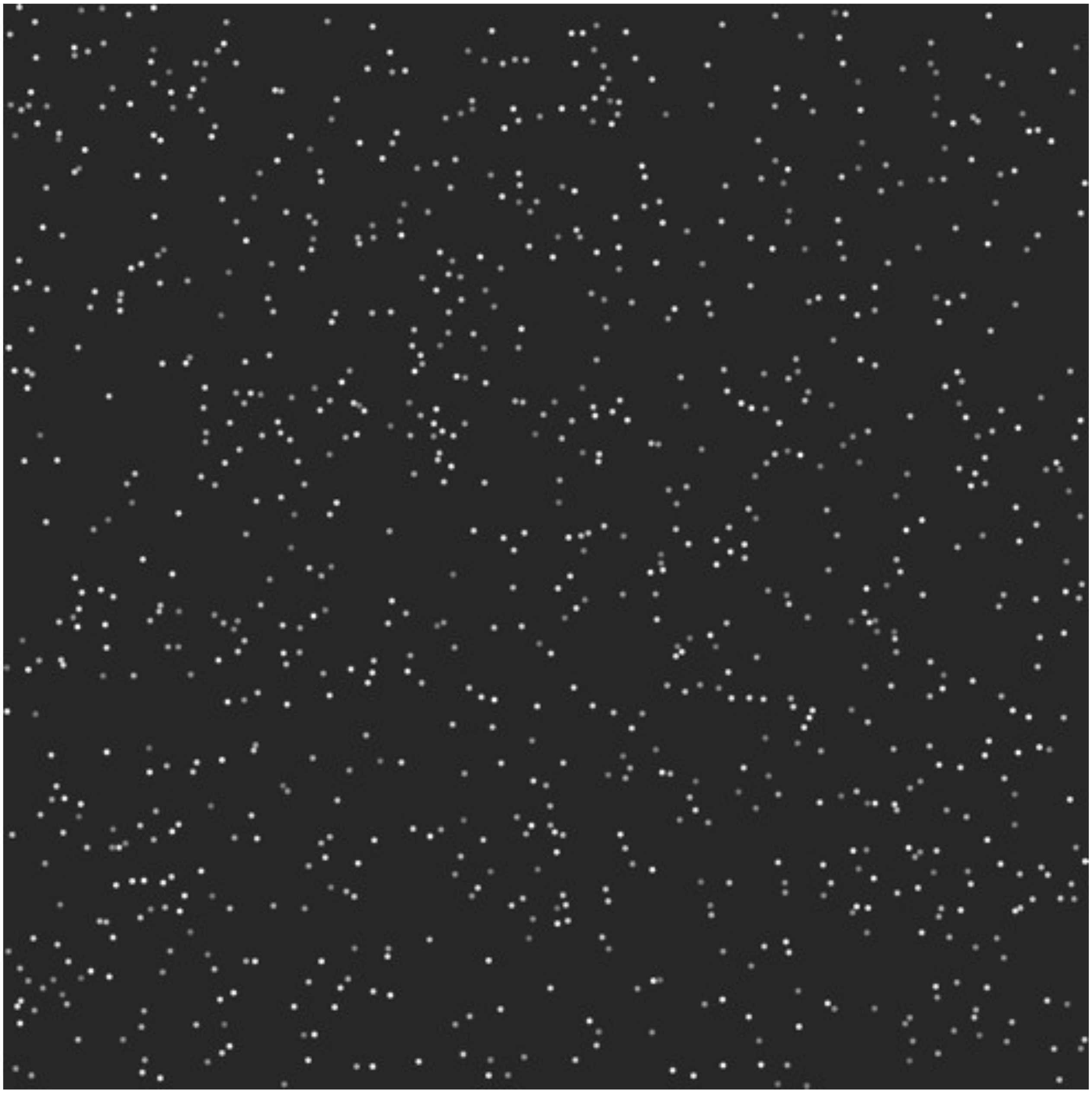

Figure A.9. Synthetic image # 1.

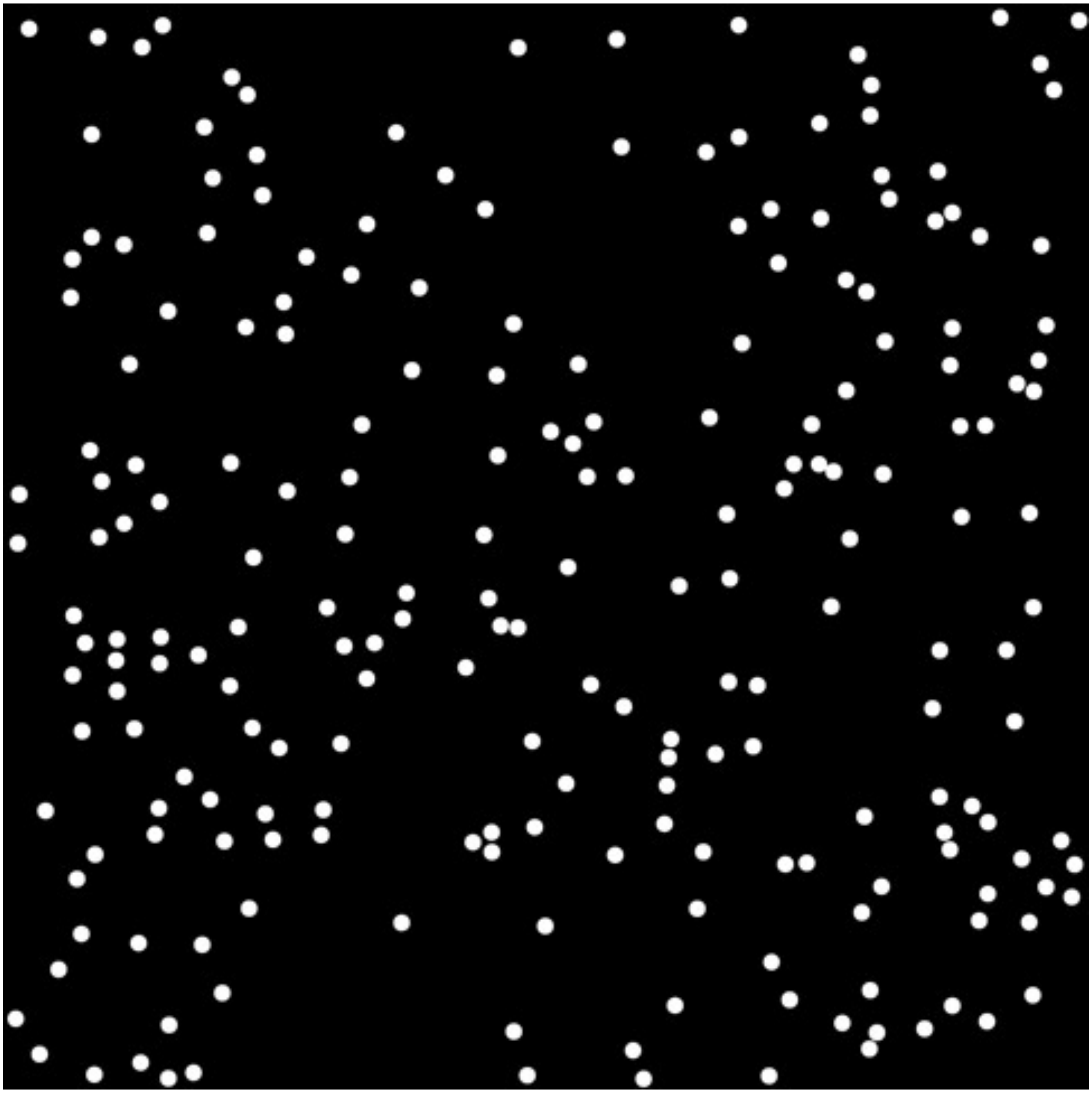

Figure A.10 Synthetic image # 2.

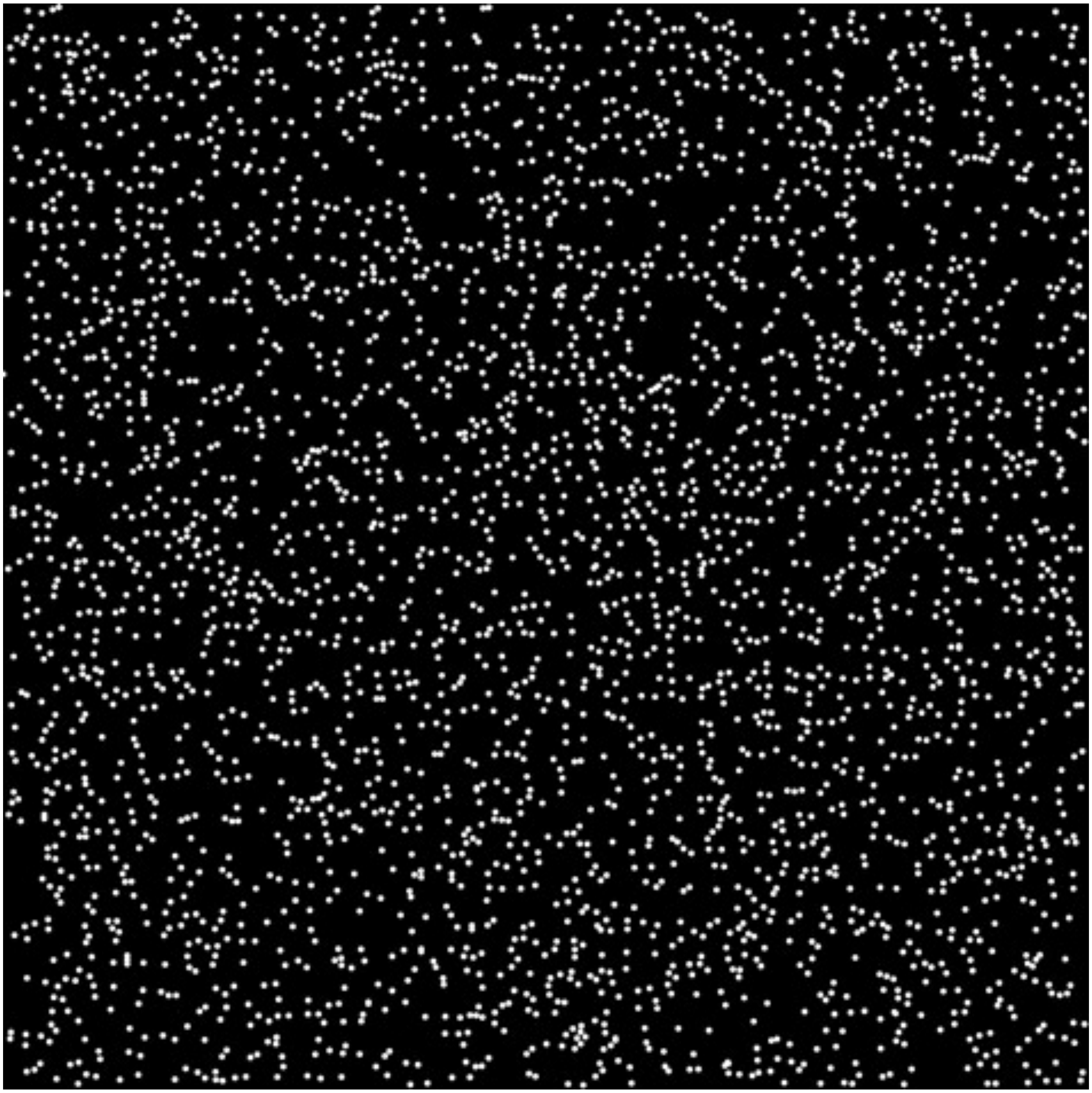

Figure A.11. Synthetic image # 3.

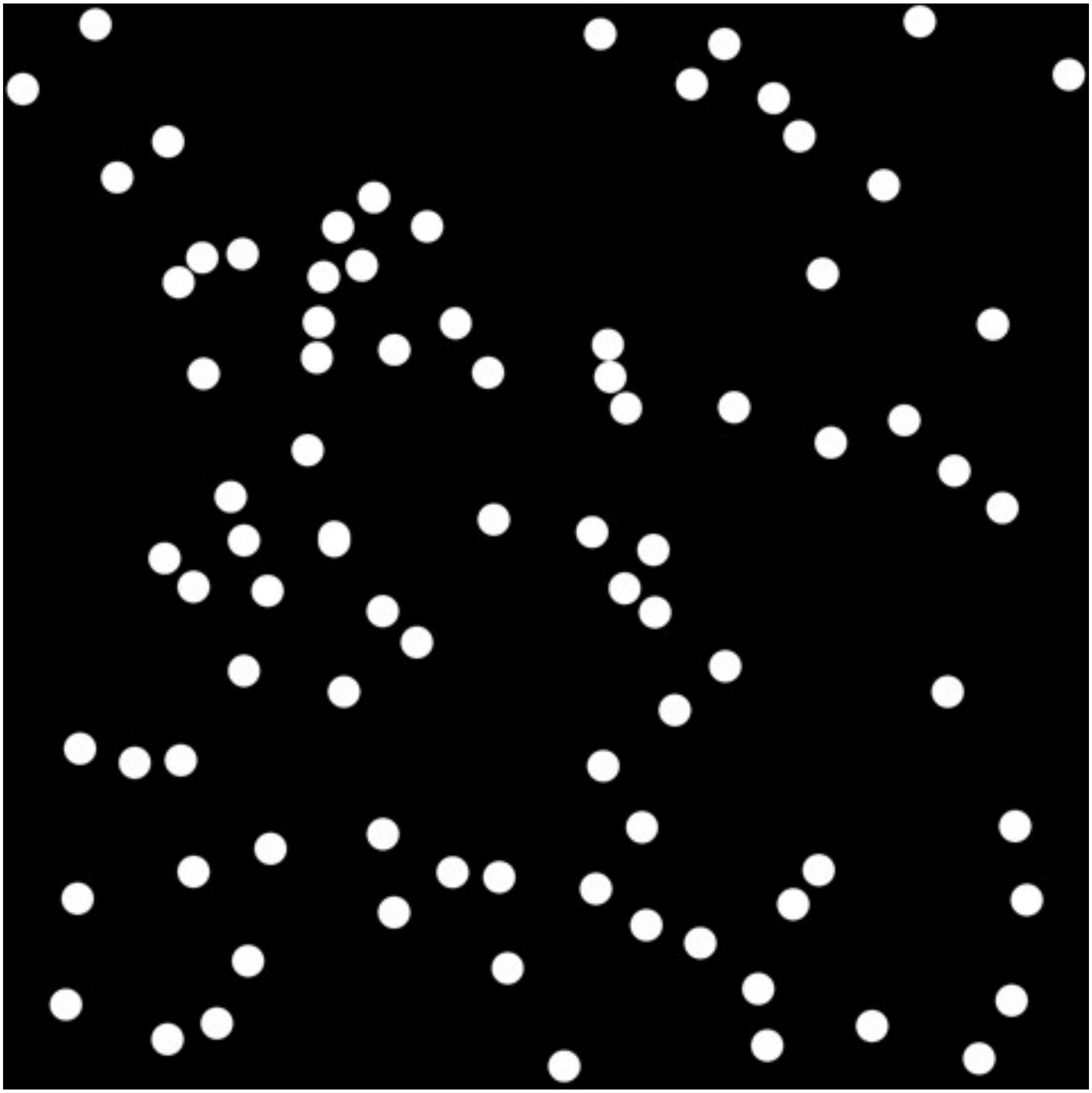

Figure A.12. Synthetic image # 4.

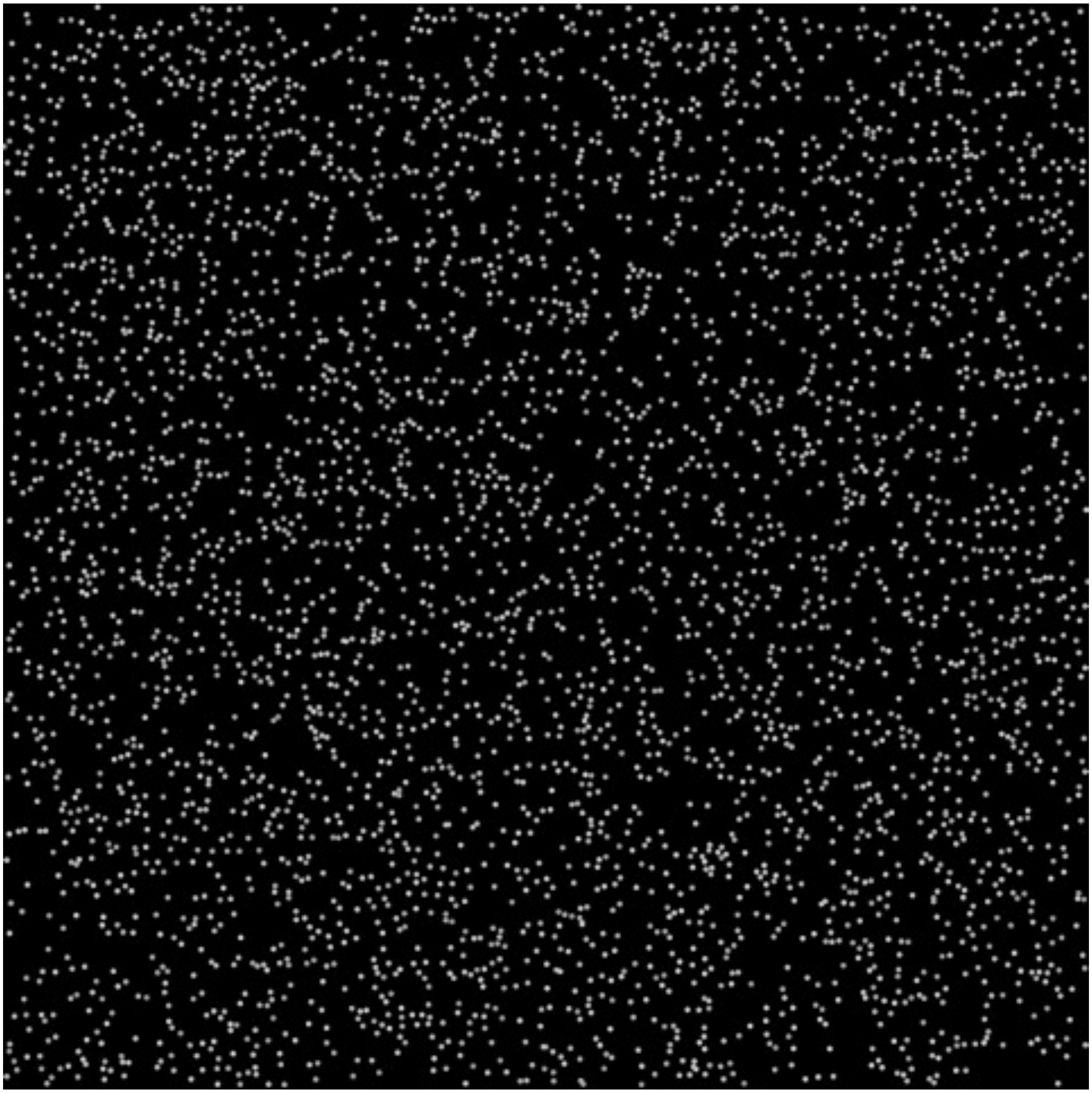

Figure A.13. Synthetic image # 5.

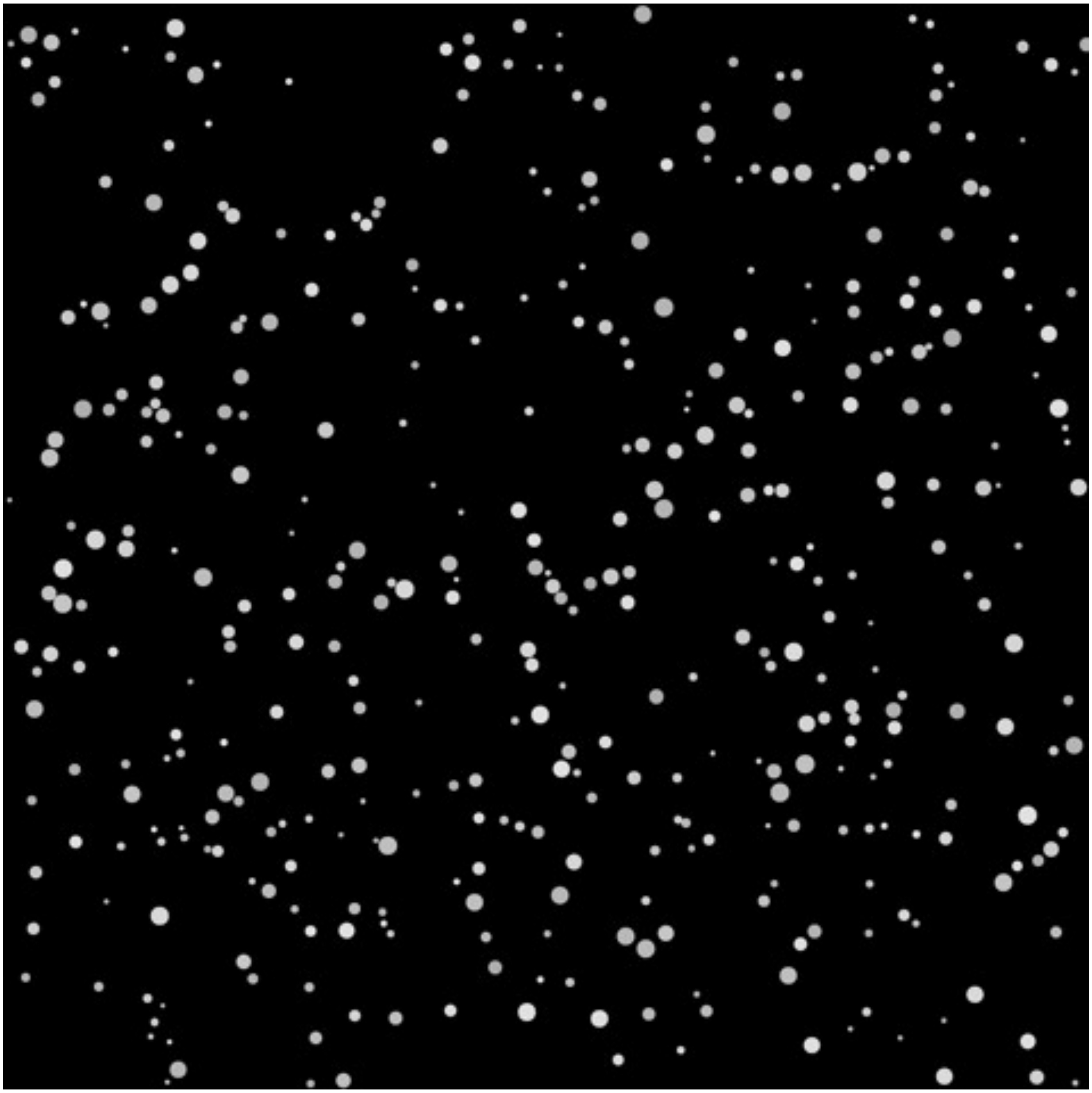

Figure A.14. Synthetic image # 6.

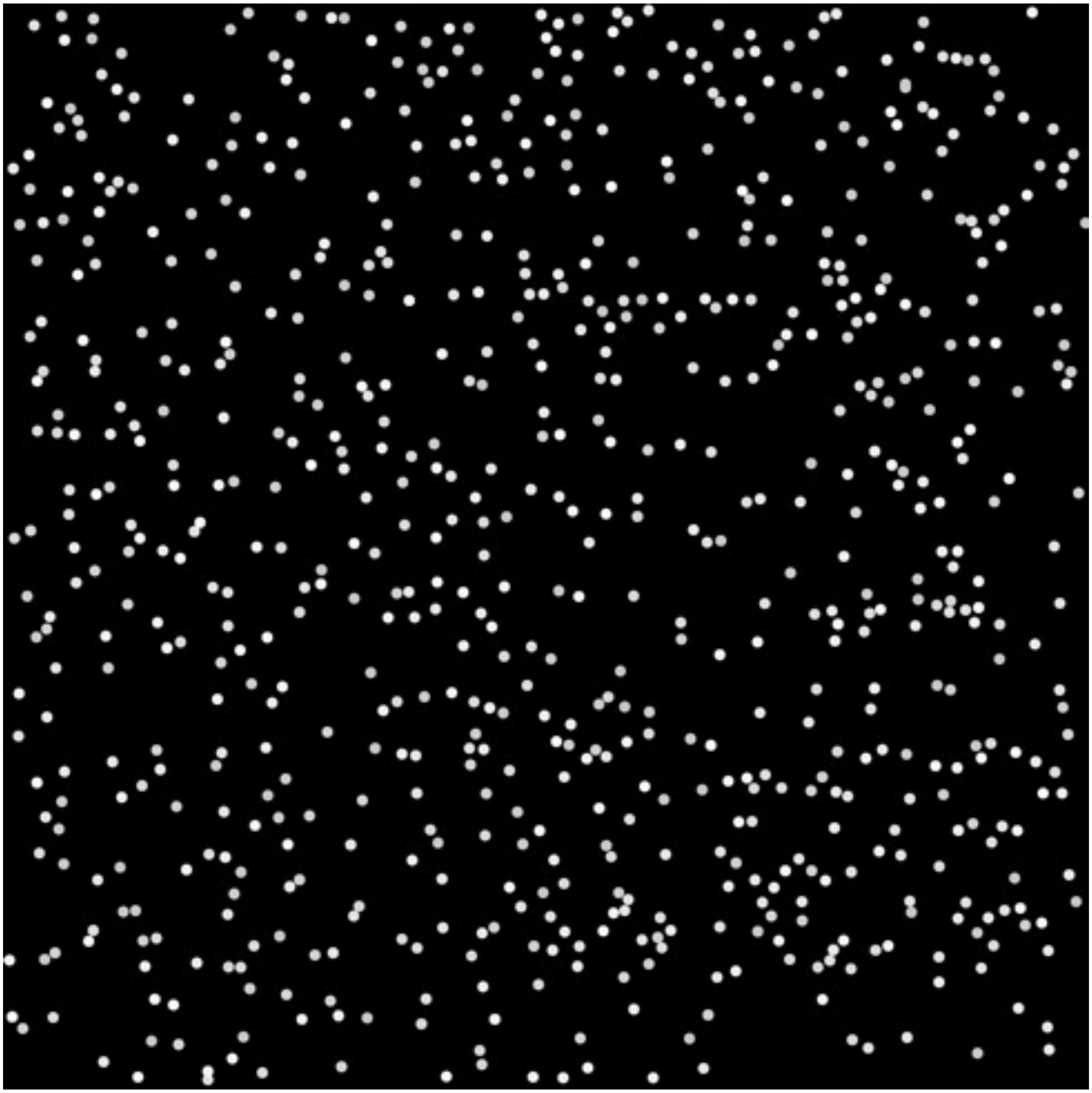

Figure A.15. Synthetic image # 7

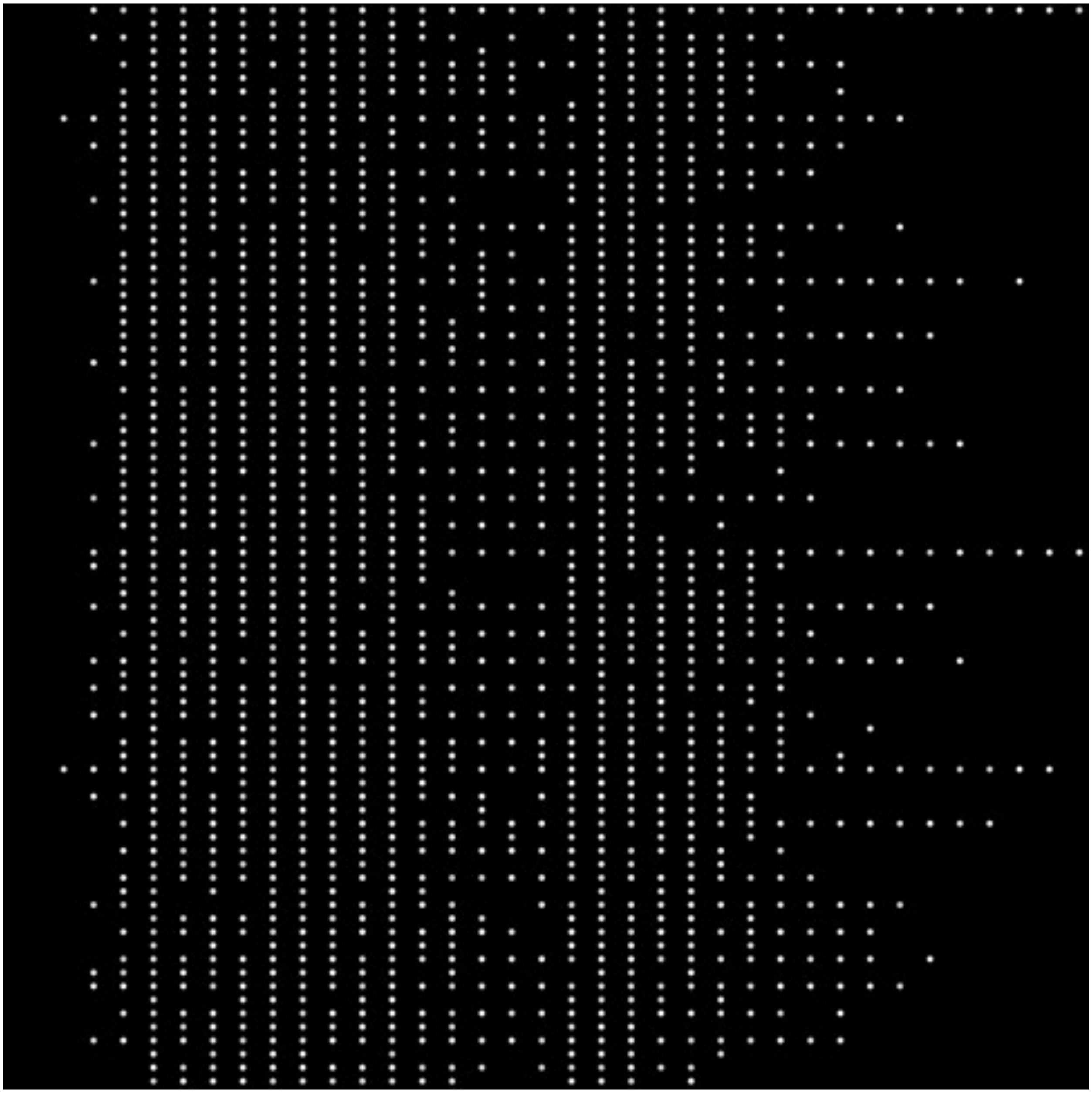

Figure A.16. Synthetic image # 8.

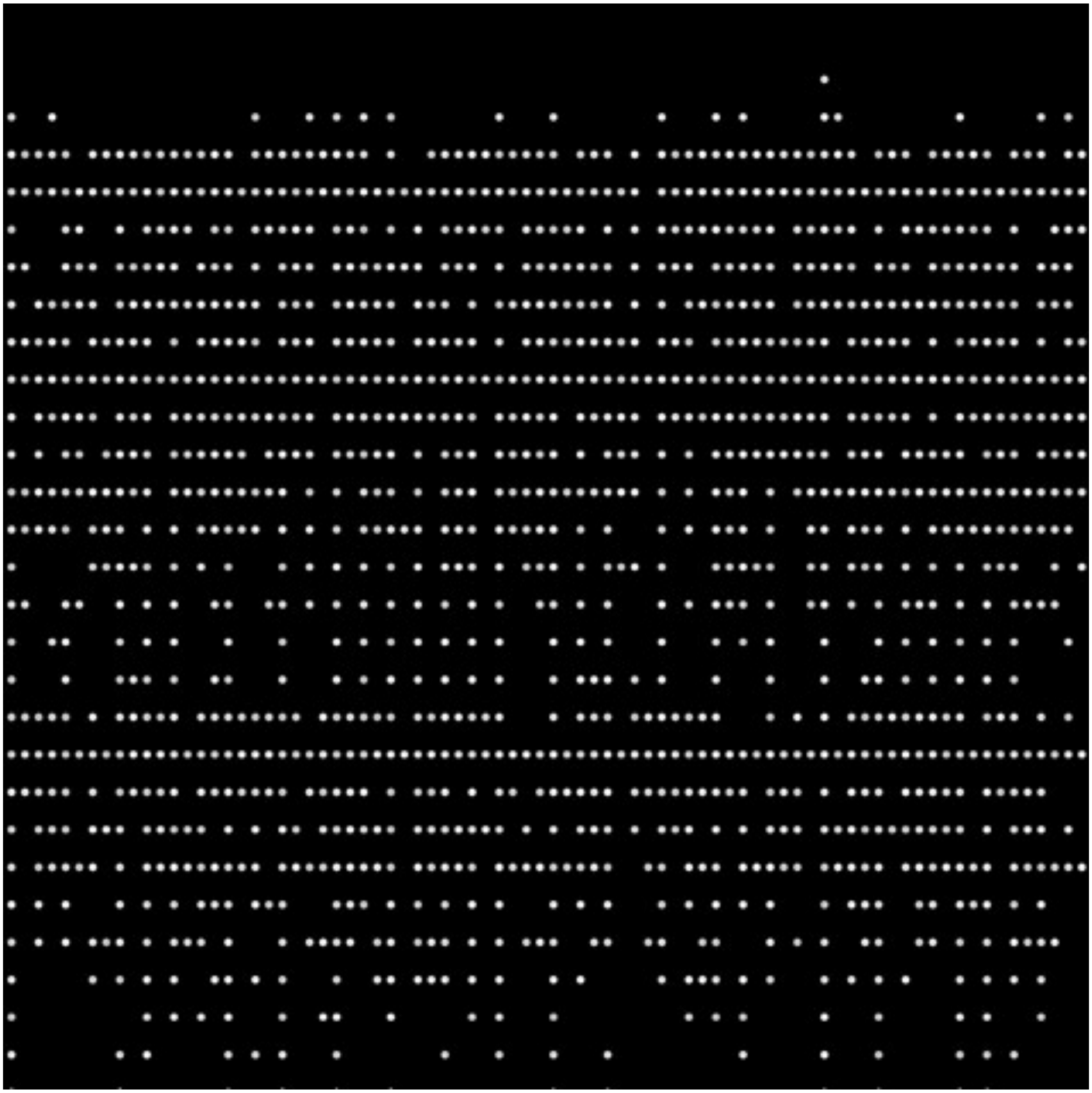

Figure A.17. Synthetic image # 9.

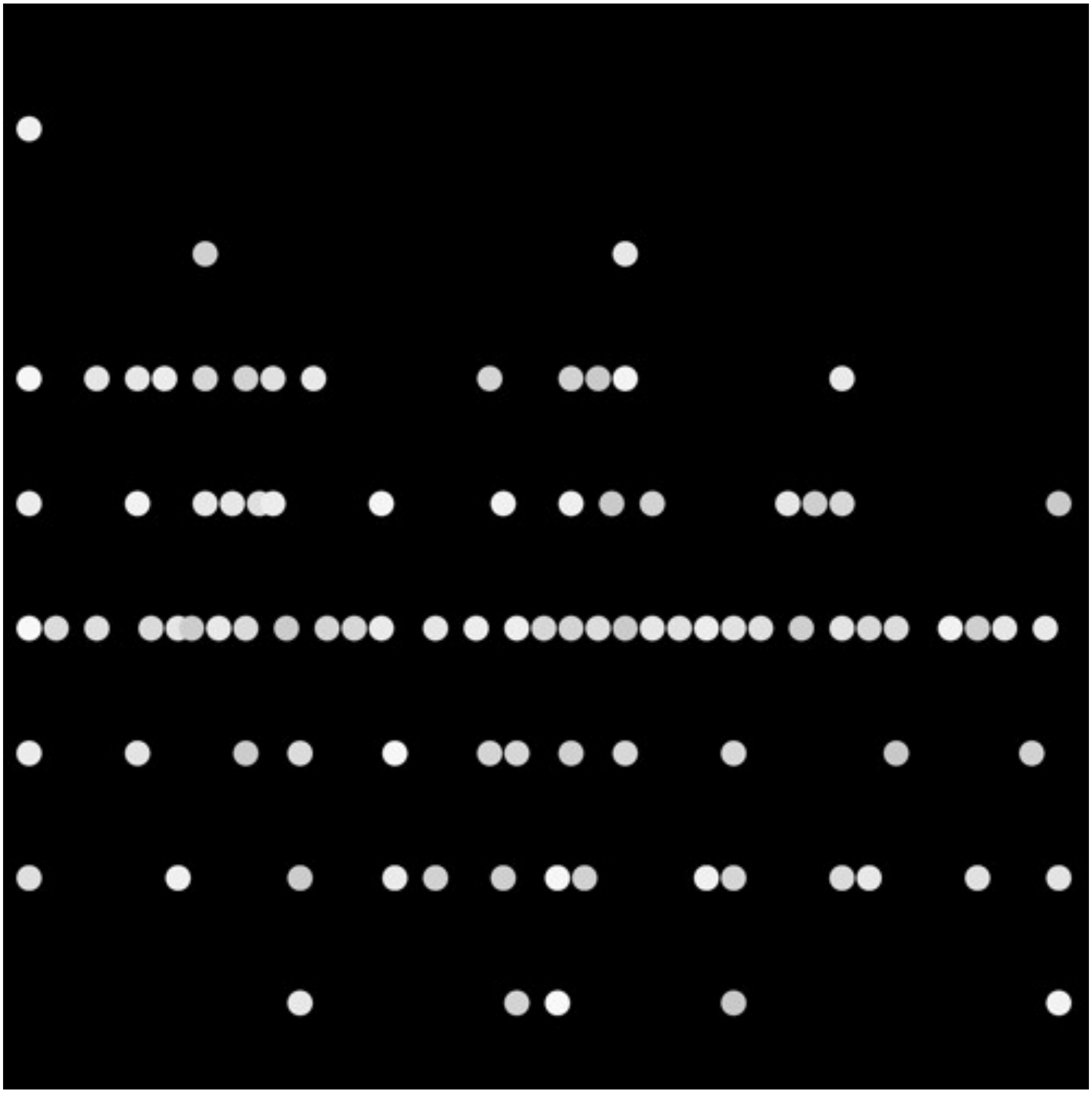

Figure A.18. Synthetic image # 10.